UNFITTED FINITE ELEMENT METHODS FOR THE STOKES PROBLEM USING THE SCOTT-VOGELIUS PAIR

by

Haoran Liu

B.A. in Mathematics, University of Rochester, 2016

Submitted to the Graduate Faculty of

the Dietrich School of Arts and Sciences in partial fulfillment

of the requirements for the degree of

Doctor of Philosophy

University of Pittsburgh

2022

UNIVERSITY OF PITTSBURGH

DIETRICH SCHOOL OF ARTS AND SCIENCES

This dissertation was presented

by

Haoran Liu

It was defended on

July 20th 2022

and approved by

Prof. Michael J. Neilan, Department of Mathematics, University of Pittsburgh

Prof. William J. Layton, Department of Mathematics, University of Pittsburgh

Prof. Ivan Yotov, Department of Mathematics, University of Pittsburgh

Prof. Maxim A. Olshanskii, Department of Mathematics, University of Houston

Copyright © by Haoran Liu
2022

UNFITTED FINITE ELEMENT METHODS FOR THE STOKES PROBLEM USING THE SCOTT-VOGELIUS PAIR

Haoran Liu, PhD

University of Pittsburgh, 2022

In this thesis, we construct and analyze two unfitted finite element methods for the Stokes problem based on the Scott-Vogelius pair on Clough-Tocher splits. For both methods, for $k \geq d$, where d is the dimension of the space, the velocity space consists of continuous piecewise polynomials of degree k, and the pressure space consists of piecewise polynomials of degree $k-1$ without continuity constraints. The discrete piecewise polynomial spaces are defined on macro-element triangulations which are not fitted to the smooth physical domain.

The first unfitted finite element method we propose is a finite element method with boundary correction for the Stokes problem on 2D domains. We introduce a Lagrange multiplier space consisting of continuous piecewise polynomials of degree k with respect to the boundary partition to enforce the boundary condition as well as to mitigate the lack of pressure robustness. We show the well-posedness of the method by proving several inf-sup conditions. In addition, we show this method has optimal order convergence rate and yields a divergenece-free velocity approximation.

The second unfitted finite element method we propose is a CutFEM for the Stokes problem on both 2D and 3D domains. Boundary conditions are imposed via penalization through the help of a Nitsche-type discretization. We ensure the stability with respect to small and anisotropic cuts of the bulk elements by adding local ghost penalty stabilization terms. We show the method is well-posed and possesses a divergence–free property of the discrete velocity outside an $O(h)$ neighborhood of

the boundary. To mitigate the error caused by the violation of the divergence-free condition around the boundary, we introduce local grad-div stablization. Through the error analysis, we show that the grad-div parameter can scale like $O(h^{-1})$, allowing a rather heavy penalty for the violation of mass conservation, while still ensuring optimal order error estimates.

Table of Contents

List of Tables

List of Figures

Preface

I would like to express my most sincere gratitude and appreciation to my advisor Professor Michael J. Neilan for his guidance and patience and invaluable advice during my PhD study. I would also like to thank Professor William Layton, Professor Maxim A. Olshanskii, and Professor Ivan Yotov for serving on my thesis committee and providing invaluable feedback.

I would like to thank all my friends for their support during my years in Pitt. Especially, I would like to thank Baris Otus for his help on the project and I would like to thank Manu Jayadharan for his advice on my career.

Last but not least, I would like to thank my parents for their unconditional love and support throughout the years.

1.0 Introduction

1.1 Finite Element Methods Applied to the Stokes Problem on Polytopal Domains

The Navier-Stokes equations are a fundamental model of incompressible flows. This model has wide applications in science and engineering. For instance, it can be used to model fluid flows in a pipe or a channel, or the air flows around the wings of an airplane. For a domain $\Omega \subset \mathbb{R}^d$, where $d \in \{2, 3\}$, and a time interval $(0, T)$, where $T < \infty$, a simple form of the Naiver-Stokes equations assumes constant fluid density, and is given as follows:

$$\partial_t \boldsymbol{u} - \nu \Delta \boldsymbol{u} + (\boldsymbol{u} \cdot \nabla)\boldsymbol{u} + \nabla p = \boldsymbol{f} \qquad \text{in } \Omega, \tag{1.1.1a}$$

$$\operatorname{div} \boldsymbol{u} = 0 \qquad \text{in } \Omega \tag{1.1.1b}$$

where $\boldsymbol{u}$ is the velocity of the fluid, p is the pressure, and ν is the viscosity, which is assumed to be constant. The right-hand function $\boldsymbol{f}$ stands for the external force, and the nonlinear term $(\boldsymbol{u} \cdot \nabla)\boldsymbol{u}$ stands for the inertial force. The Laplacian term $\Delta \boldsymbol{u}$ represents the viscous effects of the fluid. The second equation represents the incompressibility of the fluid.

As a constrained system of partial differential equaitons, the Navier-Stokes equations pose some mathematical and numerical difficulties. We consider a basic model, the stationary Stokes equations, to highlight and focus on this coupling and to study the divergence-free constraint. The Stokes equations with Dirichlet boundary conditions are given as:

$$-\nu\Delta \boldsymbol{u} + \nabla p = \boldsymbol{f} \qquad \text{in } \Omega, \tag{1.1.2a}$$

$$\operatorname{div} \boldsymbol{u} = 0 \qquad \text{in } \Omega, \tag{1.1.2b}$$

$$\boldsymbol{u} = \boldsymbol{g} \qquad \text{on } \partial\Omega. \tag{1.1.2c}$$

Since the system of Stokes equations does not have the nonlinear term $(\boldsymbol{u} \cdot \nabla)\boldsymbol{u}$ and is not time-dependent, it is obvious that this model problem is much simpler than the Navier-Stokes equations. For simplicity, we set $\boldsymbol{g} \equiv 0$.

We multiply a test function $\boldsymbol{v}$ from $\boldsymbol{H}_0^1(\Omega)$ to both sides of (1.1.2a), and a test function q from $L_0^2(\Omega)$ to both sides of (1.1.2b), then integrate both sides of the equations. Using integration-by-parts, we derive the weak formulation of the Stokes problem: Find $\boldsymbol{u} \in \boldsymbol{H}_0^1(\Omega)$ and $p \in L_0^2(\Omega)$ such that

$$\nu(\nabla \boldsymbol{u}, \nabla \boldsymbol{v}) - (p, \operatorname{div} \boldsymbol{v}) = (\boldsymbol{f}, \boldsymbol{v}) \qquad \forall\ \boldsymbol{v} \in \boldsymbol{H}_0^1(\Omega), \tag{1.1.3a}$$

$$-(\operatorname{div} \boldsymbol{u}, q) = 0 \qquad \forall\ q \in L_0^2(\Omega). \tag{1.1.3b}$$

Here we use $(\cdot, \cdot)$ to denote the L^2 inner product over Ω.

To apply finite element methods to (1.1.3), assuming Ω to be a polytopal domain here, we triangulate the domain Ω into a simplicial mesh $\mathcal{T}_h$, where h stands for the mesh parameter, and we define the following piecewise polynomial space with respect to $\mathcal{T}_h$:

$$\mathcal{P}_k(\mathcal{T}_h) = \{v \in C(\Omega) : v|_T \in \mathcal{P}(T) \quad \forall T \in \mathcal{T}_h\},$$

$$\mathcal{P}_k^{disc}(\mathcal{T}_h) = \{v \in L^2(\Omega) : v|_T \in \mathcal{P}(T) \quad \forall T \in \mathcal{T}_h\}.$$

We use boldface to denote the counterpart for vector-valued functions and spaces.

Let $\boldsymbol{V}_h \subset \boldsymbol{H}_0^1(\Omega)$ and $Q_h \subset L_0^2(\Omega)$ be finite-dimensional spaces consisting of piecewise polynomials with respect to $\mathcal{T}_h$. Then a finite element method for (1.1.2) based on (1.1.3) reads: Find a $\boldsymbol{u}_h \in \boldsymbol{V}_h$ and a $p_h \in Q_h$ such that

$$\nu(\nabla \boldsymbol{u}_h, \nabla \boldsymbol{v}) - (p_h, \operatorname{div} \boldsymbol{v}) = (\boldsymbol{f}, \boldsymbol{v}) \qquad \forall\, \boldsymbol{v} \in \boldsymbol{V}_h, \tag{1.1.4a}$$

$$-(\operatorname{div} \boldsymbol{u}_h, q) = 0 \qquad \forall\, q \in Q_h. \tag{1.1.4b}$$

We say that the pair of $\boldsymbol{V}_h \times Q_h$ for the finite element method (1.1.4) is stable if the Ladyzhenskaya–Babuška–Brezzi (LBB) condition is satisfied [8]: there exists a constant $C > 0$ that is independent of the mesh parameter h such that

$$C\|q\|_{L^2(\Omega)} \leq \sup_{\boldsymbol{v} \in \boldsymbol{V}_h \setminus \{0\}} \frac{\int_\Omega (\operatorname{div} \boldsymbol{v}) q \, dx}{\|\boldsymbol{v}\|_{H^1(\Omega)}} \qquad \forall q \in Q_h.$$

Here we list some common choice of stable Stokes pairs [8, 51]:

1. $\boldsymbol{\mathcal{P}}_d - \mathcal{P}_0$: $\boldsymbol{V}_h = \boldsymbol{\mathcal{P}}_d(\mathcal{T}_h) \cap \boldsymbol{H}_0^1(\Omega)$ and $Q_h = \mathcal{P}_0^{disc}(\mathcal{T}_h) \cap L_0^2(\Omega)$, where d represents the dimension of the domain;
2. Taylor-Hood Element: $\boldsymbol{V}_h = \boldsymbol{\mathcal{P}}_k(\mathcal{T}_h) \cap \boldsymbol{H}_0^1(\Omega)$ and $Q_h = \mathcal{P}_{k-1}(\mathcal{T}_h) \cap L_0^2(\Omega)$ for $k \geq 2$;
3. MINI element: $\boldsymbol{V}_h = (\boldsymbol{\mathcal{P}}_1(\mathcal{T}_h) + \mathcal{B}_{d+1}(\mathcal{T}_h)) \cap \boldsymbol{H}_0^1(\Omega)$ and $Q_h = \mathcal{P}_1(\mathcal{T}_h) \cap L_0^2(\Omega)$, where $\mathcal{B}_{d+1}(\mathcal{T}_h)$ denotes the space of local bubble functions of degree $d+1$. Here, d represents the dimension of the domain;

1.2 Divergence-free Elements for the Stokes Problem

We say $\boldsymbol{V}_h \times Q_h$ is a conforming, stable, and divergence-free pair for the Stokes problem if the following conditions with respect to a simplicial triangulation of the domain Ω are satisfied [21]:

1. The discrete spaces are conforming, i.e., we have $\boldsymbol{V}_h \subset \boldsymbol{H}_0^1(\Omega)$ and $Q_h \subset L_0^2(\Omega)$;
2. The discrete pair $\boldsymbol{V}_h \times Q_h$ is stable, i.e., the Ladyzhenskaja-Babuska-Brezzi (LBB) condition is satisfied.
3. the pair produces pointwise divergence-free discrete velocity solution $\boldsymbol{u}_h \in \boldsymbol{V}_h$ for the Stokes problem.

The third condition is typically satisfied by enforcing the image of the divergence operator on the velocity space $\boldsymbol{V}_h$ to be a subset of the pressure space Q_h, i.e., $\operatorname{div} \boldsymbol{V}_h \subset Q_h$. Many finite element methods have been developed over the past years: Some notable methods that fit this description are Taylor-Hood elements [8], $\boldsymbol{\mathcal{P}}_d - \mathcal{P}_0$ elements [8], MINI element [1], etc. However, most of those only satisfied the first two conditions mentioned above, with the mass conservation enforced only weakly. On the other hand, Scott and Vogelius showed that the $\boldsymbol{\mathcal{P}}_k - \mathcal{P}_{k-1}^{disc}$ pair in two dimensions satisfies all three conditions mentioned above, if the following criteria are met [51, 54]: (1) the polynomial degree k is greater or equal to 4; (2) the triangulation is quasi-uniform (this condition can be dropped according to [28]); (3) there are no singular vertices, i.e., vertices that fall on two straight lines, within the triangulation. Later, it has been shown on a barycenter refined mesh, if $k \geq 2$ in two dimensions [2], the pair is stable, conforming and divergence-free. In three dimensions, it has also been shown that on a barycenter refined quasi-uniform tetrahedral mesh, if $k \geq 3$, the pair is stable, conforming and divergence-free [55]. Some other examples of finite element

methods that satisfies all three conditions above include Guzmán-Neilan elements [25] and Falk-Neilan elements [21]. In this thesis, we focus on Scott-Vogelius element for its properties that for $k \geq d$ the pair yields exact divergence-free velocity solutions and the pair yields stable solution pair on a barycenter refined mesh [14].

Divergence–free schemes have several inherent advantages, e.g., exact conservation laws for any mesh size and long-time stability [17, 7]. In the case where the domain Ω is a polytope, divergence–free schemes also provide pressure-robustness; similar to the continuous setting, modifying the source term in the Stokes problem by a gradient field only affects the pressure approximation. This invariance leads to a decoupling in the velocity error, with abstract estimates independent of the viscosity. Thus, divergence-free schemes may be advantageous for high Reynold number flows and/or flows with large pressure gradients [49, 50, 38].

The advantages of the divergence-free elements is highlighted through a comparison between using Taylor-Hood and Scott-Vogelius for an example problem in [14]:

Example 1.2.1. Consider the following linear steady Stokes problem in $\mathbb{R}^2$, where $\Omega = (0,1) \times (0,1)$:

$$-\Delta \boldsymbol{u} + \nabla p = \mathrm{Ra} \begin{bmatrix} 0 \\ y \end{bmatrix} \qquad \text{in } \Omega, \tag{1.2.1a}$$

$$\nabla \cdot \boldsymbol{u} = 0 \qquad \text{in } \Omega, \tag{1.2.1b}$$

$$\boldsymbol{u} = 0 \qquad \text{on } \partial\Omega. \tag{1.2.1c}$$

Here, the Rayleigh number $\mathrm{Ra} = 10^3$. The solution to this system is $(\boldsymbol{u}, p) = (\boldsymbol{0}, \frac{\mathrm{Ra}}{2} y^2 - \frac{\mathrm{Ra}}{6})$. We use Netgen/NGSolve [48] to numerically solve this example. We

set the maximum mesh size to be 0.09. The velocity error $\|\nabla \boldsymbol{u} - \nabla \boldsymbol{u}_h\|_{L^2(\Omega)}$ from the approximation using $\boldsymbol{\mathcal{P}}_2 - \mathcal{P}_1$ Taylor-Hood is 162.1, which is of the same order as the Rayleigh number Ra. However, the velocity error $\|\nabla \boldsymbol{u} - \nabla \boldsymbol{u}_h\|_{L^2(\Omega)}$ from the approximation using $\boldsymbol{\mathcal{P}}_2 - \mathcal{P}_1^{disc}$ Scott-Vogelius on a barycenter refined mesh is 2.542e-14. The difference comes from the fact that the Scott-Vogelius pair is pressure robust, i.e., the velocity error can be decoupled from the pressure error, which is one of the advantages of divergence-free elements, whereas the Taylor-Hood pair is not. We illustrate the velocity error $\|\nabla \boldsymbol{u} - \nabla \boldsymbol{u}_h\|_{L^2(\Omega)}$ in Figure 1 and Figure 2 using Taylor-Hood and Scott-Vogelius, respectively:

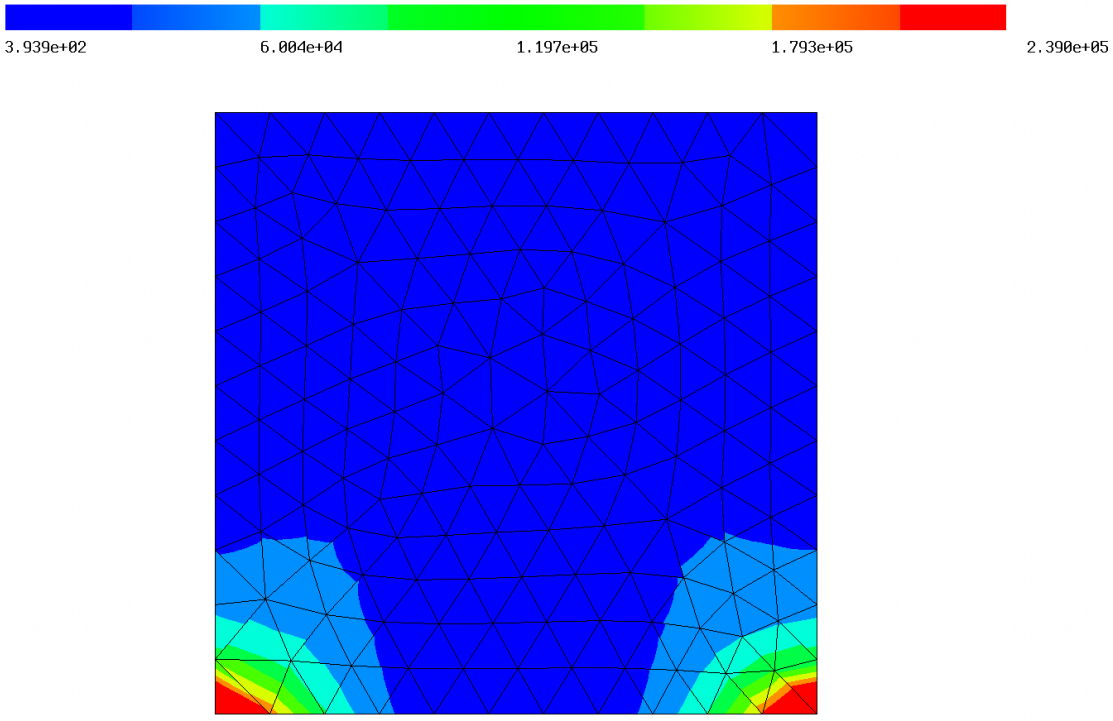

Figure 1: H^1 velocity error using Taylor-Hood

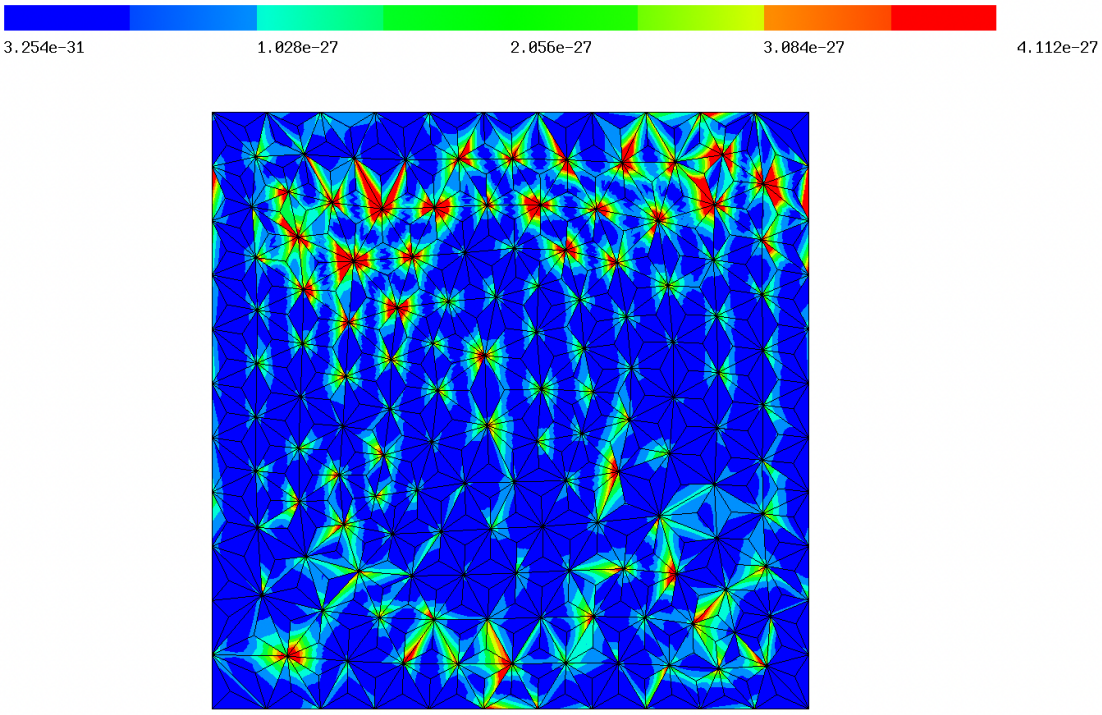

Figure 2: H^1 velocity error using Scott-Vogelius

1.3 Unfitted Finite Element Methods

In contrast to traditional finite element methods (FEMs), where the computational mesh conform to the physical domain, unfitted finite element methods include the information of the physical domain without fitting the computational mesh to the boundary of the physical domain. The most notable advantages of unfitted finite

element methods are that, for dynamic problems with moving boundary, there is no need to remesh at each time step and that it is easier to handle the problem imposed on a physical domain where the boundary is implicitly defined.

This thesis explores two classes of unfitted methods: FEMs with boundary correction and CutFEM. In particular, we look into FEMs with boundary correction and CutFEM both using divergence-free finite elements.

1. **Boundary Correction**

   FEMs with boundary correction was first proposed and analyzed in 1972 for the Poisson problem [12], and the technique has since been improved and refined recently in [13, 39, 5, 4, 3].

   The method starts with a background mesh containing the domain Ω, and the computational mesh simply consists of those elements fully contained in $\bar{\Omega}$. The method uses a standard Nitsche-based formulation to enforces Dirichlet boundary conditions via penalization. Since the computational mesh is not conformed to the physical domain, the boundary condition is corrected using an application of Taylor's theorem.

   This procedure is rather standard for the Poisson problem, but for the Stokes problem, inf-sup stability cannot be immediately proved by using standard arguments. This issue has been circumvented in [39, 4] using pressure-stabilization. However, this added stabilization leads to additional consistency errors and poor conservation properties.

2. **CutFEM**

   The precursor of CutFEM was first introduced in [6] for the Poisson problem, and there were some recent studies of the Stokes problem regarding unfitted variants of equal order pressure-velocity, Taylor–Hood and several other well-known finite

element methods [15, 11, 27, 30, 34, 35]. The CutFEM poses a similar challenge as the boundary correction method: the inf-sup stability for the method with a uniformly bounded, mesh-independent constant cannot be proved using standard arguments. However, [27] provides a framework to show discrete inf-sup stability for unfitted finite elements, and we adapted this framework in Chapter 3.

For both methods, unfitted mass-conserving elements for primitive-variable formulations of the Stokes or incompressible Navier-Stokes equations are not well developed. Based on the known divergence-free property of the Scott-Vogelius pair, in this thesis, we developed one FEM with boundary correction and one CutFEM.

For the FEM with boundary correction, we construct a boundary correction finite element method for the Stokes problem based on the Scott-Vogelius pair on Clough-Tocher splits. By the nature of the Scott-Vogelius pair, we have that the image of the divergence operator on the velocity space is a subset of the pressure space, and therefore, the scheme yields divergence-free velocity approximations. As far as we are aware, this is the first H^1-conforming divergence–free finite element method for incompressible flow on unfitted meshes. By constructing our FEM this way, we get exact enforcement of conservation laws on any mesh sizes. We carefully design the computational mesh such that it inherits a macro element structure. By doing so, we show that the resulting pair is uniformly stable on the unfitted domain with respect to the discretization parameter. As far as we are aware, this is the first uniform inf-sup stability result of a divergence-free Stokes pair on unfitted meshes. Because of the weak enforcement of boundary conditions via penalization, even though the scheme is divergence-free, it does not have pressure-robustness. We introduce an additional Lagrange multiplier that enforces the boundary conditions of the normal component of the velocity to mitigate the lack of pressure robustness in the scheme.

Since mass conservation is a favorable property for numerical solutions to equations governing the motion of fluids, we develop our CutFEM using the Scott-Vogelius pair as well. For this method, we impose a boundary condition on a surface cutting through a background mesh by using the Nitsche method [29], and we add local ghost penalty stabilization terms to ensure the stability with respect to small and anisotropic cuts of the bulk elements. The stability of pressure on cut elements requires an additional ghost penalty term defined on a thin strip of elements in a proximity of the boundary. The divergence-condition in the mixed formulation is changed by this additional stabilizing term. Thus, the scheme does not yield strictly divergence–free velocity approximations. However, we show that pointwise mass conservation holds in the volume occupied by the fluid except in an $O(h)$ strip. Moreover, we introduce local grad-div stabilization [42] to minimize the error caused by the violation of the divergence–free condition.

The remainder of the thesis is structured as follows: In chapter 2, we develop a boundary correction method based on the Scott-Vogelius pair on Clough-Tocher splits with macro-element structure: The velocity space consists of continuous piecewise polynomials of degree k, and the pressure space consists of piecewise polynomials of degree $(k-1)$ without continuity constraints. We prove the well-posedness of the method and show the method converges with optimal order and the velocity approximation is divergence–free.

In chapter 3, we develop a CutFEM discretization for the Stokes problem based on the Scott-Vogelius pair. This method does not yield exactly divergence–free velocity approximations. The CutFEM includes a local grad-div stabilization to mitigate the error brought by the violation of mass conservation property. We show the well-posedness of the method and that the method converges with optimal order.

In chapter 4, we present two numerical experiments using the boundary correction

method introduced in chapter 2 and two using numerical experiments using the CutFEM introduced in chapter 3 to illustrate the theoretic results proved in the respective chapters. In addition, we conduct two numerical experiments for the stationary Navier–Stokes equations using CutFEM.

2.0 A Divergence-Free Finite Element Method for the Stokes Problem with Boundary Correction

In this chapter, we develop and analyze a divergence-free finite element method for the Stokes problem with boundary correction.

We start with a background mesh that completely contains the physical domain Ω. Then we set the portion of the mesh that is a subset of the closure of the domain $\bar{\Omega}$ to be the computational domain. We use a standard Nitsche-based formulation as a basis for the method. The boundary conditions are then enforced through penalization. Since the computational domain does not conform to the physical domain, we use Taylor's theorem to transfer the boundary conditions on the physical domain to the computational domain.

The methodology is standard for the Possion problem, but not for the Stokes problem, mainly for the two following reasons:

(1) We cannot immediately prove the inf-sup stability using the standard approach. The standard inf-sup stability proof requires a decomposition of the Lipschitz domain into a finite number of strictly star shaped domain; however, for the non-conforming computational domain, even if the boundary of the physical domain is smooth enough, and the mesh is shape regular, the number of the strictly star-shaped domain in the decomposition of the computational domain will become unbounded as the mesh parameter h goes to 0. Therefore, the positive constant in the inf-sup condition is unbounded from below. One way to bypass this issue is to add pressure-stabilization terms to the method. However, adding pressure-stabilization terms will introduce additional consistency errors. Instead, we design the computational mesh to be macro element structure preserving and use the framework provided in [27] to

show inf-sup stability on the unfitted domain.

(2) A divergence-free method for the Stokes problem with boundary correction is not pressure robust. This is caused by the fact that we use a Nitsche-based formulation, which enforces the boundary conditions weakly via penalization. We address this issue by introducing a Lagrange multiplier space, which consists of continuous piecewise quadrtic polynomials with respect to the partition of the boundary of the computational domain, to enforce the boundary conditions of the normal component of the velocity. This Lagrange multiplier is an approximation of the pressure restricted to the computational boundary. By introducing the Lagrange multiplier space, we mitigate the lack of pressure-robustness of the method. This leads to a weakly-coupled velocity error estimate, where the dependence of the velocity error on the viscosity is weakened by a higher-order power of the mesh parameter h.

2.1 Preliminaries

We consider the Stokes problem on a two-dimensional open, bounded domain $\Omega \subset \mathbb{R}^2$,

$$-\nu\Delta \boldsymbol{u} + \nabla p = \boldsymbol{f} \qquad \text{in } \Omega, \tag{2.1.1a}$$

$$\operatorname{div} \boldsymbol{u} = 0 \qquad \text{in } \Omega, \tag{2.1.1b}$$

$$\boldsymbol{u} = \boldsymbol{g} \qquad \text{on } \partial\Omega, \tag{2.1.1c}$$

where $\nu > 0$ is the viscosity constant. For simplicity in the presentation, we present the results regarding to the problem with homogeneous boundary condition, i.e, $\boldsymbol{g} = 0$. The extension from the homogeneous boundary conditions to the non-homogeneous boundary conditions is relatively straight-forward [31].

2.1.1 Computational Domain

Let $S \subset \mathbb{R}^2$ to be an open polygon such that $\Omega \subset S$. Let $\mathcal{S}_h$ be a triangulation S consists of shape regular triangles, which means that there exists a constant $\rho_0 \in \mathbb{R}$ such that

$$\max_{T \in \mathcal{S}_h} \frac{\text{diam}T}{|T|^{\frac{1}{2}}} < \rho_0,$$

where $|T|$ denotes the measure of the triangle T in $\mathbb{R}^2$. We further assume that the triangulation $\mathcal{S}_h$ is quasi-uniform: there exists a constant $\rho \in \mathbb{R}$ such that

$$\frac{\max_{T \in \mathcal{S}_h} |T|}{\min_{T \in \mathcal{S}_h} |T|} < \rho.$$

We define $h = \max_{T \in \mathcal{S}_h} \text{diam}T$, $h_K = \text{diam}(K)$ and $h_e = \text{diam}(e)$.

We call the mesh $\mathcal{S}_h$ the background mesh, and we define the computational mesh $\mathcal{T}_h$ to be a subset of $\mathcal{S}_h$, where

$$\mathcal{T}_h = \{T \in \mathcal{S}_h : \ \bar{T} \subset \bar{\Omega}\}.$$

Correspondingly, we have the computational domain Ω_h defined as

$$\Omega_h = \text{int}\Big(\bigcup_{T \in \mathcal{T}_h} \bar{T} \Big) \subset \Omega.$$

The unrefined computational domain is illustrated in Figure 3. Furthermore, we define the set of all boundary edges of $\mathcal{T}_h$ to be $\mathcal{E}_h^B$.

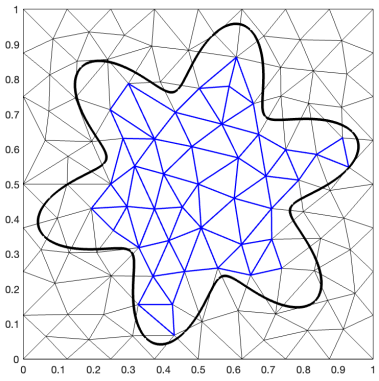

Figure 3: Ω_h is the domain consisting of triangles with blue edges.

By connecting the three vertices to the barycenter of each triangle $T \in \mathcal{S}$, we split each triangle into three and thus we get the Clough-Tocher refinement $\mathcal{S}^{ct}$ of $\mathcal{S}$. We use K to denote the triangles in the Clough-Tocher refinement $\mathcal{S}^{ct}$. We define the Clough-Tocher refinement $\mathcal{T}_h^{ct}$ of $\mathcal{T}_h$ as

$$\mathcal{T}_h^{ct} = \{K \in \mathcal{S}_h^{ct} : \ K \subset T, \ \exists T \in \mathcal{T}_h\}.$$

By our definition, for each $K \in \mathcal{T}_h^{ct}$, the parent triangle T, where $K \subset T$, is an element of $\mathcal{T}_h$. We emphasize that

$$\mathcal{T}_h^{ct} \neq \{K \in \mathcal{S}_h^{ct} : \ \bar{K} \subset \bar{\Omega}\}.$$

Therefore, we preserve the macro-element structure that is needed to prove the stability of the Scott-Vogelius pair.

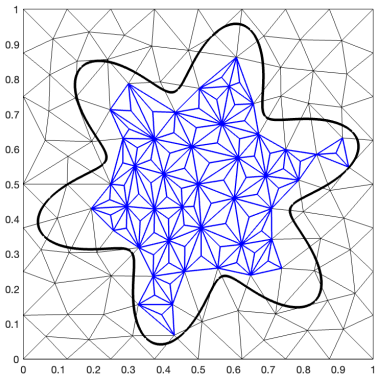

Figure 4: $\mathcal{T}_h^{ct}$ consists of triangles with blue edges.

From Figure 4, we see that the corresponding computational domain of $\mathcal{T}_h^{ct}$ is Ω_h as well. Moreover, $\mathcal{E}_h^B$ is also the set of boundary edges of $\mathcal{T}_h^{ct}$. For a piecewise smooth function q on $\partial\Omega_h$, we denote

$$\int_{\partial\Omega_h} q\, ds = \sum_{e\in\mathcal{E}_h^B} \int_e q\, ds.$$

2.2 Boundary Transfer Operator

We assume the boundary $\partial\Omega$ of the domain to be sufficiently smooth. Let ϕ be the signed distance function of the domain Ω such that we have $\phi(x) < 0$ for $x \in \Omega$, and $\phi(x) \geq 0$ for $x \notin \Omega$. Then the unit outward normal vector is $\boldsymbol{n} = \frac{\nabla\phi}{|\nabla\phi|}$. Let $\tau > 0$ be a positive real number. Then $\Gamma_\tau = \{x \in \mathbb{R}^2 : |\phi(x)| < \tau\}$ is a tubular region around the boundary $\partial\Omega$ of the domain Ω. Based on [23, Lemma 14.16] and

[12], we have that there exists a real number $\tau_0 > 0$ such that the closest-point map $p : \Gamma_{\tau_0} \longrightarrow \partial\Omega$ is well-defined, and we have the identity $p(x) = x - \phi(x)\boldsymbol{n}(p(x))$ for all $x \in \Gamma_{\tau_0}$.

In order to define the boundary correction method, we want to have a well-defined map $M : \partial\Omega_h \longrightarrow \partial\Omega$ which transfers every point on the boundary of the computational domain $\partial\Omega_h$ to a corresponding point on the boundary of the physical domain $\partial\Omega$. Let $I : \partial\Omega_h \longrightarrow \partial\Omega_h$ be the identity map. Then the transfer direction vector is defined as $\mathfrak{d}(x) = (M - I)(x)$ for all $x \in \partial\Omega_h$. The transfer distance is the magnitude of the transfer direction vector,

$$\delta(x) = |\mathfrak{d}(x)|.$$

One of the common choices for the map M is the closet-point projection p mentioned above. Suppose that the computational domain Ω_h approximates the physical domain Ω well enough such that the distance between $\partial\Omega_h$ and $\partial\Omega$ is less than the constant τ_0 mentioned above. Then the map $p : \partial\Omega_h \longrightarrow \partial\Omega$ is well-defined. Moreover, from the identity $p(x) = x - \phi(x)\boldsymbol{n}(p(x))$, and the fact that $\phi(x) < 0$ for all $x \in \partial\Omega_h$, we see that the transfer direction coincides to the outward normal vector of physical boundary $\partial\Omega$, and the transfer distance is $\delta(x) = |\phi(x)|$ for all $x \in \partial\Omega_h$.

Another possible choice for the transfer direction is the direction same as the unit outward vector $\boldsymbol{n}_h$ of the computational boundary $\partial\Omega_h$. Generally in this case, we have $\delta(x) \geq |\phi(x)|$. This choice of transfer direction creates a larger discrepancy between $\delta(x)$ and $|\phi(x)|$ than the choice of transfer direction where the transfer direction vector is $(p - I)(x)$ for all $x \in \partial\Omega_h$. However, this choice results in easier implementation.

In the rest of this chapter, we do not specify the map M explicitly. Instead, we make the assumption that the transfer distance $\delta(x)$ is sufficiently small in comparison to the mesh parameter h. Similar to [12, 13, 12, 5, 4, 3], the stability and convergence analysis in this chapter only requires this assumption. The formal assumption is given below in the stability analysis section after we define the finite element method.

Now we define the boundary transfer operator.

The idea of the boundary transfer operator stems from the Taylor expansion. Recall that for a function $f : \mathbb{R}^2 \longrightarrow \mathbb{R}^2$, $x \in \mathbb{R}^n$, $\boldsymbol{a}$ is a unit vector in $\mathbb{R}^n$, and t is a scalar, then Taylor expansion of f is

$$f(x + t\boldsymbol{a}) = \sum_{j=0}^{\infty} \frac{1}{j!} |t|^j \frac{\partial^j f}{\partial \boldsymbol{a}^j}(x).$$

The k^{th} order polynomial of f is $\sum_{j=0}^{\infty} \frac{1}{j!} |t|^j \frac{\partial^j f}{\partial \boldsymbol{a}^j}(x)$. Note that the k^{th} order polynomial of $f(x + t\boldsymbol{a})$ is an approximation of f at $x + t\boldsymbol{a}$ from x.

Setting $\boldsymbol{d} = \mathfrak{d}/\delta$, we use k^{th} order Taylor polynomial of $\boldsymbol{v}$ expanded at x in the direction of $\boldsymbol{d}$ to define the boundary transfer operator:

$$(S_h \boldsymbol{v})(x) = \sum_{j=0}^{k} \frac{1}{j!} (\delta(x))^j \frac{\partial^i \boldsymbol{v}}{\partial \boldsymbol{d}^j}(x), \qquad \text{for } x \in \partial\Omega_h$$

Since $\mathfrak{d} = M - I$, we see that $(S_h \boldsymbol{v})(x)$ is an approximation of $\boldsymbol{v}$ at $x + \mathfrak{d} = Mx$ from x.

2.3 A Divergence-Free Finite Element Method with Boundary Correction

For a subset $D \subset \Omega$, we use $\mathcal{P}_k(D)$ to denote the polynomials on D with degree at most k. We use the boldface $\boldsymbol{\mathcal{P}}_k(D)$ to denote the vector-valued polynomials on D with degree at most k.

Then we define the velocity space and pressure space to be the Scott-Vogelius pair with respect to Clough-Toucher splits as follows:

$$\begin{aligned}
\boldsymbol{V}_h &= \{\boldsymbol{v} \in \boldsymbol{H}^1(\Omega_h) : \ \boldsymbol{v}|_K \in \boldsymbol{\mathcal{P}}_k(K) \ \forall K \in \mathcal{T}_h^{ct}, \ \int_{\partial\Omega_h} (\boldsymbol{v} \cdot \boldsymbol{n}_h)\, ds = 0\}, \\
Q_h &= \{q \in L^2(\Omega_h) : \ q|_K \in \mathcal{P}_{k-1}(K) \ \forall K \in \mathcal{T}_h^{ct}\};
\end{aligned}$$

Analogously, we define the velocity space with boundary conditions and pressure space with zero mean constraint to be

$$\begin{aligned}
\mathring{\boldsymbol{V}}_h &= \boldsymbol{V}_h \cap \boldsymbol{H}_0^1(\Omega_h), \\
\mathring{Q}_h &= Q_h \cap L_0^2(\Omega_h).
\end{aligned}$$

Furthermore, we define the Lagrange multiplier space and the Lagrange multiplier space with zero mean constraint to be

$$\begin{aligned}
X_h &= \{\mu \in C(\partial\Omega_h) : \ \mu|_e \in \mathcal{P}_k(e) \ \forall e \in \mathcal{E}_h^B\} \\
\mathring{X}_h &= \{\mu \in X_h : \ \int_{\partial\Omega_h} \mu\, ds = 0\},
\end{aligned}$$

respectively.

Now, we define the mesh-dependent bilinear forms

$$a_h(\boldsymbol{u}, \boldsymbol{v}) = \nu\Big(\int_{\Omega_h} \nabla \boldsymbol{u} : \nabla \boldsymbol{v}\, dx - \int_{\partial\Omega_h} \frac{\partial \boldsymbol{u}}{\partial \boldsymbol{n}_h} \cdot \boldsymbol{v}\, ds + \int_{\partial\Omega_h} \frac{\partial \boldsymbol{v}}{\partial \boldsymbol{n}_h} \cdot (S_h \boldsymbol{u})\, ds,$$

$$+\sum_{e\in\mathcal{E}_h^B}\int_e \frac{\sigma}{h_e}(S_h\boldsymbol{u})\cdot(S_h\boldsymbol{v})\,ds\Big),$$

$$b_h(\boldsymbol{v},(q,\mu)) = -\int_{\Omega_h}(\operatorname{div}\boldsymbol{v})q\,dx + \int_{\partial\Omega_h}(\boldsymbol{v}\cdot\boldsymbol{n}_h)\mu\,ds,$$

$$b_h^e(\boldsymbol{v},(q,\mu)) = -\int_{\Omega_h}(\operatorname{div}\boldsymbol{v})q\,dx + \int_{\partial\Omega_h}((S_h\boldsymbol{v})\cdot\boldsymbol{n}_h)\mu\,ds,$$

where $\sigma > 0$ in $a_h(\cdot,\cdot)$ is a penalty parameter.

We get the bilinear form $a_h(\cdot,\cdot)$ from the standard non-symmetric "Nitsche bilinear form" associated with the Laplace operator:

$$\int_{\Omega_h}\nabla\boldsymbol{u}:\nabla\boldsymbol{v}\,dx - \int_{\partial\Omega_h}\frac{\partial\boldsymbol{u}}{\partial\boldsymbol{n}_h}\cdot\boldsymbol{v}\,ds + \int_{\partial\Omega_h}\frac{\partial\boldsymbol{v}}{\partial\boldsymbol{n}_h}\cdot(\boldsymbol{u})\,ds + \sum_{e\in\mathcal{E}_h^B}\int_e\frac{\sigma}{h_e}(\boldsymbol{u})\cdot(\boldsymbol{v})\,ds$$

by changing the $\boldsymbol{u}$ in the third term to $S_h\boldsymbol{u}$, and the $\boldsymbol{u}$, $\boldsymbol{v}$ in the fourth term to $S_h\boldsymbol{u}$, $S_h\boldsymbol{v}$, respectively [41, 46]. We make the change to improve the consistency of the scheme.

The non-symmetry of the Nitsche bilinear form is referring to the different sign in front of the term $\int_{\partial\Omega_h}\frac{\partial\boldsymbol{v}}{\partial\boldsymbol{n}_h}\cdot\boldsymbol{u}\,ds$ and the term $\int_{\partial\Omega_h}\frac{\partial\boldsymbol{u}}{\partial\boldsymbol{n}_h}\cdot\boldsymbol{v}\,ds$. The reason we based our bilinear form $a_h(\cdot,\cdot)$ on the non-symmetric Nitsche bilinear form is that the bilinear form with boundary correction based on the symmetric Nitsche bilinear form still results in a non-symmetric bilinear form [12, 39]. However, if the bilinear form is based on the non-symmetric version of Nitsche bilinear form, the penalty parameter σ will be less restrictive to ensure stability.

The two bilinear forms $b_h(\cdot,(\cdot,\cdot))$ and $b_h^e(\cdot,(\cdot,\cdot))$ are two bilinear forms associated with the continuity equations. The only difference between the two is that $b_h(\cdot,(\cdot,\cdot))$ does not have the boundary correction, whereas $b_h^e(\cdot,(\cdot,\cdot))$ does.

We set the method as follows:

find $(\boldsymbol{u}_h, p_h, \lambda_h) \in \boldsymbol{V}_h \times \mathring{Q}_h \times \mathring{X}_h$ such that

$$a_h(\boldsymbol{u}_h, \boldsymbol{v}) + b_h(\boldsymbol{v}, (p_h, \lambda_h)) = \int_{\Omega_h} \boldsymbol{f} \cdot \boldsymbol{v}\, dx \qquad \forall \boldsymbol{v} \in \boldsymbol{V}_h, \tag{2.3.1a}$$

$$b_h^e(\boldsymbol{u}_h, (q, \mu)) = 0 \qquad \forall (q, \mu) \in \mathring{Q}_h \times \mathring{X}_h. \tag{2.3.1b}$$

We choose the zero-mean constraint Lagrange multiplier space $\mathring{X}_h$ in the formulation of the method because we want to mod out the constants to ensure that the method is not ill-posed. Indeed, suppose we use the Lagrange multiplier space X_h without the zero-mean constraint. Then due to the condition $\int_{\partial\Omega_h} (\boldsymbol{v} \cdot \boldsymbol{n}_h)\, ds = 0$ from the definition of the discrete velocity space $\boldsymbol{V}_h$, we have

$$b_h(\boldsymbol{v}, (0, 1)) = 0 \quad \forall \boldsymbol{v} \in \boldsymbol{V}_h.$$

Moreover, the condition $\int_{\partial\Omega_h} (\boldsymbol{v} \cdot \boldsymbol{n}_h)\, ds = 0$ in the definition of $\boldsymbol{V}_h$ is necessary to show that the method yields a divergence-free velocity solution as we show in the next section.

2.3.1 Divergence-Free Property

Lemma 2.3.1 (Divergence–free property)**.** *If* $(\boldsymbol{u}_h, p_h, \lambda_h) \in \boldsymbol{V}_h \times \mathring{Q}_h \times \mathring{X}_h$ *satisfies* (2.3.1)*, then* $\operatorname{div} \boldsymbol{u}_h \equiv 0$ *in* Ω_h*.*

Proof. For the Stokes pair $\boldsymbol{V}_h \times \mathring{Q}_h$, since we have the constraint that for $\boldsymbol{v} \in \boldsymbol{V}_h$, $\int_{\partial\Omega_h} \boldsymbol{v} \cdot \boldsymbol{n}\, ds = 0$, by the divergence theorem, we have $\int_\Omega \operatorname{div} \boldsymbol{v}\, dx = \int_{\partial\Omega} \boldsymbol{v} \cdot \boldsymbol{n}\, ds = 0$. Thus we have that the div operator maps from $\boldsymbol{V}_h$ to $\mathring{Q}_h$, i.e, $\operatorname{div} \boldsymbol{u}_h \in \mathring{Q}_h$. We set $q = \operatorname{div} \boldsymbol{u}_h$ and $\mu = 0$ in (2.3.1b). Then we have

$$0 = b_h^e(\boldsymbol{u}_h, (q, \mu)) = b_h^e(\boldsymbol{u}_h, (\operatorname{div} \boldsymbol{u}_h, 0)) = -\|\operatorname{div} \boldsymbol{u}_h\|^2_{L^2(\Omega_h)}.$$

Thus, $\operatorname{div} \boldsymbol{u}_h \equiv 0$. □

2.4 Stability Analysis of the Finite Element Method

Throughout this chapter, the constants C and c(with or without subscripts) denote some positive constants that are independent of the mesh parameter h and the viscosity. We conduct our stability analysis and convergence analysis under the assumption mentioned in section 2.2: the transfer distance $\delta(x)$ is sufficiently small compared to the mesh parameter h, i.e, the distance between the boundary of the PDE domain Ω and the boundary of the computational domain Ω_h is sufficiently small relative to the mesh parameter h. Before we formally state the assumption, we first define for a boundary edge $e \in \mathcal{E}_h^B$,

$$\delta_e := \max_{x \in \bar{e}} \delta(x).$$

Now we state the assumption formally:

$$\max_{e \in \mathcal{E}_h^B} h_e^{-1} \delta_e \leq c_\delta < 1, \qquad \text{for } c_\delta \text{ sufficiently small.} \tag{A}$$

Assumption (A) ensures that the distance between $\partial\Omega$ and $\partial\Omega_h$ is of order $O(h)$, where the constant c_δ is sufficiently small. Similar assumptions have been made in [12, 43, 39, 5, 4]. In practice, the small distance between $\partial\Omega$ and $\partial\Omega_h$ can be achieved by shifting the position of the nodes on $\partial\Omega_h$ along the direction $\boldsymbol{n}$ as explained in [5, Remark 3].

Before we show the continuity and coercivity of the bilinear forms, we want to first define some norms for the finite element spaces.

We define three H^1-type norm on $\boldsymbol{V}_h + \boldsymbol{H}^{k+1}(\Omega)$, so that we apply the norms to both the velocity solution of the PDE and the velocity solution of the FEM:

$$\|\boldsymbol{v}\|_h^2 = \|\nabla \boldsymbol{v}\|_{L^2(\Omega_h)}^2 + \sum_{e \in \mathcal{E}_h^B} h_e^{-1} \|S_h \boldsymbol{v}\|_{L^2(e)}^2,$$

$$\|\boldsymbol{v}\|_{1,h}^2 = \|\nabla \boldsymbol{v}\|_{L^2(\Omega_h)}^2 + \sum_{e\in\mathcal{E}_h^B} h_e^{-1}\|\boldsymbol{v}\|_{L^2(e)}^2,$$
$$|||\boldsymbol{v}|||_h^2 = \|\boldsymbol{v}\|_h^2 + \sum_{e\in\mathcal{E}_h^B} h_e\|\nabla \boldsymbol{v}\|_{L^2(e)}^2.$$

In addition, we define a $H^{-1/2}$-type norm on the Lagrange multiplier space $\mathring{X}_h$:

$$\|\mu\|_{-1/2,h}^2 = \sum_{e\in\mathcal{E}_h^B} h_e\|\mu\|_{L^2(e)}^2.$$

Finally, we define a norm on the pair $\mathring{Q}_h \times \mathring{X}_h$ as

$$\|(q,\mu)\| := \|q\|_{L^2(\Omega_h)} + \|\mu\|_{-1/2,h}.$$

In the next lemma, we show that if the Assumption (A) is satisfied, then the three H^1-type norms on $\boldsymbol{V}_h + \boldsymbol{H}^{k+1}(\Omega)$ are equivalent.

Lemma 2.4.1. *Assuming* (A)*, there holds for all* $\boldsymbol{v} \in \boldsymbol{V}_h$*,*

$$\begin{aligned}\sum_{e\in\mathcal{E}_h^B} h_e^{-1}\|S_h\boldsymbol{v} - \boldsymbol{v}\|_{L^2(e)}^2 &\le Cc_\delta^2\|\nabla\boldsymbol{v}\|_{L^2(\Omega_h)}^2,\\ \sum_{e\in\mathcal{E}_h^B} h_e^{-1}\|S_h\boldsymbol{v}\|_{L^2(e)}^2 &\le C\|\boldsymbol{v}\|_{1,h}^2.\end{aligned} \tag{2.4.1}$$

In particular, $\|\cdot\|_h$*,* $\|\cdot\|_{1,h}$*, and* $|||\cdot|||_h$ *are equivalent on* $\boldsymbol{V}_h$*.*

Proof. By the definition of S_h, we have

$$h_e^{-1}\|S_h\boldsymbol{v}-\boldsymbol{v}\|_{L^2(e)}^2=\sum_{j=1}^{k}h_e^{-1}\int_e|\delta|^{2j}\Big|\frac{\partial^j\boldsymbol{v}}{\partial\boldsymbol{d}^j}\Big|^2\,ds,$$

for $e\in\mathcal{E}_h^B$.

By trace and inverse inequalities, the shape-regularity of $\mathcal{T}_h$ and (A), there holds for $e\in\mathcal{E}_h^B$,

$$\begin{aligned}h_e^{-1}\int_e|\delta|^{2j}\Big|\frac{\partial^j\boldsymbol{v}}{\partial\boldsymbol{d}^j}\Big|^2\,ds&\le C\delta_e^{2j}h_e^{-2}\|\boldsymbol{D}^j\boldsymbol{v}\|_{L^2(e)}^2\\&\le C\delta_e^{2j}h_e^{-2j}\|\nabla\boldsymbol{v}\|_{L^2(T_e)}^2\\&\le Cc_\delta^{2j}\|\nabla\boldsymbol{v}\|_{L^2(T_e)}^2\quad j=1,2,...,k,\end{aligned}\tag{2.4.2}$$

where $T_e\in\mathcal{T}_h$ satisfies $e\subset\partial T$, and $\boldsymbol{D}^j$ is the j^{th} derivative of $\boldsymbol{v}$. The estimate (2.4.2) implies the first inequality in (2.4.1). The estimate (2.4.2) also implies the second inequality in (2.4.1) since

$$\sum_{e\in\mathcal{E}_h^B}h_e^{-1}\|S_h\boldsymbol{v}\|_{L^2(e)}^2\le C\sum_{e\in\mathcal{E}_h^B}\sum_{j=0}^{k}h_e^{-1}\int_e|\delta|^{2j}\Big|\frac{\partial^j\boldsymbol{v}}{\partial\boldsymbol{d}^j}\Big|^2\,ds\le C\|\boldsymbol{v}\|_{1,h}^2.$$

The second inequality in (2.4.1) immediately yields $\|\boldsymbol{v}\|_h\le C\|\boldsymbol{v}\|_{1,h}$ from the definition of $\|\cdot\|_h$ and $\|\cdot\|_{1,h}$. Moreover, standard arguments involving the trace and inverse inequalities show $\|\boldsymbol{v}\|_h\le|||\boldsymbol{v}|||_h\le C\|\boldsymbol{v}\|_h$ on $\boldsymbol{V}_h$. Thus, to complete the proof, it suffices to show $\|\boldsymbol{v}\|_{1,h}\le C\|\boldsymbol{v}\|_h$.

We once again use (2.4.2) to obtain

$$\sum_{e\in\mathcal{E}_h^B}h_e^{-1}\|\boldsymbol{v}\|_{L^2(e)}^2\le 2\sum_{e\in\mathcal{E}_h^B}h_e^{-1}\|S_h\boldsymbol{v}\|_{L^2(e)}^2+2\sum_{e\in\mathcal{E}_h^B}h_e^{-1}\|S_h\boldsymbol{v}-\boldsymbol{v}\|_{L^2(e)}^2$$

$$\leq 2\sum_{e\in\mathcal{E}_h^B} h_e^{-1}\|S_h\boldsymbol{v}\|_{L^2(e)}^2 + C\sum_{e\in\mathcal{E}_h^B} h_e^{-1}\sum_{j=1}^{k}\int_e |\delta|^{2j}\big|\frac{\partial^j \boldsymbol{v}}{\partial \boldsymbol{d}^j}\big|^2\, ds$$
$$\leq 2\sum_{e\in\mathcal{E}_h^B} h_e^{-1}\|S_h\boldsymbol{v}\|_{L^2(e)}^2 + C\|\nabla\boldsymbol{v}\|_{L^2(\Omega_h)}^2.$$

This inequality implies $\|\boldsymbol{v}\|_{1,h} \leq C\|\boldsymbol{v}\|_h$.

□

2.4.1 Continuity and Coercivity of the Bilinear Forms

Lemma 2.4.2. *There holds*

$$|a_h(\boldsymbol{v},\boldsymbol{w})| \leq c_2(1+\sigma)\nu|||\boldsymbol{v}|||_h|||\boldsymbol{w}|||_h \qquad \forall \boldsymbol{v},\boldsymbol{w}\in \boldsymbol{V}_h + H^3(\Omega_h), \quad (2.4.3)$$

$$\big|b_h(\boldsymbol{v},(q,\mu))\big| \leq C\|\boldsymbol{v}\|_{1,h}\|(q,\mu)\| \qquad \forall (q,\mu)\in \mathring{Q}_h\times\mathring{X}_h, \quad (2.4.4)$$

$$\big|b_h(\boldsymbol{v},(q,\mu)) - b_h^e(\boldsymbol{v},(q,\mu))\big| \leq Cc_\delta\|\boldsymbol{v}\|_{1,h}\|(q,\mu)\| \quad \forall \boldsymbol{v}\in\boldsymbol{V}_h,\ \forall (q,\mu)\in\mathring{Q}_h\times\mathring{X}_h, \quad (2.4.5)$$

$$\big|b_h^e(\boldsymbol{v},(q,\mu))\big| \leq C(1+c_\delta)\|\boldsymbol{v}\|_{1,h}\|(q,\mu)\| \qquad \forall (q,\mu)\in\mathring{Q}_h\times\mathring{X}_h \quad (2.4.6)$$

Proof. The proof of the continuity estimate of (2.4.3) is given in [5, Proposition 1] (with superficial modifications). We show the details for the completeness of the proof.

From the definiton of $a_h(\cdot,\cdot)$ and the Cauchy-Schwarz inequality, we get

$$\begin{aligned}|a_h(\boldsymbol{v},\boldsymbol{w})| &= |\nu\Big(\int_{\Omega_h}\nabla\boldsymbol{v}:\nabla\boldsymbol{w}\,dx - \int_{\partial\Omega_h}\frac{\partial\boldsymbol{v}}{\partial\boldsymbol{n}_h}\cdot\boldsymbol{w}\,ds\\ &\quad + \int_{\partial\Omega_h}\frac{\partial\boldsymbol{w}}{\partial\boldsymbol{n}_h}\cdot(S_h\boldsymbol{v})\,ds + \sum_{e\in\mathcal{E}_h^B}\int_e\frac{\sigma}{h_e}(S_h\boldsymbol{v})\cdot(S_h\boldsymbol{w})\,ds\Big)|\\ &\leq \nu\Big(\|\nabla\boldsymbol{v}\|_{L^2(\Omega)}\|\nabla\boldsymbol{w}\|_{L^2(\Omega)} + \|h^{\frac{1}{2}}\nabla\boldsymbol{v}\cdot\boldsymbol{n}_h\|_{L^2(\partial\Omega_h)}\|h^{-\frac{1}{2}}\boldsymbol{w}\|_{L^2(\partial\Omega_h)}\end{aligned}$$

$$+ \|h^{\frac{1}{2}}\nabla \boldsymbol{w}\cdot \boldsymbol{n}_h\|_{L^2(\partial\Omega_h)}\|h^{-\frac{1}{2}}S_h\boldsymbol{v}\|_{L^2(\partial\Omega_h)} + \sigma\|h^{-\frac{1}{2}}S_h\boldsymbol{v}\|_{L^2(\partial\Omega_h)}\|h^{-\frac{1}{2}}S_h\boldsymbol{w}\|_{L^2(\partial\Omega_h)}\Big),$$

Using the definition of $|||\cdot|||_h$, and the equivalence between $|||\cdot|||_h$ and $\|\cdot\|_{1,h}$ we have

$$\|h^{\frac{1}{2}}\nabla \boldsymbol{v}\cdot \boldsymbol{n}_h\|_{L^2(\partial\Omega_h)}\|h^{-\frac{1}{2}}\boldsymbol{w}\|_{L^2(\partial\Omega_h)} \leq C_1|||\boldsymbol{v}|||_h|||\boldsymbol{w}|||_h,$$

and

$$\|h^{\frac{1}{2}}\nabla \boldsymbol{w}\cdot \boldsymbol{n}_h\|_{L^2(\partial\Omega_h)} \leq C_2|||\boldsymbol{w}|||_h.$$

Combined the above results with the definition of $|||\cdot|||_h$, we have

$$|a_h(\boldsymbol{v},\boldsymbol{w})| \leq \nu\Big(|||\boldsymbol{v}|||_h|||\boldsymbol{w}|||_h + C_1|||\boldsymbol{v}|||_h|||\boldsymbol{w}|||_h + C_2|||\boldsymbol{v}|||_h|||\boldsymbol{w}|||_h + \sigma|||\boldsymbol{v}|||_h|||\boldsymbol{w}|||_h\Big).$$

Then we find c_2 such that

$$|a_h(\boldsymbol{v},\boldsymbol{w})| \leq c_2(1+\sigma)\nu|||\boldsymbol{v}|||_h|||\boldsymbol{w}|||_h$$

The continuity estimate of $b_h(\cdot,\cdot)$ (2.4.4) follows directly from the Cauchy-Schwarz inequality:

$$\begin{aligned}|b_h(\boldsymbol{v},(q,\mu))| &\leq |\int_{\Omega_h}(\operatorname{div}\boldsymbol{v})q\,dx| + |\int_{\partial\Omega_h}(\boldsymbol{v}\cdot\boldsymbol{n}_h)\mu\,ds| \\ &\leq C_1\|\nabla\boldsymbol{v}\|_{L^2(\Omega_h)}\|q\|_{L^2(\Omega_h)} + C_2\sum_{e\in\mathcal{E}_h^B} h_e^{-\frac{1}{2}}\|\boldsymbol{v}\|_{L^2(e)}h^{\frac{1}{2}}\|\mu\|_{L^2(e)} \qquad (2.4.7)\end{aligned}$$

By the definition of $\|\boldsymbol{v}\|_{1,h}$, we have

$$\|\nabla\boldsymbol{v}\|_{L^2(\Omega_h)} \leq \|\boldsymbol{v}\|_{1,h}.$$

Applying Cauchy-Schwarz inequality, we have

$$\begin{aligned}\sum_{e\in\mathcal{E}_h^B} h_e^{-\frac{1}{2}}\|\boldsymbol{v}\|_{L^2(e)}h_e^{\frac{1}{2}}\|\mu\|_{L^2(e)} &\leq \Big(\sum_{e\in\mathcal{E}_h^B} h_e^{-1}\|\boldsymbol{v}\|^2_{L^2(e)}\Big)^{\frac{1}{2}}\Big(\sum_{e\in\mathcal{E}_h^B} h_e\|\mu\|^2_{L^2(e)}\Big)^{\frac{1}{2}} \\ &\leq \|\boldsymbol{v}\|_{1,h}\|\mu\|_{-1/2,h}.\end{aligned}$$

Combining the two inequalities above with (2.4.7) and using the definition of $\|(q,\mu)\|$, we find a constant C independent of the mesh such that

$$\begin{aligned}|b_h(\boldsymbol{v},(q,\mu))| &\leq C_1\|\boldsymbol{v}\|_{1,h}\|q\|_{L^2(\Omega_h)} + C_2\|\boldsymbol{v}\|_{1,h}\|\mu\|_{-1/2,h} \\ &\leq C|\boldsymbol{v}\|_{1,h}\|(q,\mu)\|.\end{aligned}$$

This third estimate (2.4.5) follows from the definition of the forms, the Cauchy-Schwarz inequality, and (2.4.2):

$$\begin{aligned}\big|b_h(\boldsymbol{v},(q,\mu)) - b_h^e(\boldsymbol{v},(q,\mu))\big| &= \Big|\sum_{e\in\mathcal{E}_h^B}\int_e \big((\boldsymbol{v}-S_h\boldsymbol{v})\cdot\boldsymbol{n}_h\big)\mu\,ds\Big| \\ &\leq C\Big(\sum_{e\in\mathcal{E}_h^B}\sum_{j=1}^{k} h_e^{-1}\int_e |\delta|^{2j}\big|\frac{\partial^j\boldsymbol{v}}{\partial\boldsymbol{d}^j}\big|^2\Big)^{1/2}\|\mu\|_{-1/2,h} \\ &\leq Cc_\delta\|\boldsymbol{v}\|_{1,h}\|\mu\|_{-1/2,h}.\end{aligned}$$

From (2.4.4) and (2.4.5) and using the triangle inequality, we have

$$\begin{aligned}|b_h^e(\boldsymbol{v},(q,\mu))| &\leq |b_h(\boldsymbol{v},(q,\mu))| + |b_h^e(\boldsymbol{v},(q,\mu)) - b_h^e(\boldsymbol{v},(q,\mu))| \\ &\leq C(1+c_\delta)\|\boldsymbol{v}\|_{1,h}\|(q,\mu)\|\end{aligned}$$

□

Lemma 2.4.3. *Suppose that Assumption* (A) *is satisfied for c_δ sufficiently small. Then there holds,*

$$c_1\nu\|\boldsymbol{v}\|_{1,h}^2 \leq a_h(\boldsymbol{v},\boldsymbol{v}) \qquad \forall\boldsymbol{v}\in\boldsymbol{V}_h,$$

for $c_1 > 0$ independent of h and ν, and for any positive penalty parameter $\sigma > 0$.

Proof. By definition of the bilinear form $a_h(\cdot,\cdot)$,

$$a_h(\boldsymbol{v},\boldsymbol{v}) = \nu\Big(\|\nabla \boldsymbol{v}\|^2_{L^2(\Omega_h)} + \sum_{e\in\mathcal{E}_h^B}\Big(\int_e \frac{\partial \boldsymbol{v}}{\partial \boldsymbol{n}_h}\cdot(S_h\boldsymbol{v}-\boldsymbol{v})\,ds + \frac{\sigma}{h_e}\|S_h\boldsymbol{v}\|^2_{L^2(e)}\Big)\Big)$$

A discrete trace inequality with (2.4.1) yields

$$\Big|\sum_{e\in\mathcal{E}_h^B}\int_e \frac{\partial \boldsymbol{v}}{\partial \boldsymbol{n}_h}\cdot(S_h\boldsymbol{v}-\boldsymbol{v})\,ds\Big| \le Cc_\delta\|\nabla\boldsymbol{v}\|^2_{L^2(\Omega_h)}. \tag{2.4.8}$$

Thus, we find

$$a_h(\boldsymbol{v},\boldsymbol{v}) \ge \nu\Big((1-Cc_\delta)\|\nabla\boldsymbol{v}\|^2_{L^2(\Omega_h)} + \sum_{e\in\mathcal{E}_h^B}\frac{\sigma}{h_e}\|S_h\boldsymbol{v}\|^2_{L^2(e)}\Big)\Big) \ge C\nu\|\boldsymbol{v}\|^2_h \ge C\nu\|\boldsymbol{v}\|^2_{1,h}$$

for c_δ sufficiently small and for $\sigma > 0$.

□

2.4.2 Inf-Sup Conditions

In this section we prove the discrete inf-sup (LBB) condition for the Stokes pair $\mathring{\boldsymbol{V}}_h \times \mathring{Q}_h$ with stability constants independent of h and the inf-sup condition for the Lagrange multiplier part of the bilinear form $b_h(\cdot,\cdot)$. We use these two inf-sup conditions to derive the inf-sup condition for the bilinear form $b_h(\cdot,\cdot)$ in the next section.

The LBB stability for this pair is well-known (cf. [2, 45, 26]) for the fixed polygonal domain; however, we cannot extend these results to the unfitted domain Ω_h directly. In particular, the proofs in [2, 45, 26] (directly or indirectly) rely on the Nečas inequality:

$$\mathfrak{c}_h \|q\|_{L^2(\Omega_h)} \leq \sup_{\boldsymbol{v}\in \boldsymbol{H}_0^1(\Omega_h)\setminus\{0\}} \frac{\int_{\Omega_h} (\operatorname{div} \boldsymbol{v}) q \, dx}{\|\nabla \boldsymbol{v}\|_{L^2(\Omega_h)}} \qquad \forall q \in L_0^2(\Omega_h)$$

for some $\mathfrak{c}_h > 0$ depending on the domain Ω_h. As explained in [27], it is unclear if the constant $\mathfrak{c}_h$ in this inequality is independent of h.

To extend the LBB condition to an unfitted domain Ω_h with a constant that is independent of h, we combine the local stability of the Scott-Vogelius pair with the stability of the $\boldsymbol{\mathcal{P}}_k \times \mathcal{P}_{k-2}$ pair. For a (macro) element $T \in \mathcal{T}_h$, we define the local spaces with boundary conditions

$$\begin{aligned} \boldsymbol{V}_0(T) &= \{\boldsymbol{v} \in \boldsymbol{H}_0^1(T) : \ \boldsymbol{v}|_K \in \boldsymbol{\mathcal{P}}_k(K) \ \forall K \subset T, \ K \in \mathcal{T}_h^{ct}\}, \\ Q_0(T) &= \{q \in L_0^2(T) : \ q|_K \in \mathcal{P}_{k-1}(K) \ \forall K \subset T, \ K \in \mathcal{T}_h^{ct}\}. \end{aligned}$$

We first state a local surjectivity [26, Theorem 3.1] of the divergence operator acting on these spaces.

Lemma 2.4.4. *For every $q \in Q_0(T)$, there exists $\boldsymbol{v} \in \boldsymbol{V}_0(T)$ such that* $\operatorname{div} \boldsymbol{v} = q$ *and* $\|\nabla \boldsymbol{v}\|_{L^2(T)} \leq \beta_T^{-1} \|q\|_{L^2(T)}$. *Here, the constant $\beta_T > 0$ depends only on the shape-regularity of T.*

Proof. The proof for the general cases can be found in [26, Theorem 3.1]. Here we present a simpler proof for the 2D case.

Set $\boldsymbol{Z}(T) = \{\boldsymbol{v} \in \boldsymbol{V}_0(T) : \operatorname{div} \boldsymbol{v} = 0\}$. Since $\boldsymbol{v} \in \boldsymbol{H}_0^1(T)$ and $\boldsymbol{v}$ is piecewise polynomial of degree k on $K \subset T$ and $K \in \mathcal{T}_h^{ct}$, we have $\psi \in H_0^2(T)$ such that $\boldsymbol{v} = \mathbf{curl}\, \psi$, and ψ is piecewise polynomial of degree $k+1$ on $K \subset T$ and $K \in \mathcal{T}_h^{ct}$.

Set $\Sigma(T) = \{\psi \in H_0^2(T) : \psi \in \mathcal{P}_{k+1}(K)\}$. Clearly, we have $\boldsymbol{Z}(T) = \mathbf{curl}\, \Sigma(T)$. Note that if $\psi \in \Sigma(T)$, and $\mathbf{curl}\, \psi = 0$, then $\psi \in \mathbb{R}$. Since $\psi|_{\partial T} = 0$, we have that $\psi \equiv 0$ on T. Since the **curl** operator has trivial kernel for $\Sigma(T)$, we have $\dim\Sigma(T) = \dim\mathbf{curl}\, \Sigma(T)$. From [19], we get $\dim\Sigma(T) = \frac{3}{2}k^2 - \frac{9}{2}k + 3$. By the rank-nullity theorem, we have

$$
\begin{aligned}
\operatorname{dimdiv} \boldsymbol{V}_0(T) &= \dim \boldsymbol{V}_0(T) - \dim \boldsymbol{Z}(T) \\
&= \dim \boldsymbol{V}_0(T) - \dim \Sigma(T) \\
&= 2(1 + 3(k-1) + \frac{3}{2}(k-1)(k-2)) - (\frac{3}{2}k^2 - \frac{9}{2}k + 3) \\
&= \frac{3}{2}k^2 + \frac{3}{2}k - 1 \\
&= 3 \cdot \frac{1}{2}k(k+1) - 1 \\
&= \dim Q_0(T)
\end{aligned}
$$

Thus, we have shown that the divergence operator is surjective from $\boldsymbol{V}_0(T)$ to $Q_0(T)$.

Next we use a scaling argument to show $\|\nabla \boldsymbol{v}\|_{L^2(T)} \leq \beta_T^{-1} \|q\|_{L^2(T)}$.

Let $\hat{T}$ be a reference triangle, and $\hat{T}^{ct}$ be the CT refinement of $\hat{T}$.

Claim: for any $\hat{q} \in \mathcal{P}_{k-1}^{disc}(\hat{T}^{ct}) \cap L_0^2(\hat{T})$, there exists a $\hat{\boldsymbol{v}} \in \boldsymbol{\mathcal{P}}_k(\hat{T}^{ct}) \cap H_0^1(\hat{T})$ such that $\widehat{\operatorname{div}}\,\hat{\boldsymbol{v}} = \hat{q}$ and $\|\hat{\nabla}\hat{\boldsymbol{v}}\|_{L^2(\hat{T})} \leq C\|\hat{q}\|_{L^2(\hat{T})}$. Proof of the claim: We set $\hat{\boldsymbol{Z}} = \{\hat{\boldsymbol{w}} \in \boldsymbol{\mathcal{P}}_k(\hat{T}^{ct}) \cap H_0^1(\hat{T}) : \widehat{\operatorname{div}}\,\hat{\boldsymbol{w}} = 0\}$, and $\hat{\boldsymbol{Z}}^{\perp} = \{\hat{\boldsymbol{v}} \in \boldsymbol{\mathcal{P}}_k(\hat{T}^{ct}) \cap H_0^1(\hat{T}) : \int_{\hat{T}} \hat{\nabla}\hat{\boldsymbol{v}} : \hat{\nabla}\hat{\boldsymbol{w}} = 0,\ \forall \hat{\boldsymbol{w}} \in \hat{\boldsymbol{Z}}\}$.

Since for all $\hat{\boldsymbol{v}} \in \hat{\boldsymbol{Z}}^{\perp}$, $\|\widehat{\operatorname{div}}\,\hat{\boldsymbol{v}}\|_{L^2(\hat{T})} = 0$ implies that $\hat{\boldsymbol{v}} = 0$. Thus, $\|\widehat{\operatorname{div}}\,\hat{\boldsymbol{v}}\|_{L^2(\hat{T})}$ is a norm for $\hat{\boldsymbol{v}} \in \hat{\boldsymbol{Z}}^{\perp}$. Therefore, by the equivalence of norms, we have $\|\hat{\nabla}\hat{\boldsymbol{v}}\|_{L^2(\hat{T})} \leq C\|\widehat{\operatorname{div}}\,\hat{\boldsymbol{v}}\|_{L^2(\hat{T})}$, for all $\hat{\boldsymbol{v}} \in \hat{\boldsymbol{Z}}^{\perp}$.

By the same counting argument showed above, we have that $\widehat{\operatorname{div}} : \boldsymbol{\mathcal{P}}_k(\hat{T}^{ct}) \cap H_0^1(\hat{T}) \to \mathcal{P}_{k-1}^{disc}(\hat{T}^{ct}) \cap L_0^2(\hat{T})$ is surjective. We select $\hat{\boldsymbol{v}} \in \boldsymbol{\mathcal{P}}_k(\hat{T}^{ct}) \cap H_0^1(\hat{T})$ such that $\widehat{\operatorname{div}}\,\hat{\boldsymbol{v}} = \hat{q}$.

We write $\hat{\boldsymbol{v}} = \hat{\boldsymbol{z}} + \hat{\boldsymbol{v}}^{\perp}$, where $\hat{\boldsymbol{z}} \in \hat{\boldsymbol{Z}}$ and $\hat{\boldsymbol{v}}^{\perp} \in \hat{\boldsymbol{Z}}^{\perp}$.

Since $\widehat{\operatorname{div}}\,\hat{\boldsymbol{z}} = 0$, we have $\widehat{\operatorname{div}}\,\hat{\boldsymbol{v}}^{\perp} = \widehat{\operatorname{div}}\,\hat{\boldsymbol{v}} = \hat{q}$, and therefore,

$$\|\hat{\nabla}\hat{\boldsymbol{v}}^{\perp}\|_{L^2(\hat{T})} \leq C\|\widehat{\operatorname{div}}\,\hat{\boldsymbol{v}}^{\perp}\|_{L^2(\hat{T})} = C\|\hat{q}\|_{L^2(\hat{T})}.$$

This completes the proof of the claim.

Let $q \in \mathcal{P}_{k-1}^{disc}(T^{ct}) \cap L_0^2(T)$. We set $\hat{q} : \hat{T} \to \mathbb{R}$ such that $\hat{q}(\hat{x}) = q(x)$, where $x = F_T(\hat{x})$. F_T is a linear map where $F_T(\hat{x}) = A\hat{x} + b$. Thus, we have $\hat{q} \in \mathcal{P}_{k-1}^{disc}(\hat{T}^{ct}) \cap L_0^2(\hat{T})$. By claim, there exists $\hat{\boldsymbol{v}} \in \boldsymbol{\mathcal{P}}_k(\hat{T}^{ct}) \cap H_0^1(\hat{T})$ such that $\widehat{\boldsymbol{v}} = \hat{q}$ and $\|\hat{\nabla}\hat{\boldsymbol{v}}\|_{L^2(\hat{T})} \leq C\|\hat{q}\|_{L^2(\hat{T})}$.

We set $\boldsymbol{v} \in \boldsymbol{\mathcal{P}}_k(T^{ct}) \cap H_0^1(T)$ such that $\boldsymbol{v}(x) = A\hat{\boldsymbol{v}}(\hat{x})$. Then $(\operatorname{div}\boldsymbol{v})(x) = (\widehat{\operatorname{div}}\,\hat{\boldsymbol{v}})(\hat{x}) = \hat{q}(\hat{x}) = q(x)$.

Hence, we have

$$\begin{aligned}
\|\nabla\boldsymbol{v}\|_{L^(T)}^2 = \int_T |\nabla\boldsymbol{v}|^2\,dx &= 2|T| \int_{\hat{T}} |A\hat{\nabla}\hat{\boldsymbol{v}}A^{-1}|^2\,dx \\
&\leq C|T|\|\hat{\nabla}\hat{\boldsymbol{v}}\|_{L^2(T)}^2 \\
&\leq C|T|\|\hat{q}\|_{L^(\hat{T})}
\end{aligned}$$

$$\leq C\|q\|_{L^2(T)}.$$

We set $\beta_T = C^{-1}$, and we have the desired result. □

For the next step, we use the stability of the $\boldsymbol{\mathcal{P}}_k \times \mathcal{P}_{k-2}$ pair on unfitted domains. This result can be found in [27, Theorem 1, Section 6.3, Remark 1].

Lemma 2.4.5. *Define the space of piecewise polynomials of degree* $(k-2)$ *with respect to the mesh* $\mathcal{T}_h$*:*

$$\mathring{Y}_h = \{q \in L_0^2(\Omega_h) : \ q|_T \in \mathcal{P}_{k-2}(T) \ \forall T \in \mathcal{T}_h\} \subset \mathring{Q}_h.$$

There exist $\beta_0 > 0$ *and* $h_0 > 0$ *such that for* $h \leq h_0$*, there holds*

$$\sup_{\boldsymbol{v} \in \mathring{\boldsymbol{V}}_h \setminus \{0\}} \frac{\int_{\Omega_h} (\operatorname{div} \boldsymbol{v}) q \, dx}{\|\nabla \boldsymbol{v}\|_{L^2(\Omega_h)}} \geq \beta_0 \|q\|_{L^2(\Omega_h)} \qquad \forall q \in \mathring{Y}_h.$$

Combining Lemma 2.4.4 and Lemma 2.4.5, we derive the following discrete inf-sup (LBB) condition for the Stokes pair $\mathring{\boldsymbol{V}}_h \times \mathring{Q}_h$ with stability constants independent of h:

Lemma 2.4.6 (Inf-Sup Stability I)**.** *There exists* $\beta_1 > 0$ *independent of* h *such that*

$$\sup_{\boldsymbol{v} \in \mathring{\boldsymbol{V}}_h \setminus \{0\}} \frac{\int_{\Omega_h} (\operatorname{div} \boldsymbol{v}) q \, dx}{\|\nabla \boldsymbol{v}\|_{L^2(\Omega_h)}} \geq \beta_1 \|q\|_{L^2(\Omega_h)} \qquad \forall q \in \mathring{Q}_h.$$

for $h \leq h_0$*.*

Proof. This proof essentially follows arguments from [2, 45, 26] using Lemma 2.4.4 and 2.4.5.

For a $q \in \mathring{Q}_h$, we set $\bar{q}$ to be the piecewise average of q on each macro element $T \in \mathcal{T}_h$: $\bar{q}|_T = |T|^{-1} \int_T q \, dx \, \forall T \in \mathcal{T}_h$. Then, we have $q - \bar{q}$ is mean value zero on each macro element $T \in \mathcal{T}_h$. Thus, we have $q - \bar{q}|_T \in Q_0(T)$ for each $T \in \mathcal{T}_h$. Using Lemma 2.4.4, for each $T \in \mathcal{T}_h$, we find $\boldsymbol{v}_{1,T} \in \boldsymbol{V}_0(T)$ such that $\operatorname{div} \boldsymbol{v}_{1,T} = (q - \bar{q})|_T$ and $\|\nabla \boldsymbol{v}\|_{L^2(T)} \leq \beta_T^{-1} \|q - \bar{q}\|_{L^2(T)}$. Then we define $\boldsymbol{v}_1$ such that $\boldsymbol{v}_1|_T = \boldsymbol{v}_{1,T}$ for all $T \in \mathcal{T}_h$. Then we have $\operatorname{div} \boldsymbol{v}_1 = q - \bar{q}$ on Ω_h, and $\|\nabla \boldsymbol{v}_1\| \leq \beta_*^{-1} \|q - \bar{q}\|_{L^2(\Omega_h)}$, where $\beta_* = \min_{T \in \mathcal{T}_h} \beta_T$. Since β_T are all independent of h, we have β_* independent of h.

Since we have

$$\frac{\int_{\Omega_h} (\operatorname{div} \boldsymbol{v}) \bar{q} \, dx}{\|\nabla \boldsymbol{v}\|_{L^2(\Omega_h)}} = \frac{\int_{\Omega_h} (\operatorname{div} \boldsymbol{v}) q \, dx}{\|\nabla \boldsymbol{v}\|_{L^2(\Omega_h)}} + \frac{\int_{\Omega_h} (\operatorname{div} \boldsymbol{v})(\bar{q} - q) \, dx}{\|\nabla \boldsymbol{v}\|_{L^2(\Omega_h)}},$$

and, from the Cauchy Schwarz inequality, we have

$$\frac{\int_{\Omega_h} (\operatorname{div} \boldsymbol{v})(\bar{q} - q) \, dx}{\|\nabla \boldsymbol{v}\|_{L^2(\Omega_h)}} \leq \frac{\|\nabla \boldsymbol{v}\|_{L^2(\Omega_h)} \|q - \bar{q}\|_{L^2(\Omega_h)}}{\|\nabla \boldsymbol{v}\|_{L^2(\Omega_h)}}$$

for all $\boldsymbol{v} \in \mathring{\boldsymbol{V}}_h \backslash \{0\}$, we derive

$$\sup_{\boldsymbol{v} \in \mathring{\boldsymbol{V}}_h \backslash \{0\}} \frac{\int_{\Omega_h} (\operatorname{div} \boldsymbol{v})(\bar{q} - q) \, dx}{\|\nabla \boldsymbol{v}\|_{L^2(\Omega_h)}} \leq \|q - \bar{q}\|_{L^2(\Omega_h)}. \tag{2.4.9}$$

Since $\|\nabla \boldsymbol{v}_1\| \leq \beta_*^{-1} \|q - \bar{q}\|_{L^2(\Omega_h)}$ and $\operatorname{div} \boldsymbol{v}_1 = q - \bar{q}$ on Ω_h, we have

$$\begin{aligned} \frac{\int_{\Omega_h} (\operatorname{div} \boldsymbol{v}_1)(q - \bar{q}) \, dx}{\|\nabla \boldsymbol{v}_1\|_{L^2(\Omega_h)}} &= \frac{\|q - \bar{q}\|_{L^2(\Omega_h)}^2}{\|\nabla \boldsymbol{v}_1\|_{L^2(\Omega_h)}} \\ &\geq \frac{\|q - \bar{q}\|_{L^2(\Omega_h)}^2}{\beta^{-1} \|q - \bar{q}\|_{L^2(\Omega_h)}} \\ &= \beta \|q - \bar{q}\|_{L^2(\Omega_h)}. \end{aligned}$$

Thus we have

$$\|q-\bar{q}\|_{L^2(\Omega_h)} \le \beta^{-1} \sup_{\boldsymbol{v}\in\mathring{\boldsymbol{V}}_h\setminus\{0\}} \frac{\int_{\Omega_h}(\operatorname{div}\boldsymbol{v})q\,dx}{\|\nabla\boldsymbol{v}\|_{L^2(\Omega_h)}}. \tag{2.4.10}$$

Combining Lemma 2.4.5, (2.4.9) and (2.4.10), we have

$$\begin{aligned}\beta_0\|\bar{q}\|_{L^2(\Omega_h)} &\le \sup_{\boldsymbol{v}\in\mathring{\boldsymbol{V}}_h\setminus\{0\}} \frac{\int_{\Omega_h}(\operatorname{div}\boldsymbol{v})\bar{q}\,dx}{\|\nabla\boldsymbol{v}\|_{L^2(\Omega_h)}}\\ &\le \sup_{\boldsymbol{v}\in\mathring{\boldsymbol{V}}_h\setminus\{0\}} \frac{\int_{\Omega_h}(\operatorname{div}\boldsymbol{v})q\,dx}{\|\nabla\boldsymbol{v}\|_{L^2(\Omega_h)}} + \|q-\bar{q}\|_{L^2(\Omega_h)}\\ &\le (1+\beta_*^{-1}) \sup_{\boldsymbol{v}\in\mathring{\boldsymbol{V}}_h\setminus\{0\}} \frac{\int_{\Omega_h}(\operatorname{div}\boldsymbol{v})q\,dx}{\|\nabla\boldsymbol{v}\|_{L^2(\Omega_h)}}.\end{aligned}$$

Using the triangle inequality and (2.4.10), we have

$$\|q\|_{L^2(\Omega_h)} \le \|q-\bar{q}\|_{L^2(\Omega_h)} + \|\bar{q}\|_{L^2(\Omega_h)} \le \big(\beta_*^{-1}+\beta_0^{-1}(1+\beta_*^{-1})\big) \sup_{\boldsymbol{v}\in\mathring{\boldsymbol{V}}_h\setminus\{0\}} \frac{\int_{\Omega_h}(\operatorname{div}\boldsymbol{v})q\,dx}{\|\nabla\boldsymbol{v}\|_{L^2(\Omega_h)}}.$$

Since both β_* and β_1 are independent of the mesh parameter h, we have $\beta_*^{-1} + \beta_0^{-1}(1+\beta_*^{-1})$ independent of the mesh parameter h. By setting $\beta_1 = \beta_*^{-1} + \beta_0^{-1}(1+\beta_*^{-1})$, we complete the proof. □

The next lemma states the inf-sup condition for the Lagrange multiplier part of the bilinear form $b_h(\cdot,\cdot)$.

Lemma 2.4.7 (Inf-Sup Stability II)**.** *Assume the triangulation $\mathcal{T}_h$ is quasi-uniform. Then there holds*

$$\sup_{\boldsymbol{v}\in\boldsymbol{V}_h\setminus\{0\}} \frac{\int_{\partial\Omega_h}(\boldsymbol{v}\cdot\boldsymbol{n}_h)\mu\,ds}{\|\boldsymbol{v}\|_{1,h}} \ge \beta_2\|\mu\|_{-1/2,h} \qquad \forall\mu\in\mathring{X}_h. \tag{2.4.11}$$

for some $\beta_2 > 0$ independent of h.

Proof. On the boundary of the computational domain Ω_h, we have equal number of edges and vertices. We label the boundary edges as $\{e_j\}_{j=1}^N = \mathcal{E}_h^B$, and denote the boundary vertices by $\{a_j\}_{j=1}^N = \mathcal{V}_h^B$, labeled such that e_j has vertices a_j and a_{j+1}, with the convention that $a_{N+1} = a_1$. For a boundary edge $e \in \mathcal{E}_h^B$, let $\mathcal{M}_h^e = \{m_j\}_{j=1}^{k-1}$ denote the canonical interior degrees of freedom on the edge e, and set $\mathcal{M}_h^B = \cup_{e\in\mathcal{E}_h^B}\mathcal{M}_h^e$. Let $\boldsymbol{n}_j$ be the normal vector of $\partial\Omega_h$ restricted to the edge e_j, and let $\boldsymbol{t}_j$ be the tangent vector obtained by rotating $\boldsymbol{n}_j$ 90 degrees clockwise. Without loss of generality, we assume that $\boldsymbol{t}_j$ is parallel to $a_{j+1} - a_j$. We further denote by $\mathcal{V}_h^C$ the set of boundary corner vertices, i.e., if $a_j \in \mathcal{V}_h^C$, then the outward unit normals $\boldsymbol{n}_j, \boldsymbol{n}_{j-1}$ of the edges touching a_j are linearly independent. The set of flat boundary vertices are defined as $\mathcal{V}_h^F = \mathcal{V}_h^B \backslash \mathcal{V}_h^C$. Note that $\boldsymbol{n}_j = \boldsymbol{n}_{j-1}$ and $\boldsymbol{t}_j = \boldsymbol{t}_{j-1}$ for $a_j \in \mathcal{V}_h^F$.

We let $h_I \in X_h$ denote the continuous, piecewise linear polynomial with respect to the partition $\mathcal{E}_h^B$ satisfying $h_I(a_j) = \frac{1}{2}(h_{e_{j-1}} + h_{e_j})$. Given $\mu \in \mathring{X}_h$, we let $P_h(h_I\mu) \in \mathring{X}_h$ be the L^2-projection of $h_I\mu$, i.e.,

$$\int_{\partial\Omega_h} P_h(h_I\mu)\kappa \, ds = \int_{\partial\Omega_h} h_I\mu\kappa \, ds \qquad \forall \kappa \in \mathring{X}_h.$$

We then define $\boldsymbol{v} \in \boldsymbol{V}_h$ by the conditions

$$\begin{aligned}
&(\boldsymbol{v}\cdot\boldsymbol{n}_j)(a_j) = P_h(h_I\mu)(a_j), && (\boldsymbol{v}\cdot\boldsymbol{n}_{j-1})(a_j) = P_h(h_I\mu)(a_j) && \forall a_j \in \mathcal{V}_h^C,\\
&(\boldsymbol{v}\cdot\boldsymbol{n}_j)(a_j) = P_h(h_I\mu)(a_j), && (\boldsymbol{v}\cdot\boldsymbol{t}_j)(a_j) = 0 && \forall a_j \in \mathcal{V}_h^F,\\
&(\boldsymbol{v}\cdot\boldsymbol{n}_j)(m_j) = P_h(h_I\mu)(m_j), && (\boldsymbol{v}\cdot\boldsymbol{t}_j)(m_j) = 0 && \forall m_j \in \mathcal{M}_h^e, \forall e \in \mathcal{E}_h^B.
\end{aligned} \tag{2.4.12}$$

All other (Lagrange) degrees of freedom of $\boldsymbol{v}$ are set to zero.

Since $(\boldsymbol{v}\cdot\boldsymbol{n}_j - P_h(h_I\mu))|_{e_j}$ is a polynomial of degree k on each $e_j \in \mathcal{E}_h^B$, and $\boldsymbol{v}\cdot\boldsymbol{n}_j = P_h(h_I\mu)$ at $(k+1)$ distinct points on e_j, we have $\boldsymbol{v}\cdot\boldsymbol{n}_j - P_h(h_I\mu)|_{e_j} = 0$. Thus by shape regularity,

$$\int_{\partial\Omega_h} (\boldsymbol{v}\cdot\boldsymbol{n}_h)\mu\, ds = \int_{\partial\Omega_h} P_h(h_I\mu)\mu\, ds = \int_{\partial\Omega_h} h_I\mu^2\, ds \geq C\|\mu\|^2_{-1/2,h}. \tag{2.4.13}$$

It remains to show that $\|\boldsymbol{v}\|_{1,h} \leq C\|\mu\|_{-1/2,h}$ to complete the proof.

For $K \in \mathcal{T}_h^{ct}$, let $\mathcal{V}_K^B, \mathcal{V}_K^C, \mathcal{V}_K^F, \mathcal{M}_K^B$ be the sets of elements in $\mathcal{V}_h^B, \mathcal{V}_h^C, \mathcal{V}_h^F, \mathcal{M}_h^B$ contained in $\bar{K}$, respectively. By a standard scaling argument and (2.4.12), we get $(m = 0, 1)$

$$\begin{aligned}\|\boldsymbol{v}\|^2_{H^m(K)} &\leq C \sum_{c_j\in\mathcal{V}_K^B\cup\mathcal{M}_K^B} h_{e_j}^{2-2m}|\boldsymbol{v}(c_j)|^2 \\ &= C\Big(\sum_{a_j\in\mathcal{V}_K^C} h_{e_j}^{2-2m}|\boldsymbol{v}(a_j)|^2 + \sum_{c_j\in\mathcal{V}_K^F\cup\mathcal{M}_K^B} h_{e_j}^{2-2m}|P_h(h_I\mu)(c_j)|^2\Big).\end{aligned} \tag{2.4.14}$$

Claim: $|\boldsymbol{v}(a_j)| \leq C|P_h(h_I\mu)(a_j)|$ for all $a_j \in \mathcal{V}_K^C$, where $C > 0$ is uniformly bounded and independent of h, $\boldsymbol{n}_j$ and $\boldsymbol{n}_{j-1}$.

Proof of the claim: Assume that $\mathcal{V}_K^C$ is non-empty for otherwise the proof is trivial. For $a_j \in \mathcal{V}_K^C$, we write $\boldsymbol{v}(a_j)$ in terms of the basis $\{\boldsymbol{t}_j, \boldsymbol{t}_{j-1}\}$, use (2.4.12), and apply some elementary vector identities:

$$\begin{aligned}\boldsymbol{v}(a_j) &= \frac{1}{\boldsymbol{t}_{j-1}\cdot\boldsymbol{n}_j}(\boldsymbol{v}\cdot\boldsymbol{n}_j)(a_j)\boldsymbol{t}_{j-1} + \frac{1}{\boldsymbol{t}_j\cdot\boldsymbol{n}_{j-1}}(\boldsymbol{v}\cdot\boldsymbol{n}_{j-1})(a_j)\boldsymbol{t}_j \\ &= P_h(h_I\mu)(a_j)\Big(\frac{1}{\boldsymbol{t}_{j-1}\cdot\boldsymbol{n}_j}\boldsymbol{t}_{j-1} + \frac{1}{\boldsymbol{t}_j\cdot\boldsymbol{n}_{j-1}}\boldsymbol{t}_j\Big) \\ &= P_h(h_I\mu)(a_j)\Big(\frac{\boldsymbol{t}_j - \boldsymbol{t}_{j-1}}{\boldsymbol{t}_j\cdot\boldsymbol{n}_{j-1}}\Big).\end{aligned} \tag{2.4.15}$$

We now show $\left|\frac{\boldsymbol{t}_j-\boldsymbol{t}_{j-1}}{\boldsymbol{t}_j\cdot\boldsymbol{n}_{j-1}}\right|$ is bounded. Write $\boldsymbol{t}_j = (\cos(\theta_j),\sin(\theta_j))^\intercal$ with $\theta_{j-1},\theta_j \in [-\pi,\pi]$, so that

$$\frac{\boldsymbol{t}_j-\boldsymbol{t}_{j-1}}{\boldsymbol{t}_j\cdot\boldsymbol{n}_{j-1}} = \frac{(\cos(\theta_j)-\cos(\theta_{j-1}),\sin(\theta_j)-\sin(\theta_{j-1}))^\intercal}{\sin(\theta_j-\theta_{j-1})}.$$

Since

$$\begin{aligned}\lim_{\theta_j\to\theta_{j-1}} \frac{(\cos\theta_j-\cos\theta_{j-1},\sin\theta_j-\sin\theta_{j-1})^\intercal}{\sin(\theta_j-\theta_{j-1})} &= \lim_{\theta_j\to\theta_{j-1}} \frac{(-\sin\theta_j,\cos\theta_j)^\intercal}{\cos(\theta_j-\theta_{j-1})}\\ &= (-\sin\theta_{j-1},\cos\theta_{j-1})^\intercal,\end{aligned}$$

and due to the shape regularity of the mesh, we conclude $\left|\frac{\boldsymbol{t}_j-\boldsymbol{t}_{j-1}}{\boldsymbol{t}_j\cdot\boldsymbol{n}_{j-1}}\right|$ is bounded in the case $|\boldsymbol{t}_j\cdot\boldsymbol{n}_{j-1}| \ll 1$, in particular, for "nearly flat boundary vertices". Therefore, $\left|\frac{\boldsymbol{t}_j-\boldsymbol{t}_{j-1}}{\boldsymbol{t}_j\cdot\boldsymbol{n}_{j-1}}\right| \le C$ on shape-regular triangulations for some $C>0$ independent of h and $\{\boldsymbol{n}_{j-1},\boldsymbol{n}_j\}$. With (2.4.15), this yields $|\boldsymbol{v}(a_j)| \le C|P_h(h_I\mu)(a_j)|$ for all $a_j \in \mathcal{V}_K^C$, which concludes the proof of the claim.

Applying the claim to (2.4.14) and a scaling argument yields

$$\|\boldsymbol{v}\|^2_{H^m(K)} \le C \sum_{c_j\in\mathcal{V}_K^B\cup\mathcal{M}_K^B} h_{e_j}^{2-2m}|P_h(h_I\mu)(c_j)|^2 \le C \sum_{\substack{e\in\mathcal{E}_h^B\\ a_j\in\bar{e}:\ a_j\in\mathcal{V}_K^B}} h_e^{1-2m}\|P_h(h_I\mu)\|^2_{L^2(e)}.$$

Therefore, by an inverse inequality and shape-regularity of $\mathcal{T}_h^{ct}$,

$$\begin{aligned}\|\boldsymbol{v}\|^2_{1,h} &= \|\nabla\boldsymbol{v}\|^2_{L^2(\Omega_h)} + \sum_{e\in\mathcal{E}_h^B}\frac{1}{h_e}\|\boldsymbol{v}\|^2_{L^2(e)}\\ &\le \|\nabla\boldsymbol{v}\|^2_{L^2(\Omega_h)} + C\sum_{K\in\mathcal{T}_h^{ct}} h_K^{-2}\|\boldsymbol{v}\|^2_{L^2(K)} \le C\sum_{e\in\mathcal{E}_h^B} h_e^{-1}\|P_h(h_I\mu)\|^2_{L^2(e)}.\end{aligned}$$

Finally, using the L^2-stability of $P_h(h_I\mu)$ and the quasi-uniform assumption, we have

$$\begin{aligned}\|\boldsymbol{v}\|_{1,h}^2 &\leq C\sum_{e\in\mathcal{E}_h^B} h_e^{-1}\|P_h(h_I\mu)\|_{L^2(e)}^2 \\ &\leq Ch^{-1}\|P_h(h_I\mu)\|_{L^2(\partial\Omega_h)}^2 \leq Ch^{-1}\|h_I\mu\|_{L^2(\partial\Omega_h)}^2 \leq C\|\mu\|_{-1/2,h}^2.\end{aligned} \tag{2.4.16}$$

Combining this estimate with (2.4.13) yields the desired inf-sup condition (2.4.11).

□

Remark 2.4.8. The proof of Lemma 2.4.7, and in particular the proof of the claim, relies on the continuity properties of the Lagrange multiplier space at nearly flat corner vertices.

2.4.3 Main Stability Results

With Lemma 2.4.6 and Lemma 2.4.7, we show the main inf-sup condition for the bilinear form $b_h(\cdot,\cdot)$ in the next theorem. We show inf-sup condition for the bilinear form with boundary correction term $b_h^e(\cdot,\cdot)$ in the corollary after.

Theorem 2.4.9. *Assume $\mathcal{T}_h$ is quasi-uniform. Then there exists $\beta > 0$ depending only on β_1 and β_2 such that*

$$\beta\|(q,\mu)\| \leq \sup_{\boldsymbol{v}\in\boldsymbol{V}_h\setminus\{0\}} \frac{b_h(\boldsymbol{v},(q,\mu))}{\|\boldsymbol{v}\|_{1,h}} \qquad \forall (q,\mu)\in \mathring{Q}_h\times\mathring{X}_h. \tag{2.4.17}$$

Proof. We use Lemmas 2.4.6 and 2.4.7 and follow the arguments in [32, Theorem 3.1].

Fix $(q,\mu)\in\mathring{Q}_h\times\mathring{X}_h$.

We first bound the Lagrange multiplier part of the bilinear form $b_h(\cdot,(\cdot,\cdot))$ using Lemma 2.4.7. The statement (2.4.11) implies the existence of $\boldsymbol{v}_2 \in \boldsymbol{V}_h$ such that $\|\boldsymbol{v}_2\|_{1,h} \leq 1$ and

$$\int_{\partial\Omega_h} (\boldsymbol{v}_2 \cdot \boldsymbol{n}_h)\mu \, ds \geq \beta_2 \|\mu\|_{-1/2,h}.$$

Then, we use the LBB condition for the unfitted domain to bound the divergence part of the bilinear form $b_h(\cdot,(\cdot,\cdot))$. By Lemma 2.4.6 there exists $\boldsymbol{v}_1 \in \mathring{\boldsymbol{V}}_h$ satisfying $\|\nabla \boldsymbol{v}_1\|_{L^2(\Omega_h)} = \|\boldsymbol{v}_1\|_{1,h} \leq 1$ and

$$-\int_{\Omega_h} (\operatorname{div} \boldsymbol{v}_1) q \geq \beta_1 \|q\|_{L^2(\Omega_h)}.$$

Set $\boldsymbol{v} = c\boldsymbol{v}_1 + \boldsymbol{v}_2$ for some $c > 0$, so that $\|\boldsymbol{v}\|_{1,h} \leq (1+c)$, and

$$\begin{aligned}
-\int_{\Omega_h} (\operatorname{div} \boldsymbol{v}) q \, dx &\geq c\beta_1 \|q\|_{L^2(\Omega_h)} - \|\operatorname{div} \boldsymbol{v}_2\|_{L^2(\Omega_h)} \|q\|_{L^2(\Omega_h)} \\
&\geq c\beta_1 \|q\|_{L^2(\Omega_h)} - \sqrt{2} \|\nabla \boldsymbol{v}_2\|_{L^2(\Omega_h)} \|q\|_{L^2(\Omega_h)} \\
&\geq c\beta_1 \|q\|_{L^2(\Omega_h)} - \sqrt{2} \|\boldsymbol{v}_2\|_{1,h} \|q\|_{L^2(\Omega_h)} \\
&= \big(c\beta_1 - \sqrt{2}\big) \|q\|_{L^2(\Omega_h)}.
\end{aligned}$$

Because $\boldsymbol{v}_1|_{\partial\Omega_h} = 0$, we have

$$\int_{\partial\Omega_h} (\boldsymbol{v} \cdot \boldsymbol{n}_h)\mu \, ds = \int_{\partial\Omega_h} (\boldsymbol{v}_2 \cdot \boldsymbol{n}_h)\mu \, ds \geq \beta_2 \|\mu\|_{-1/2,h}.$$

Therefore,

$$\begin{aligned}
b_h(\boldsymbol{v},(q,\mu)) &\geq \big(c\beta_1 - \sqrt{2}\big) \|q\|_{L^2(\Omega_h)} + \beta_2 \|\mu\|_{-1/2,h} \\
&\geq (1+c)^{-1} \Big(\big(c\beta_1 - \sqrt{2}\big) \|q\|_{L^2(\Omega_h)} + \beta_2 \|\mu\|_{-1/2,h} \Big) \|\boldsymbol{v}\|_{1,h}
\end{aligned}$$

for some $c > 0$ sufficiently large.

Now we set $\beta = \min\{\frac{c\beta_1 - \sqrt{2}}{1+c}, \frac{\beta_2}{1+c}\}$ to get the desired results. □

Corollary 2.4.10. *Provided Assumption* (A) *is satisfied and the mesh* $\mathcal{T}_h$ *is quasi-uniform, there exists* $\beta_e > 0$ *independent of* h *such that there holds*

$$\beta_e \|(q,\mu)\| \leq \sup_{\boldsymbol{v}\in \boldsymbol{V}_h\setminus\{0\}} \frac{b_h^e(\boldsymbol{v},(q,\mu))}{\|\boldsymbol{v}\|_{1,h}} \qquad \forall (q,\mu)\in \mathring{Q}_h \times \mathring{X}_h. \tag{2.4.18}$$

Proof. From Theorem 2.4.9, and the triangle inequality, we have

$$\begin{aligned}
\beta\|(q,\mu)\| &\leq \sup_{\boldsymbol{v}\in \boldsymbol{V}_h\setminus\{0\}} \frac{b_h(\boldsymbol{v},(q,\mu))}{\|\boldsymbol{v}\|_{1,h}} \\
&= \sup_{\boldsymbol{v}\in \boldsymbol{V}_h\setminus\{0\}} \frac{b_h(\boldsymbol{v},(q,\mu)) + b_h^e(\boldsymbol{v},(q,\mu)) - b_h(\boldsymbol{v},(q,\mu))}{\|\boldsymbol{v}\|_{1,h}} \\
&\leq \sup_{\boldsymbol{v}\in \boldsymbol{V}_h\setminus\{0\}} \frac{b_h(\boldsymbol{v},(q,\mu))}{\|\boldsymbol{v}\|_{1,h}} + \sup_{\boldsymbol{v}\in \boldsymbol{V}_h\setminus\{0\}} \frac{|b_h^e(\boldsymbol{v},(q,\mu)) - b_h(\boldsymbol{v},(q,\mu))|}{\|\boldsymbol{v}\|_{1,h}}.
\end{aligned} \tag{2.4.19}$$

From Lemma 2.4.2, we have

$$\begin{aligned}
\sup_{\boldsymbol{v}\in \boldsymbol{V}_h\setminus\{0\}} \frac{|b_h^e(\boldsymbol{v},(q,\mu)) - b_h(\boldsymbol{v},(q,\mu))|}{\|\boldsymbol{v}\|_{1,h}} &\leq \sup_{\boldsymbol{v}\in \boldsymbol{V}_h\setminus\{0\}} \frac{Cc_\delta \|\boldsymbol{v}\|_{1,h}\|(q,\mu)\|}{\|\boldsymbol{v}\|_{1,h}} \\
&= Cc_\delta \|(q,\mu)\|.
\end{aligned} \tag{2.4.20}$$

Combining (2.4.19) and (2.4.20), we get

$$\beta\|(q,\mu)\| \leq \sup_{\boldsymbol{v}\in \boldsymbol{V}_h\setminus\{0\}} \frac{b_h^e(\boldsymbol{v},(q,\mu))}{\|\boldsymbol{v}\|_{1,h}} + Cc_\delta\|(q,\mu)\| \qquad \forall (q,\mu)\in \mathring{Q}_h \times \mathring{X}_h.$$

For c_δ to be sufficiently small, $\beta - Cc_\delta$ is positive and set $\beta_e = \beta - Cc_\delta$. We then get the desired result (2.4.18). □

With the main inf-sup condition from Theorem 2.4.9, we now show the following stability estimates.

Theorem 2.4.11. *Let* $(\boldsymbol{u}_h, p_h, \lambda_h) \in \boldsymbol{V}_h \times \mathring{Q}_h \times \mathring{X}_h$ *satisfy* (2.3.1). *Then, provided* c_δ *in Assumption* (A) *is sufficiently small and the mesh* $\mathcal{T}_h$ *is quasi-uniform, there holds*

$$\nu\|\boldsymbol{u}_h\|_{1,h} + \|(p_h, \lambda_h)\| \leq C\|\boldsymbol{f}\|_{-1,h}, \tag{2.4.21}$$

where $\|\boldsymbol{f}\|_{-1,h} = \sup_{\boldsymbol{v}\in\boldsymbol{V}_h\setminus\{0\}} \frac{\int_{\Omega_h} \boldsymbol{f}\cdot\boldsymbol{v}\,dx}{\|\boldsymbol{v}\|_{1,h}}$. *Consequently, there exists a unique solution to* (2.3.1).

Proof. We prove this Theorem using an energy argument. Setting $\boldsymbol{v} = \boldsymbol{u}_h$ in (2.3.1a), $(q, \mu) = (p_h, \lambda_h)$ in (2.3.1b), and subtracting the resulting expressions yields

$$a_h(\boldsymbol{u}_h, \boldsymbol{u}_h) = \int_{\Omega_h} \boldsymbol{f}\cdot\boldsymbol{u}_h\,dx + \int_{\partial\Omega_h} \big((S_h\boldsymbol{u}_h - \boldsymbol{u}_h)\cdot\boldsymbol{n}_h\big)\lambda_h\,ds.$$

By using (2.4.1), and the definition of $\|\cdot\|_{-1/2,h}$, and the Cauchy-Schwarz inequality we have

$$\begin{aligned}\int_{\partial\Omega_h} \big((S_h\boldsymbol{u}_h - \boldsymbol{u}_h)\cdot\boldsymbol{n}_h\big)\lambda_h\,ds &= \Big(\sum_{e\in\mathcal{E}_h^B} h_e^{-1}\|S_h\boldsymbol{u}_h - \boldsymbol{u}_h\|^2_{L^2(e)}\Big)^{\frac{1}{2}}\Big(\sum_{e\in\mathcal{E}_h^B} h_e\|\lambda_h\|^2_{L^2(e)}\Big)^{\frac{1}{2}}\\ &\leq Cc_\delta\|\boldsymbol{u}_h\|_{1,h}\|\lambda_h\|_{-1/2,h}.\end{aligned} \tag{2.4.22}$$

We apply the coercivity result in Lemma 2.4.3, the Cauchy-Schwarz inequality, and (2.4.22) to get

$$\begin{aligned}\nu c_1\|\boldsymbol{u}_h\|^2_{1,h} &\leq a_h(\boldsymbol{u}_h, \boldsymbol{u}_h)\\ &\leq \|\boldsymbol{f}\|_{-1,h}\|\boldsymbol{u}_h\|_{1,h} + Cc_\delta\|\boldsymbol{u}_h\|_{1,h}\|\lambda_h\|_{-1/2,h}.\end{aligned} \tag{2.4.23}$$

On the other hand, we use inf-sup stability (2.4.17) and triangle inequality to conclude

$$\beta\|(p_h, \lambda_h)\|_{-1/2,h} \leq \sup_{\boldsymbol{v}\in\boldsymbol{V}_h\setminus\{0\}} \frac{b_h(\boldsymbol{v}, (p_h, \lambda_h))}{\|\boldsymbol{v}\|_{1,h}}$$

$$\leq \sup_{\boldsymbol{v}\in\boldsymbol{V}_h\setminus\{0\}} \frac{\int_{\Omega_h} \boldsymbol{f}\cdot\boldsymbol{v}\,dx - a_h(\boldsymbol{u}_h,\boldsymbol{v})}{\|\boldsymbol{v}\|_{1,h}}$$
$$\leq \sup_{\boldsymbol{v}\in\boldsymbol{V}_h\setminus\{0\}} \frac{\int_{\Omega_h} \boldsymbol{f}\cdot\boldsymbol{v}\,dx}{\|\boldsymbol{v}\|_{1,h}} + \sup_{\boldsymbol{v}\in\boldsymbol{V}_h\setminus\{0\}} \frac{|a_h(\boldsymbol{u}_h,\boldsymbol{v})|}{\|\boldsymbol{v}\|_{1,h}}.$$

Using the continuity estimate (2.4.3) and the definition of $\|(p_h,\lambda_h)\|$, we get

$$\beta\|\lambda_h\|_{-1/2,h} \leq \beta\|(p_h,\lambda_h)\| \leq \|\boldsymbol{f}\|_{-1,h} + C(1+\sigma)\nu\|\boldsymbol{u}_h\|_{1,h}. \tag{2.4.24}$$

Inserting this estimate into (2.4.23), we obtain

$$\nu\big(c_1 - Cc_\delta\beta^{-1}(1+\sigma)\big)\|\boldsymbol{u}_h\|_{1,h} \leq (1+Cc_\delta\beta^{-1})\|\boldsymbol{f}\|_{-1,h}.$$

Thus, $\|\boldsymbol{u}_h\|_{1,h} \leq C\nu^{-1}\|\boldsymbol{f}\|_{-1,h}$ for c_δ sufficiently small. This, combined with (2.4.24), yields the desired stability result (2.4.21).

□

2.5 Convergence Analysis of the Finite Element Method

In this section, we show that the solution of the finite element method (2.3.1) converges with optimal order provided the exact solution is sufficiently smooth. Throughout this section, we assume that the hypotheses of Theorem 2.4.11 are satisfied, i.e., Assumption A is satisfied and the mesh $\mathcal{T}_h$ is quasi-uniform.

2.5.1 Consistency Estimates of the Method

The following lemma bounds the boundary correction operator acting on the exact velocity function. Note that since we assume homogeneous Dirichlet boundary condition on $\partial\Omega$, there holds $S_h\boldsymbol{u} + R_h\boldsymbol{u} = 0$, where $R_h\boldsymbol{u}$ is the Taylor remainder. The result is essentially an estimate on $R_h\boldsymbol{u}$ and follows from similar arguments in [3, Proposition 3] (also see [12]).

Lemma 2.5.1. *For any $\boldsymbol{u} \in \boldsymbol{H}^{k+1}(\Omega) \cap \boldsymbol{H}_0^1(\Omega)$, there holds*

$$\sum_{e\in\mathcal{E}_h^B} h_e^{-1} \int_e \left|S_h\boldsymbol{u}\right|^2 ds \le Ch^{2k}\|\boldsymbol{u}\|^2_{H^{k+1}(\Omega)}.$$

Proof. For a boundary edge $e \in \mathcal{E}_h^B$ with endpoints a_1, a_2, let $x(t) = a_1 + th_e^{-1}(a_2 - a_1)$ $(0 \le t \le h_e)$ be its parameterization, and introduce the 2D parameterization for the area between the computation boundary $\partial\Omega_h$ and the physical boundary $\partial\Omega$ corresponding to each boundary edge e: $\varphi(t,s) = x(t) + s\boldsymbol{d}(x(t))$ for $0 \le t \le h_e$ and $0 \le s \le \delta(x(t))$. The Taylor remainder estimation with $S_h\boldsymbol{u} + R_h\boldsymbol{u} = 0$ yields

$$|S_h\boldsymbol{u}(x(t))| = |R_h\boldsymbol{u}(x(t))| = \frac{1}{k!}\Big|\int_0^{\delta(x(t))} \frac{\partial^{k+1}\boldsymbol{u}}{\partial\boldsymbol{d}^{k+1}}(\varphi(t,s))(\delta(x(t)) - s)^k\, ds\Big|.$$

Applying the Cauchy-Schwarz inequality, we obtain

$$|S_h\boldsymbol{u}(x(t))| \le C\delta(x(t))^{k+1/2}\Big(\int_0^{\delta(x(t))} \Big|\frac{\partial^{k+1}\boldsymbol{u}}{\partial\boldsymbol{d}^{k+1}}(\varphi(t,s))\Big|^2 ds\Big)^{1/2},$$

and therefore

$$\begin{aligned} h_e^{-1}\|S_h\boldsymbol{u}\|^2_{L^2(e)} &\le Ch_e^{-1}\delta_e^{2k+1}\int_0^{h_e}\int_0^{\delta(x(t))} \Big|\frac{\partial^{k+1}\boldsymbol{u}}{\partial\boldsymbol{d}^{k+1}}(\varphi(t,s))\Big|^2 ds\, dt \\ &\le Ch_e^{2k}\int_0^{h_e}\int_0^{\delta(x(t))} \Big|\frac{\partial^{k+1}\boldsymbol{u}}{\partial\boldsymbol{d}^{k+1}}(\varphi(t,s))\Big|^2 ds\, dt, \end{aligned}$$

where we used Assumption A in the last inequality. The estimate in Lemma 2.5.1 now follows from a change of variables (cf. [43, 3]) and summing over $e \in \mathcal{E}_h^B$. □

Lemma 2.5.2. *There holds for all* $\boldsymbol{u} \in \boldsymbol{H}^{k+1}(\Omega) \cap \boldsymbol{H}_0^1(\Omega)$,

$$\Big| -\nu \int_{\Omega_h} \Delta \boldsymbol{u} \cdot \boldsymbol{v}\, dx - a_h(\boldsymbol{u}, \boldsymbol{v}) \Big| \leq C\nu h^k \|\boldsymbol{u}\|_{H^{k+1}(\Omega)} \|\boldsymbol{v}\|_{1,h} \qquad \forall \boldsymbol{v} \in \boldsymbol{V}_h. \tag{2.5.1}$$

If $\operatorname{div} \boldsymbol{u} = 0$ *in* Ω, *then*

$$\big| b_h^e(\boldsymbol{u}, (q, \mu)) \big| \leq C h^k \|\boldsymbol{u}\|_{H^{k+1}(\Omega)} \|(q, \mu)\| \qquad \forall (q, \mu) \in \mathring{Q}_h \times \mathring{X}_h.$$

Proof. Using the integrate-by-parts technique, we have

$$-\nu \int_{\Omega_h} \Delta \boldsymbol{u} \cdot \boldsymbol{v}\, dx = \nu \Big(\int_{\Omega_h} \nabla \boldsymbol{u} : \nabla \boldsymbol{v}\, dx - \int_{\partial \Omega_h} \frac{\partial \boldsymbol{u}}{\partial \boldsymbol{n}_h} \cdot \boldsymbol{v}\, ds \Big).$$

Then by the definition of $a_h(\cdot, \cdot)$, we have

$$\Big| -\nu \int_{\Omega_h} \Delta \boldsymbol{u} \cdot \boldsymbol{v}\, dx - a_h(\boldsymbol{u}, \boldsymbol{v}) \Big| = \nu \Big| \sum_{e \in \mathcal{E}_h^B} \int_e \frac{\partial \boldsymbol{v}}{\partial \boldsymbol{n}_h} \cdot (S_h \boldsymbol{u})\, ds + \sum_{e \in \mathcal{E}_h^B} \frac{\sigma}{h_e} \int_e (S_h \boldsymbol{u}) \cdot (S_h \boldsymbol{v})\, ds \Big|.$$

Next, we estimate the two terms on the right hand side of the above equality by using the Cauchy-Schwarz inequality, trace and inverse inequalities, along with Lemmas 2.4.1 and 2.5.1 as follows:

$$\begin{aligned} \Big| \sum_{e \in \mathcal{E}_h^B} \int_e \frac{\partial \boldsymbol{v}}{\partial \boldsymbol{n}_h} \cdot (S_h \boldsymbol{u})\, ds \Big| &\leq \Big(\sum_{e \in \mathcal{E}_h^B} h_e \int_e \big| \frac{\partial \boldsymbol{v}}{\partial \boldsymbol{n}_h} \big|^2\, ds \Big)^{1/2} \Big(\sum_{e \in \mathcal{E}_h^B} h_e^{-1} \int_e |S_h \boldsymbol{u}|^2\, ds \Big)^{1/2} \\ &\leq C h^k \|\boldsymbol{u}\|_{H^{k+1}(\Omega)} \|\boldsymbol{v}\|_{1,h}, \end{aligned}$$

and

$$\begin{aligned} \Big| \sum_{e \in \mathcal{E}_h^B} \frac{\sigma}{h_e} \int_e (S_h \boldsymbol{u}) \cdot (S_h \boldsymbol{v})\, ds \Big| &\leq \sigma \Big(\sum_{e \in \mathcal{E}_h^B} h_e^{-1} \int_e |S_h \boldsymbol{u}|^2\, ds \Big)^{1/2} \Big(\sum_{e \in \mathcal{E}_h^B} h_e^{-1} \int_e |S_h \boldsymbol{v}|^2\, ds \Big)^{1/2} \\ &\leq C h^k \|\boldsymbol{u}\|_{H^{k+1}(\Omega)} \|\boldsymbol{v}\|_{1,h}. \end{aligned}$$

Thus, the first estimate (2.5.1) holds.

Similarly, another use of the Cauchy-Schwarz inequality with Lemma 2.5.1 yields

$$\begin{aligned}\big|b_h^e(\boldsymbol{u},(q,\mu))\big| &= \Big|\sum_{e\in\mathcal{E}_h^B}\int_e (S_h\boldsymbol{u}\cdot\boldsymbol{n}_h)\mu\,ds\Big| \\ &\le \Big(\sum_{e\in\mathcal{E}_h^B} h_e^{-1}\int_e |S_h\boldsymbol{u}|^2\,ds\Big)^{1/2}\Big(\sum_{e\in\mathcal{E}_h^B} h_e\|\mu\|_{L^2(e))}^2\,ds\Big)^{1/2} \\ &\le Ch^k\|\boldsymbol{u}\|_{H^{k+1}(\Omega)}\|\mu\|_{-1/2,h},\end{aligned}$$

and this completes the proof. □

2.5.2 Approximation Properties of the Kernel

We define the discrete kernel as

$$\boldsymbol{Z}_h = \{\boldsymbol{v}\in\boldsymbol{V}_h:\ b_h^e(\boldsymbol{v},(q,\mu))=0,\ \forall(q,\mu)\in\mathring{Q}_h\times\mathring{X}_h\}.$$

Note that if $\boldsymbol{v}\in\boldsymbol{Z}_h$, then $\operatorname{div}\boldsymbol{v}=0$ in Ω_h (cf. Lemma 2.3.1), and

$$\int_{\partial\Omega_h}((S_h\boldsymbol{v})\cdot\boldsymbol{n}_h)\mu\,ds=0 \qquad \forall\mu\in\mathring{X}_h. \tag{2.5.2}$$

In this section, we show that the kernel $\boldsymbol{Z}_h$ has optimal order approximation properties with respect to divergence-free smooth functions. Finally, we define the orthogonal complement of $\boldsymbol{Z}_h$ as

$$\boldsymbol{Z}_h^\perp := \{\boldsymbol{v}\in\boldsymbol{V}_h:\ (\boldsymbol{v},\boldsymbol{w})_{1,h}=0\ \ \forall\boldsymbol{w}\in\boldsymbol{Z}_h\},$$

where $(\cdot,\cdot)_{1,h}$ is the inner product on $\boldsymbol{V}_h$ that induces the norm $\|\cdot\|_{1,h}$.

Lemma 2.5.3. *There holds*

$$\beta_e\|\boldsymbol{w}\|_{1,h}\le\sup_{(q,\mu)\in\mathring{Q}_h\times\mathring{X}_h\setminus\{0\}}\frac{b_h^e(\boldsymbol{w},(q,\mu))}{\|(q,\mu)\|} \qquad \forall\boldsymbol{w}\in\boldsymbol{Z}_h^\perp.$$

Proof. The result follows from Corollary 2.4.10 and standard results in mixed finite element theory (cf. [9, Lemma 12.5.10]). □

Theorem 2.5.4. *For any* $\boldsymbol{u} \in \boldsymbol{H}^{k+1}(\Omega) \cap \boldsymbol{H}_0^1(\Omega)$ *with* $\operatorname{div} \boldsymbol{u} = 0$*, there holds*

$$\inf_{\boldsymbol{w} \in \boldsymbol{Z}_h} |||\boldsymbol{u} - \boldsymbol{w}|||_h \leq C h^k \|\boldsymbol{u}\|_{H^{k+1}(\Omega)}. \tag{2.5.3}$$

Proof. Let $\boldsymbol{v} \in \boldsymbol{V}_h$ be arbitrary. By Lemma 2.5.3, we find $\boldsymbol{y} \in \boldsymbol{Z}_h^\perp$ such that

$$b_h^e(\boldsymbol{y}, (q, \mu)) = b_h^e(\boldsymbol{u} - \boldsymbol{v}, (q, \mu)) \qquad \forall (q, \mu) \in \mathring{Q}_h \times \mathring{X}_h,$$

and

$$\|\boldsymbol{y}\|_{1,h} \leq C \beta_e^{-1} \|\boldsymbol{u} - \boldsymbol{v}\|_{1,h},$$

where $C > 0$ is the continuity constant of the bilinear form b_h^e (cf. (2.4.6)). Similarly, we find $\boldsymbol{z} \in \boldsymbol{Z}_h^\perp$ satisfy

$$b_h^e(\boldsymbol{z}, (q, \mu)) = -b_h^e(\boldsymbol{u}, (q, \mu)) \qquad \forall (q, \mu) \in \mathring{Q}_h \times \mathring{X}_h.$$

Then $\boldsymbol{w} := \boldsymbol{v} + \boldsymbol{y} + \boldsymbol{z} \in \boldsymbol{Z}_h$, and

$$\begin{aligned} \|\boldsymbol{u} - \boldsymbol{w}\|_{1,h} &\leq \|\boldsymbol{u} - \boldsymbol{v}\|_{1,h} + \|\boldsymbol{y}\|_{1,h} + \|\boldsymbol{z}\|_{1,h} \\ &\leq (1 + C\beta_e^{-1}) \|\boldsymbol{u} - \boldsymbol{v}\|_{1,h} + \|\boldsymbol{z}\|_{1,h}. \end{aligned}$$

By Lemma 2.5.3 and Lemma 2.5.2,

$$\beta_e \|\boldsymbol{z}\|_{1,h} \leq \sup_{(q,\mu) \in \mathring{Q}_h \times \mathring{X}_h \setminus \{0\}} \frac{b_h^e(\boldsymbol{u}, (q, \mu))}{\|(q, \mu)\|} \leq C h^k \|\boldsymbol{u}\|_{H^{k+1}(\Omega)},$$

and so, by Lemma 2.4.1,

$$\begin{aligned} |||\boldsymbol{u} - \boldsymbol{w}|||_h &\leq |||\boldsymbol{u} - \boldsymbol{v}|||_h + C\|\boldsymbol{v} - \boldsymbol{w}\|_{1,h} \leq C\big(|||\boldsymbol{u} - \boldsymbol{v}|||_h + \|\boldsymbol{u} - \boldsymbol{w}\|_{1,h}\big) \\ &\leq C(1 + \beta_e^{-1})\big(|||\boldsymbol{u} - \boldsymbol{v}|||_h + \|\boldsymbol{u} - \boldsymbol{v}\|_{1,h} + h^k \|\boldsymbol{u}\|_{H^{k+1}(\Omega)}\big) \qquad \forall \boldsymbol{v} \in \boldsymbol{V}_h. \end{aligned}$$

Taking $\boldsymbol{v}$ to be the nodal interpolant of $\boldsymbol{u}$, we obtain the desired result. □

2.5.3 Error Estimates of the Method

In this section, we show an error estimate for both velocity and pressure. Both error estimates are of optimal order. In particular, we show that with the inclusion of the Lagrange multiplier in the method, there is an additional power of h in the velocity error, compensating its dependence on the inverse of the viscosity and mitigating the lack of pressure robustness.

Theorem 2.5.5. *Suppose that the solution of* (2.1.1) *has regularity* $(\boldsymbol{u}, p) \in \boldsymbol{H}^{k+1}(\Omega) \cap \boldsymbol{H}^1_0(\Omega) \times H^1(\Omega)$. *Furthermore, without loss of generality, assume that* $p|_{\Omega_h} \in L^2_0(\Omega_h)$. *Then,*

$$\|\boldsymbol{u} - \boldsymbol{u}_h\|_{1,h} \leq C\big(h^k \|\boldsymbol{u}\|_{H^{k+1}(\Omega)} + \nu^{-1} \inf_{\mu \in X_h} \|p - \mu\|_{-1/2,h}\big), \tag{2.5.4a}$$

$$\|p - p_h\|_{L^2(\Omega_h)} \leq C(\nu h^k \|\boldsymbol{u}\|_{H^{k+1}(\Omega)} + \inf_{\mu \in X_h} \|p - \mu\|_{-1/2,h} + \inf_{q_h \in \hat{Q}_h} \|p - q_h\|_{L^2(\Omega)}), \tag{2.5.4b}$$

$$\|\mathring{p} - \lambda_h\|_{-1/2,h} \leq C\Big(\nu h^k \|\boldsymbol{u}\|_{H^{k+1}(\Omega)} + \inf_{\mu \in X_h} \|p - \mu\|_{-1/2,h}\Big), \tag{2.5.4c}$$

where $\mathring{p} := p - \frac{1}{|\partial\Omega_h|} \int_{\partial\Omega_h} p \, ds$. *In particular, if* $p \in H^{k+1}(\Omega)$ *there holds*

$$\|\boldsymbol{u} - \boldsymbol{u}_h\|_{1,h} \leq C\big(h^k \|\boldsymbol{u}\|_{H^{k+1}(\Omega)} + \nu^{-1} h^{k+1} \|p\|_{H^{k+1}(\Omega)}\big), \tag{2.5.5a}$$

$$\|p - p_h\|_{L^2(\Omega_h)} \leq C\big(\nu h^k \|\boldsymbol{u}\|_{H^{k+1}(\Omega)} + h^k \|p\|_{H^k(\Omega)}\big), \tag{2.5.5b}$$

$$\|\mathring{p} - \lambda_h\|_{-1/2,h} \leq C\big(\nu h^k \|\boldsymbol{u}\|_{H^{k+1}(\Omega)} + h^{k+1} \|p\|_{H^{k+1}(\Omega)}\big). \tag{2.5.5c}$$

Proof. Let $\boldsymbol{w} \in \boldsymbol{Z}_h$ be arbitrary. Note that we have mean value zero constraint for $\boldsymbol{v} \cdot \boldsymbol{n}_h$ on $\partial\Omega_h$ for all $\boldsymbol{v} \in \boldsymbol{V}_h$. Denote $\mathring{\mu} = \mu - \frac{1}{|\partial\Omega_h|} \int_{\partial\Omega_h} \mu \, ds \in \mathring{X}_h$.

Then we have

$$\int_{\partial\Omega_h} (\boldsymbol{v} \cdot \boldsymbol{n}_h)(\lambda_h - \mathring{\mu}) \, ds = \int_{\partial\Omega_h} (\boldsymbol{v} \cdot \boldsymbol{n}_h)(\lambda_h - \mu) \, ds$$

We then have, for all $\boldsymbol{v} \in \boldsymbol{Z}_h$ and $\mu \in X_h$,

$$\begin{aligned} a_h(\boldsymbol{u}_h - \boldsymbol{w}, \boldsymbol{v}) &= \int_{\Omega_h} \boldsymbol{f} \cdot \boldsymbol{v} - a_h(\boldsymbol{w}, \boldsymbol{v}) - b_h(\boldsymbol{v}, (p_h, \lambda_h)) \\ &= -\nu \int_{\Omega_h} \Delta \boldsymbol{u} \cdot \boldsymbol{v} \, dx - a_h(\boldsymbol{w}, \boldsymbol{v}) - \int_{\partial\Omega_h} (\boldsymbol{v} \cdot \boldsymbol{n}_h)(\lambda_h - p) \, ds \\ &= -\nu \int_{\Omega_h} \Delta \boldsymbol{u} \cdot \boldsymbol{v} \, dx - a_h(\boldsymbol{w}, \boldsymbol{v}) - \int_{\partial\Omega_h} (\boldsymbol{v} \cdot \boldsymbol{n}_h)(\mu - p) \, ds \\ &\quad - \int_{\partial\Omega_h} (\boldsymbol{v} \cdot \boldsymbol{n}_h)(\lambda_h - \mathring{\mu}) \, ds. \end{aligned}$$

Therefore by Lemma 2.5.2, the continuity of $a_h(\cdot, \cdot)$ (cf. (2.4.3)), and the Cauchy-Schwarz inequality,

$$\begin{aligned} a_h(\boldsymbol{u}_h - \boldsymbol{w}, \boldsymbol{v}) &\le C\big(\nu h^k \|\boldsymbol{u}\|_{H^{k+1}(\Omega)} + \|p - \mu\|_{-1/2,h}\big)\|\boldsymbol{v}\|_{1,h} \\ &\quad + a_h(\boldsymbol{u} - \boldsymbol{w}, \boldsymbol{v}) - \int_{\partial\Omega_h} (\boldsymbol{v} \cdot \boldsymbol{n}_h)(\lambda_h - \mathring{\mu}) \, ds \\ &\le C\big(\nu h^k \|\boldsymbol{u}\|_{H^{k+1}(\Omega)} + \nu(1+\sigma)|||\boldsymbol{u} - \boldsymbol{w}|||_h + \|p - \mu\|_{-1/2,h}\big)\|\boldsymbol{v}\|_{1,h} \\ &\quad - \int_{\partial\Omega_h} (\boldsymbol{v} \cdot \boldsymbol{n}_h)(\lambda_h - \mathring{\mu}) \, ds. \end{aligned}$$

We then use (2.5.2) and (2.4.1) to obtain

$$\int_{\partial\Omega_h} (\boldsymbol{v} \cdot \boldsymbol{n}_h)(\lambda_h - \mathring{\mu}) \, ds = \int_{\partial\Omega_h} \big((\boldsymbol{v} - S_h\boldsymbol{v}) \cdot \boldsymbol{n}_h\big)(\lambda_h - \mathring{\mu}) \, ds \le C c_\delta \|\boldsymbol{v}\|_{1,h} \|\lambda_h - \mathring{\mu}\|_{-1/2,h}.$$

Setting $\boldsymbol{v} = \boldsymbol{u}_h - \boldsymbol{w}$, applying the coercivity of $a_h(\cdot, \cdot)$ and Theorem 2.5.4, we obtain

$$c_1 \nu \|\boldsymbol{u}_h - \boldsymbol{w}\|_{1,h} \le C\big(\nu(1+\sigma) h^k \|\boldsymbol{u}\|_{H^{k+1}(\Omega)} + \|p - \mu\|_{-1/2,h} + c_\delta \|\lambda_h - \mathring{\mu}\|_{-1/2,h}\big) \quad (2.5.6)$$

for $\boldsymbol{w} \in \boldsymbol{Z}_h$ satisfying (2.5.3).

Next, let $P_h \in \mathring{Q}_h$ be the L^2-projection of p and note that, due to the definitions of the finite element spaces, $\int_{\Omega_h} (\operatorname{div} \boldsymbol{v})(p - P_h)\, dx = 0$ for all $\boldsymbol{v} \in \boldsymbol{V}_h$. This identity, along with the inf-sup stability estimate given in Theorem 2.4.9 yields

$$\begin{aligned}\beta \|(p_h - P_h, \lambda_h - \mathring{\mu})\| &\leq \sup_{\boldsymbol{v} \in \boldsymbol{V}_h \setminus \{0\}} \frac{b_h(\boldsymbol{v}, (p_h - P_h, \lambda_h - \mathring{\mu}))}{\|\boldsymbol{v}\|_{1,h}} \\ &= \sup_{\boldsymbol{v} \in \boldsymbol{V}_h \setminus \{0\}} \frac{b_h(\boldsymbol{v}, (p_h - p, \lambda_h - \mathring{\mu}))}{\|\boldsymbol{v}\|_{1,h}}.\end{aligned}$$

Using Lemma 2.5.2, we write the numerator as

$$\begin{aligned}b_h(\boldsymbol{v}, (p_h - p, \lambda_h - \mathring{\mu})) &= b_h(\boldsymbol{v}, (p_h, \lambda_h)) - b_h(\boldsymbol{v}, (p, \mathring{\mu})) \\ &= \int_{\Omega_h} \boldsymbol{f} \cdot \boldsymbol{v}\, dx - a_h(\boldsymbol{u}_h, \boldsymbol{v}) + \int_{\Omega_h} (\operatorname{div} \boldsymbol{v}) p\, dx - \int_{\partial\Omega_h} (\boldsymbol{v} \cdot \boldsymbol{n}_h) \mu\, ds \\ &\leq C\nu h^k \|\boldsymbol{u}\|_{H^{k+1}(\Omega)} \|\boldsymbol{v}\|_{1,h} + a_h(\boldsymbol{u} - \boldsymbol{u}_h, \boldsymbol{v}) \\ &\quad - \int_{\partial\Omega_h} (\boldsymbol{v} \cdot \boldsymbol{n}_h)(\mu - p)\, ds.\end{aligned}$$

By continuity and the Cauchy-Schwarz inequality,

$$\beta \|(p_h - P_h, \lambda_h - \mathring{\mu})\| \leq C\big(\nu h^k \|\boldsymbol{u}\|_{H^{k+1}(\Omega)} + c_2\nu(1+\sigma)|||\boldsymbol{u} - \boldsymbol{u}_h|||_h + \|p - \mu\|_{-1/2,h}\big) \tag{2.5.7}$$

$$\begin{aligned}&\leq C\big(\nu h^k \|\boldsymbol{u}\|_{H^{k+1}(\Omega)} + c_2\nu(1+\sigma)\big(|||\boldsymbol{u} - \boldsymbol{w}|||_h + \|\boldsymbol{u}_h - \boldsymbol{w}\|_{1,h}\big) + \|p - \mu\|_{-1/2,h}\big) \\ &\leq C\big(\nu(1+\sigma) h^k \|\boldsymbol{u}\|_{H^{k+1}(\Omega)} + c_2\nu(1+\sigma)\|\boldsymbol{u}_h - \boldsymbol{w}\|_{1,h} + \|p - \mu\|_{-1/2,h}\big).\end{aligned}$$

Inserting this estimate into (2.5.6), we get

$$\nu\big(c_1 - C\beta^{-1} c_2 (1+\sigma) c_\delta\big)\|\boldsymbol{u}_h - \boldsymbol{w}\|_{1,h} \leq C\nu(1+\sigma) h^k \|\boldsymbol{u}\|_{H^{k+1}(\Omega)} + C\|p - \mu\|_{-1/2,h}. \tag{2.5.8}$$

Using the approximation properties of the discrete kernel once again (cf. Theorem 2.5.4), and for c_δ sufficiently small,

$$\|\boldsymbol{u} - \boldsymbol{u}_h\|_{1,h} \leq C\big(h^k \|\boldsymbol{u}\|_{H^{k+1}(\Omega)} + \nu^{-1} \inf_{\mu \in X_h} \|p - \mu\|_{-1/2,h}\big).$$

This establishes the velocity estimate (2.5.4a).

To obtain the estimate for the pressure approximation (2.5.4b), we use the triangle inequality and the approximation properties of the L^2-projection:

$$\|p - p_h\|_{L^2(\Omega_h)} \leq \|p_h - P_h\|_{L^2(\Omega_h)} + \inf_{q_h \in \mathring{Q}_h} \|p - q_h\|_{L^2(\Omega_h)}.$$

Inserting (2.5.7) and (2.5.8) into the right-hand side yields the desired bound for the pressure. Likewise, combining (2.5.7) and (2.5.8) yields

$$\|\mathring{p} - \lambda_h\|_{-1/2,h} \leq C\Big(\nu h^k \|\boldsymbol{u}\|_{H^{k+1}(\Omega)} + \inf_{\mu \in X_h} \big(\|p - \mu\|_{-1/2,h} + \|\mathring{p} - \mathring{\mu}\|_{-1/2,h}\big)\Big).$$

Applications of the Cauchy-Schwarz inequality show $\|\mathring{p} - \mathring{\mu}\|_{-1/2,h} \leq C\|p - \mu\|_{-1/2,h}$ on quasi-uniform meshes, and therefore (2.5.4c) holds.

Next, we estimate the term $\inf_{\mu \in X_h} \|p - \mu\|_{-1/2,h}$ for $p \in H^{k+1}(\Omega)$. With an abuse of notation, let μ_I denote the kth degree nodal Lagrange interpolant of p on Ω_h with respect to $\mathfrak{T}_h^{ct}$. Notice that $\mu_I|_{\partial\Omega_h} \in X_h$. Applying a trace inequality, followed by standard interpolation estimates and shape regularity of $\mathfrak{T}_h^{ct}$, we obtain for each $e \in \mathcal{E}_h^B$,

$$\|p - \mu_I\|_{L^2(e)}^2 \leq C\big(h_e^{-1}\|p - \mu_I\|_{L^2(T_e)}^2 + h_e\|\nabla(p - \mu_I)\|_{L^2(T_e)}^2\big) \leq C h_e^{2k+1}\|p\|_{H^{k+1}(T_e)}^2,$$

where $T_e \in \mathfrak{T}_h^{ct}$ satisfies $e \subset \partial T_e$. We thus conclude from the definition of $\|\cdot\|_{-1/2,h}$ that

$$\inf_{\mu \in X_h} \|p - \mu\|_{-1/2,h} \leq C h^{k+1} \|p\|_{H^{k+1}(\Omega)}. \tag{2.5.9}$$

Finally, the estimates (2.5.5a)-(2.5.5c) follow from (2.5.4a)-(2.5.4c), interpolation estimates, and (2.5.9). □

3.0 A CutFEM Divergence–Free Discretization for the Stokes Problem

CutFEM [10] is one of the prevalent classes of unfitted finite element method that uses a Nitsche-based formulation. The basic idea is to enforce boundary conditions via penalization, and to add ghost penalty stabilization.

Several rigorous stability and convergence analysis of the unfitted finite elements have been done since the a CutFEM was introduced in [6]. For instance, the $\boldsymbol{\mathcal{P}}_1^{bubble} - \mathcal{P}_1$ unfitted finite element was studied in [16], and the optimal order of convergence was achieved in the energy norm.

In this chapter, we construct and analyze a CutFEM for the Stokes problem based on the Scott-Vogelius pair $\boldsymbol{\mathcal{P}}_k - \mathcal{P}_{k-1}^{disc}$ on Clough-Tocher splits. For CutFEM, we start with a background mesh $\mathcal{S}_h$, that contains the physical domain Ω similar to the construction of the Boundary Correction method. However, we have two computational domain in this case. One is an interior computational domain consists of all the triangles in $\mathcal{S}_h$ that are strictly contained in $\bar{\Omega}$; the other one is an exterior computational domain that consists of both the triangles in the interior computational domain and the triangles in $\mathcal{S}_h$ that are cut by the boundary of the physical domain.

Similar to the Boundary Correction method, the discrete inf-sup condition cannot be immediately obtained by standard results due to the unfitted nature of the method. The uniform stability results with respect to the mesh parameter h have been shown for many unfitted finite elements over the years. The uniform stability condition was shown for the lowest order Taylor-Hood element $\boldsymbol{\mathcal{P}}_2 - \mathcal{P}_1$ in [33]. The same uniform stability condition was also shown for a wider range of elements including $\boldsymbol{\mathcal{P}}_{k+1} - \mathcal{P}_k$, where $k \geq 1$ and $\boldsymbol{\mathcal{P}}_{k+d} - \mathcal{P}_k$, where $d = 2$ if the problem is in

2D and $d = 3$ if the problem is in 3D in [27]. We show the same uniform results for the general Scott-Vogelius pair $\boldsymbol{\mathcal{P}}_k - \mathcal{P}_{k-1}^{disc}$ on Clough-Tocher splits, using the same technique used in the Boundary Correction project and the framework provided in [27]. Additionally, even though we cannot produce a exactly divergence-free velocity solution like in the domain-fitted case, because of the ghost penalty terms in the CutFEM, we still show a divergence-free property for the velocity solution on a mesh-dependent interior domain.

3.1 Preliminaries

We consider the Stokes problem on a bounded, open domain $\Omega \subset \mathbb{R}^d$ with smooth boundary:

$$-\Delta \boldsymbol{u} + \nabla p = \boldsymbol{f} \qquad \text{in } \Omega, \tag{3.1.1a}$$

$$\operatorname{div} \boldsymbol{u} = 0 \qquad \text{in } \Omega, \tag{3.1.1b}$$

$$\boldsymbol{u} = 0 \qquad \text{on } \Gamma := \partial\Omega. \tag{3.1.1c}$$

We embed the PDE domain Ω into an open, polytopal domain to formulate the finite element method for 3.1.1. Let $S \subset \mathbb{R}^d$ be a polygon where $\Omega \subset S$. Denote the quasi-uniform triangulation of S with shape-regular triangles by $\mathcal{S}_h$, and every $T \in \mathcal{S}_h$ is a closed set. Then, we define the interior computational mesh and the associated domain:

$$\mathcal{T}_h^i = \{T \in \mathcal{S}_h : \bar{T} \subset \bar{\Omega}\}, \qquad \Omega_h^i = \operatorname{int}\Big(\bigcup_{T \in \mathcal{T}_h^i} \bar{T} \Big) \subset \bar{\Omega}.$$

By connecting the vertices of each triangle $T \in \mathcal{S}_h$ to its barycenter, we obtain the Clough-Tocher refinement of $\mathcal{S}_h$, $\mathcal{S}_h^{ct}$. We then define the analogous set with respect to the Clough-Tocher refinement:

$$\mathcal{T}_h^{ct,i} := \{K \in \mathcal{S}_h^{ct} : \ K \subset T, \ \exists T \in \mathcal{T}_h^i\}.$$

Remark 3.1.1. Note that

$$\Omega_h^i = \mathrm{Int}\Big(\bigcup_{K \in \mathcal{T}_h^{ct,i}} \bar{K} \Big).$$

However,

$$\mathcal{T}_h^{ct,i} \subset \{K \in \mathcal{S}_h^{ct} : K \subset \Omega\}$$

and this inclusion is generally strict.

On the interior domain, we define $\mathcal{F}_h^i$ to be the set of $(d-1)$-dimensional interior faces of the unrefined triangulation $\mathcal{T}_h^i$. We also let

$$\mathcal{T}_h^\Gamma := \{T \in \mathcal{S}_h : \mathrm{meas}_{d-1}(T \cap \Gamma) > 0\}, \qquad \Omega_h^\Gamma = \mathrm{Int}\Big(\bigcup_{T \in \mathcal{T}_h^\Gamma} \bar{T} \Big)$$

to be the set of simplices that cut through the interface Γ and the corresponding domain, respectively.

Define

$$\mathcal{T}_h^e := \{T \in \mathcal{S}_h : T \in \mathcal{T}_h^i \text{ or } T \in \mathcal{T}_h^\Gamma\}, \qquad \Omega_h^e = \mathrm{Int}\Big(\bigcup_{T \in \mathcal{T}_h^e} \bar{T} \Big)$$

to be the set of triangles that are either interior or cut through the interface Γ and the corresponding domain, respectively. We refer to these quantities as the exterior triangulation and exterior domain, respectively. The analogous sets with respect to the Clough-Tocher refinement are given by

$$\mathcal{T}_h^{ct,\Gamma} := \{K \in \mathcal{S}_h^{ct} : \ K \subset T, \ \exists T \in \mathcal{T}_h^\Gamma\},$$

$$\mathcal{T}_h^{ct,e} := \{K \in \mathcal{S}_h^{ct} : \ K \subset T, \ \exists T \in \mathcal{T}_h^e\}.$$

Note that now we have

$$\Omega_h^\Gamma = \mathrm{Int}\Big(\bigcup_{K \in \mathcal{T}_h^{ct,\Gamma}} \bar{K} \Big), \quad \text{and} \quad \Omega_h^e = \mathrm{Int}\Big(\bigcup_{K \in \mathcal{T}_h^{ct,e}} \bar{K} \Big).$$

In Figure 5, we illustrate the different computational mesh in different colors.

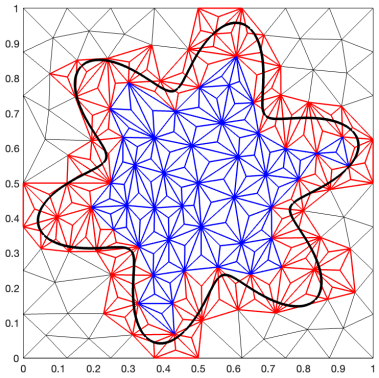

Figure 5: $\mathcal{T}_h^{ct,\Gamma}$ consists of triangles with red edges. $\mathcal{T}_h^{ct,i}$ consists of triangles with blue edges. $\mathcal{T}_h^{ct,e}$ consists of all the colored triangles.

Remark 3.1.2. Note that, in general, there exists $K \in \mathcal{T}_h^{ct,\Gamma}$ such that $\bar{K} \cap \bar{\Omega} = \emptyset$. We illustrate those triangles in Figure 6. Consequently, in the finite element method presented below, there exists active basis functions with support strictly outside the physical domain Ω.

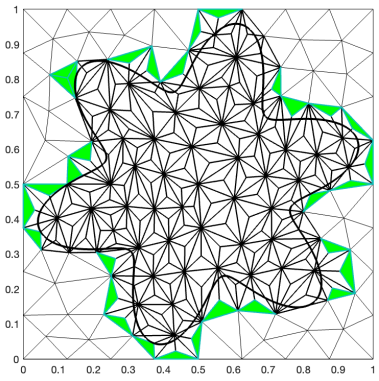

Figure 6: The green triangles are $K \in \mathcal{T}_h^{ct,\Gamma}$ where $\bar{K} \cap \bar{\Omega} = \emptyset$

We define the sets of faces:

$$\mathcal{F}^{\Gamma} := \{F : \ F \text{ is a face in } \mathcal{T}_h^{\Gamma}, \ F \not\subset \partial\Omega_h^e\},$$
$$\mathcal{F}^{e} := \{F : \ F \text{ is an interior face in } \mathcal{T}_h^{e}\},$$
$$\mathcal{F}^{ct,\Gamma} := \{F : \ F \text{ is a face in } \mathcal{T}_h^{ct,\Gamma}, \ F \not\subset \partial\Omega_h^e\},$$
$$\mathcal{F}^{ct,e} := \{F : \ F \text{ is an interior face in } \mathcal{T}_h^{ct,e}\}.$$

For $K \in \mathcal{T}_h^{ct,\Gamma}$, we define $K_\Gamma = \overline{K} \cap \Gamma$, so that $\sum_{K \in \mathcal{T}_h^{ct,\Gamma}} |K_\Gamma| = |\Gamma|$. For a simplex K, we set $h_F = \text{diam}(F)$, and for a face F, we set. Note that, because of the quasi-uniformity and shape-regularity assumption, there holds $h_K \approx h := \max_{T \in \mathcal{T}_h} h_T$ for all $K \in \mathcal{T}_h^{ct,e}$ and $h_F \approx h$ for all $F \in \mathcal{F}^{ct,e}$. We denote by $\boldsymbol{n}$ an outward normal of a domain which will be clear from its context. The constant C (with or without subscripts) will denote a generic positive constant that is independent of h, how the boundary Γ cuts the mesh, or any method-dependent parameters.

Same as the previous chapter, we use $\mathcal{P}_k(D)$ to denote the polynomials on D with degree at most k, for a subset $D \subset \Omega$, and the boldface $\boldsymbol{\mathcal{P}}_k(D)$ to denote the vector-valued polynomials on D with degree at most k, for a subset $D \subset \Omega$.

For an integer $k \geq d$, define the finite element spaces with respect to $\mathcal{T}_h^{ct,e}$:

$$\boldsymbol{V}_h = \{\boldsymbol{v} \in \boldsymbol{H}^1(\Omega_h^e) : \ \boldsymbol{v}|_K \in \boldsymbol{\mathcal{P}}_k(K) \ \forall K \in \mathcal{T}_h^{ct,e}, \ \int_{\partial\Omega_h^i} \boldsymbol{v} \cdot \boldsymbol{n} = 0\},$$
$$Q_h = \{q \in L^2(\Omega_h^e) : \ q|_K \in \mathcal{P}_{k-1}(K) \ \forall K \in \mathcal{T}_h^{ct,e}, \ \int_{\Omega_h^i} q = 0\},$$

and the analogous spaces with respect to the interior mesh

$$\boldsymbol{V}_h^i = \{\boldsymbol{v} \in \boldsymbol{H}_0^1(\Omega_h^i) : \ \boldsymbol{v}|_K \in \boldsymbol{\mathcal{P}}_k(K) \ \forall K \in \mathcal{T}_h^{ct,i}\},$$
$$Q_h^i = \{q \in L_0^2(\Omega_h^i) : \ q|_K \in \mathcal{P}_{k-1}(K) \ \forall K \in \mathcal{T}_h^{ct,i}\}.$$

The definitions of the spaces imply that the divergence maps $\boldsymbol{V}_h$ into Q_h. Likewise, the divergence maps $\boldsymbol{V}_h^i$ into Q_h^i.

3.2 A Divergence-Free CutFEM

We modify the finite element method proposed in [27, Section 3.2] based on the Scott-Vogelius pair:

We first define a mesh-dependent bilinear form with grad-div stabilization:

$$a_h(\boldsymbol{u}, \boldsymbol{v}) := (\nabla \boldsymbol{u}, \nabla \boldsymbol{v}) + \gamma(\operatorname{div} \boldsymbol{u}, \operatorname{div} \boldsymbol{v}) + s_h(\boldsymbol{u}, \boldsymbol{v}) + \mathbf{j}_h(\boldsymbol{u}, \boldsymbol{v}) + \eta j_h(\boldsymbol{u}, \boldsymbol{v}),$$

where $(\cdot, \cdot)$ denotes the L^2 inner product over Ω, $\gamma \geq 0$ is the grad-div parameter, and $\eta > 0$ is a Nitsche-type penalty parameter,

$$s_h(\boldsymbol{u}, \boldsymbol{v}) = -\int_\Gamma ((\boldsymbol{n}^\intercal \nabla \boldsymbol{u}) \cdot \boldsymbol{v} + (\boldsymbol{n}^\intercal \nabla \boldsymbol{v}) \cdot \boldsymbol{u}),$$

$$j_h(\boldsymbol{u},\boldsymbol{v}) = \sum_{K\in\mathcal{T}_h^{ct,\Gamma}} \frac{1}{h_K}\int_{K_\Gamma} \boldsymbol{u}\cdot\boldsymbol{v},$$

$$\mathbf{j}_h(\boldsymbol{u},\boldsymbol{v}) = \sum_{F\in\mathcal{F}^{ct,\Gamma}} \sum_{\ell=1}^{k} h_F^{2\ell-1}\int_F [\partial_n^\ell \boldsymbol{u}][\partial_n^\ell \boldsymbol{v}].$$

We use $\partial_n^\ell \boldsymbol{v}$ to denote the derivative of order ℓ of $\boldsymbol{v}$ in the direction $\boldsymbol{n}$, and $[\boldsymbol{w}]|_F$ denotes the jump of a function $\boldsymbol{w}$ across F. The continuity equations are discretized via the bilinear form

$$b(p,\boldsymbol{v}) := -(p,\operatorname{div}\boldsymbol{v}) + \int_\Gamma (\boldsymbol{v}\cdot\boldsymbol{n})p.$$

The finite element method reads: Find $(\boldsymbol{u}_h, p_h)\in \boldsymbol{V}_h\times Q_h$ such that

$$\begin{cases} a_h(\boldsymbol{u}_h,\boldsymbol{v}_h) + b(p_h,\boldsymbol{v}_h) = (\boldsymbol{f},\boldsymbol{v}_h), \\ b(q_h,\boldsymbol{u}_h) - \frac{1}{1+\gamma} J_h(p_h,q_h) = 0 \end{cases} \tag{3.2.1}$$

for all $\boldsymbol{v}_h\in\boldsymbol{V}_h$, $q_h\in Q_h$, where

$$J_h(q,p) = \sum_{F\in\mathcal{F}^{ct,\Gamma}} \sum_{\ell=0}^{k-1} h_F^{2\ell+1}\int_F [\partial_n^\ell q][\partial_n^\ell p].$$

The main differences between our CutFEM discretizations and the other CutFEM discretizations [11, 10, 30, 27] are the terms $\mathbf{j}_h(\boldsymbol{u},\boldsymbol{v})$, and $J_h(q,p)$. In particular, for $\mathbf{j}_h(\boldsymbol{u},\boldsymbol{v})$, and $J_h(q,p)$, instead of summing over all faces F in $\mathcal{F}^\Gamma$, we are now summing over all faces F from $\mathcal{F}^{ct,\Gamma}$. Such faces may be completely outside the physical domain Ω.

Note that although for the term $j_h(\boldsymbol{u},\boldsymbol{v})$, we modified it to be summing over the triangles $K\in\mathcal{T}_h^{ct,\Gamma}$ from summing over the triangles $T\in\mathcal{T}_h^\Gamma$, we have $\bigcup_{K\in\mathcal{T}_h^{ct,\Gamma}}|K_\Gamma| = \bigcup_{T\in\mathcal{T}_h^\Gamma}|T_\Gamma| = |\Gamma|$. Therefore, $j_h(\boldsymbol{u},\boldsymbol{v})$ is equivalent to the analogous term in, e.g., [27].

3.2.1 Divergence-Free Property

A domain-fitted Scott-Vogelius FEM produces exactly divergence-free solution, but due to the stability term $J_h(\cdot,\cdot)$ in the discrete continuity equations, we do not have exactly divergence-free velocity solution to (3.2.1) on either the physical or the computational domain. However, the velocity solution to (3.2.1) does possess a divergence-free property on a mesh-dependent interior domain which is a subset of the interior computational domain Ω_h^i.

We define the set $\widetilde{\mathcal{T}}_h^{ct,\Gamma}$ to be the set of all simplices in $\mathcal{T}_h^{ct,\Gamma}$ together with those in $\mathcal{T}_h^{ct,i}$ that are touching these simplices :

$$\widetilde{\mathcal{T}}_h^{ct,\Gamma} = \{K \in \mathcal{T}_h^{ct,e} : \ \mathrm{meas}_{d-1}(\bar{K} \cap \bar{K}') > 0 \ \exists K' \in \mathcal{T}_h^{ct,\Gamma}\}.$$

This set's complement is given by a set of interior elements:

$$\widetilde{\mathcal{T}}_h^{ct,i} = \mathcal{T}_h^{ct,e} \backslash \widetilde{\mathcal{T}}_h^{ct,\Gamma} \subset \mathcal{T}_h^{ct,i},$$

and we define the domains

$$\widetilde{\Omega}_h^{ct,\Gamma} = \mathrm{Int}\Big(\bigcup_{K \in \widetilde{\mathcal{T}}_h^{ct,\Gamma}} \bar{K} \Big), \qquad \widetilde{\Omega}_h^{ct,i} = \mathrm{Int}\Big(\bigcup_{T \in \widetilde{\mathcal{T}}_h^{ct,i}} \bar{K} \Big).$$

We illustrate these two domains in Figure 7:

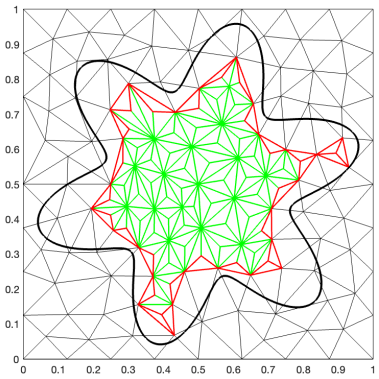

Figure 7: $\widetilde{\mathcal{T}_h^{ct,i}}$ consists of triangles with green edges, $\mathcal{T}_h^{ct,i}$ consists of all colored triangles.

Lemma 3.2.1. *(Divergence-free property) Suppose that* $\boldsymbol{u}_h \in \boldsymbol{V}_h$ *satisfies* (3.2.1). *Then* $\operatorname{div} \boldsymbol{u}_h = 0$ *on* $\widetilde{\Omega}_h^{ct,i}$.

Proof. We show the result in four steps.

1. Fix $K_* \in \widetilde{\mathcal{T}}_h^{ct,i}$, and set

$$q_1 = \begin{cases} 1 & \text{on } \widetilde{\Omega}_h^{ct,\Gamma}, \\ -(|\widetilde{\Omega}_h^{ct,\Gamma}| - |\Omega_h^{\Gamma}|)/|K_*| & \text{on } K_*, \\ 0 & \text{otherwise.} \end{cases}$$

We then have

$$\int_{\Omega_h^i} q_1 = \int_{\widetilde{\Omega}_h^{ct,\Gamma} \setminus \Omega_h^{\Gamma}} q_1 + \int_{K_*} q_1 = (|\widetilde{\Omega}_h^{ct,\Gamma}| - |\Omega_h^{\Gamma}|) + |K_*| \Big(- (|\widetilde{\Omega}_h^{ct,\Gamma}| - |\Omega_h^{\Gamma}|)/|K_*| \Big) = 0.$$

Thus, $q_1 \in Q_h$. We also have $J(p_h, q_1) = 0$ because q_1 being constant on $\Omega_h^{ct,\Gamma} \subset \widetilde{\Omega}_h^{ct,\Gamma}$ imples that $[\partial_n^l q_1] = 0$ on all $F \in \mathcal{F}^{ct,\Gamma}$. It then follows from (3.2.1) that

$$b(q_1, \boldsymbol{u}_h) = \int_{K_*} q_1 \mathrm{div}\, \boldsymbol{u}_h + \int_{\Omega \cap \widetilde{\Omega}_h^{ct,\Gamma}} q_1 \mathrm{div}\, \boldsymbol{u}_h - \int_\Gamma q_1 (\boldsymbol{u}_h \cdot \boldsymbol{n}) = 0$$

Then by plugging into the values of q_1, we have

$$-\frac{(|\widetilde{\Omega}_h^{ct,\Gamma}| - |\Omega_h^\Gamma|)}{|K_*|} \int_{K_*} \mathrm{div}\, \boldsymbol{u}_h + \int_{\Omega \cap \widetilde{\Omega}_h^{ct,\Gamma}} \mathrm{div}\, \boldsymbol{u}_h - \int_\Gamma \boldsymbol{u}_h \cdot \boldsymbol{n} = 0$$

By the Divergence Theorem, we have $\int_\Gamma \boldsymbol{u}_h \cdot \boldsymbol{n} = \int_\Omega \mathrm{div}\, \boldsymbol{u}_h$ and by the definition of $\widetilde{\Omega}_h^{ct,\Gamma}$ and $\widetilde{\Omega}_h^{ct,i}$, we have $\widetilde{\Omega}_h^{ct,i} = \Omega \backslash (\Omega \cap \widetilde{\Omega}_h^{ct,\Gamma})$. Therefore,

$$\begin{aligned} \frac{1}{|K_*|} \int_{K_*} \mathrm{div}\, \boldsymbol{u}_h &= \frac{1}{|\widetilde{\Omega}_h^{ct,\Gamma}| - |\Omega_h^\Gamma|} \Big(\int_{\Omega \cap \widetilde{\Omega}_h^{ct,\Gamma}} \mathrm{div}\, \boldsymbol{u}_h - \int_\Omega \mathrm{div}\, \boldsymbol{u}_h \Big) \\ &= \frac{-1}{|\widetilde{\Omega}_h^{ct,\Gamma}| - |\Omega_h^\Gamma|} \int_{\widetilde{\Omega}_h^{ct,i}} \mathrm{div}\, \boldsymbol{u}_h. \end{aligned} \tag{3.2.2}$$

2. Fix $K \in \widetilde{\mathcal{T}}_h^{ct,i} \backslash \{K_*\}$, and set

$$q_2 = \begin{cases} 1 & \text{on } K, \\ -\frac{|K|}{|K_*|} & \text{on } K_*, \\ 0 & \text{otherwise.} \end{cases}$$

Then $q_2 \in Q_h$, and $J_h(p_h, q_2) = 0$. By (3.2.1), we have

$$b(p_h, q_2) = \int_K q_2 \mathrm{div}\, \boldsymbol{u}_h + \int_{K_*} q_2 \mathrm{div}\, \boldsymbol{u}_h - \int_\Gamma q_2 (\boldsymbol{u}_h \cdot \boldsymbol{n}) = 0.$$

By plugging into the value of q_2, we conclude

$$\int_K \mathrm{div}\, \boldsymbol{u}_h = \frac{|K|}{|K_*|} \int_{K_*} \mathrm{div}\, \boldsymbol{u}_h.$$

We also have the trivial case where

$$\int_{K_*} \operatorname{div} \boldsymbol{u}_h = \frac{|K_*|}{|K_*|} \int_{K_*} \operatorname{div} \boldsymbol{u}_h$$

We then sum this expression over $K \in \widetilde{\mathcal{T}}_h^{ct,i}$ to conclude

$$\begin{aligned} \int_{\widetilde{\Omega}_h^{ct,i}} \operatorname{div} \boldsymbol{u}_h &= \sum_{K \in \widetilde{\mathcal{T}}_h^{ct,i}} \frac{|K|}{|K_*|} \int_{K_*} \operatorname{div} \boldsymbol{u}_h. \\ &= \frac{|\widetilde{\Omega}_h^{ct,i}|}{|K_*|} \int_{K_*} \operatorname{div} \boldsymbol{u}_h. \end{aligned} \tag{3.2.3}$$

3. We combine (3.2.2) and (3.2.3) to obtain

$$\int_{\widetilde{\Omega}_h^{ct,i}} \operatorname{div} \boldsymbol{u}_h = -\frac{|\widetilde{\Omega}_h^{ct,i}|}{|\widetilde{\Omega}_h^{ct,\Gamma}| - |\Omega_h^{\Gamma}|} \int_{\widetilde{\Omega}_h^{ct,i}} \operatorname{div} \boldsymbol{u}_h,$$

which implies

$$\int_{\widetilde{\Omega}_h^{ct,i}} \operatorname{div} \boldsymbol{u}_h = 0.$$

Using (3.2.2), and noting that $K_* \in \widetilde{\mathcal{T}}_h^{ct,i}$ was arbitrary, we have

$$\int_K \operatorname{div} \boldsymbol{u}_h = 0 \qquad \forall K \in \widetilde{\mathcal{T}}_h^{ct,i}.$$

4. Fix $K, K_\dagger \in \widetilde{\mathcal{T}}_h^{ct,i}$, and set

$$q_3 = \begin{cases} \operatorname{div} \boldsymbol{u}_h & \text{on } K_\dagger, \\ c & \text{on } K, \\ 0 & \text{otherwise,} \end{cases}$$

where $c \in \mathbb{R}$ is chosen such that $q_3 \in Q_h$. Then using (3.2.1),

$$\int_{K_\dagger} |\operatorname{div} \boldsymbol{u}_h|^2 = -c \int_K \operatorname{div} \boldsymbol{u}_h = 0.$$

Thus, $\operatorname{div} \boldsymbol{u}_h = 0$ on $\widetilde{\Omega}_h^{ct,i}$. □

3.3 Stability Analysis of the CutFEM

In this section, we show the inf-sup stability result for the CutFEM and using the inf-sup stability to derive a prior estimate.

We first define two mesh-dependent H^1-type norms:

$$\|\boldsymbol{u}\|_{\boldsymbol{V}_{0,h}}^2 = |\boldsymbol{u}|_{H^1(\Omega)}^2 + \eta j_h(\boldsymbol{u},\boldsymbol{u}) + \mathbf{j}_h(\boldsymbol{u},\boldsymbol{u}),$$
$$\|\boldsymbol{u}\|_{\boldsymbol{V}_h}^2 = \|\boldsymbol{u}\|_{\boldsymbol{V}_{0,h}}^2 + \gamma\|\mathrm{div}\,\boldsymbol{u}\|_{L^2(\Omega)}^2.$$

Note that we have $\|\mathrm{div}\,\boldsymbol{z}\|_{L^2(\Omega)}^2 \leq \|\boldsymbol{z}\|_{\boldsymbol{V}_{0,h}}^2$, for all $\boldsymbol{z} \in \boldsymbol{V}_h$. Therefore, by the definition of the two mesh-dependent norms, we have $\|\boldsymbol{z}\|_{\boldsymbol{V}_h} \leq (1+\gamma)^{1/2}\|\boldsymbol{z}\|_{\boldsymbol{V}_{0,h}}$, for all $\boldsymbol{z} \in \boldsymbol{V}_h$. Correspondingly, we have an associated dual norm for the right-hand data:

$$\|\boldsymbol{f}\|_{\boldsymbol{V}_h'} = \sup_{\boldsymbol{v}\in\boldsymbol{V}_h} \frac{(\boldsymbol{f},\boldsymbol{v})}{\|\boldsymbol{v}\|_{\boldsymbol{V}_h}}.$$

3.3.1 Inf-Sup Stability

Before we prove the main inf-sup stability result for the CutFEM, we first show a inf-sup condition with respect to the finite element spaces with support only on the interior computational domain Ω_h^i.

Theorem 3.3.1. *There exists a constant $\theta > 0$ and a constant $h_0 > 0$ such that we have the following result for $h \leq h_0$*

$$\theta\|q\|_{L^2(\Omega_h^i)} \leq \sup_{\boldsymbol{v}\in\boldsymbol{V}_h^i\setminus\{0\}} \frac{\int_{\Omega_h^i}(\mathrm{div}\,\boldsymbol{v})q}{\|\boldsymbol{v}\|_{H^1(\Omega_h^i)}} \qquad \forall q \in Q_h^i. \tag{3.3.1}$$

The constant $\theta > 0$ is independent and h.

Similar to the case in the Boundary Correction finite element method, due to the unfitted nature of the interior computational domain Ω_h^i, we cannot extend the standard LBB stability argument to find a constant θ independent of the mesh parameter h that satisfies the inf-sup condition with respect to the finite element spaces on the interior mesh.

Note that for the $k \geq d = 2$ case, Theorem 3.3.1 is exactly Lemma 2.4.6, since Ω_h from the previous chapter is exactly the interior computational domain Ω_h^i in this chapter, and the associated finite element spaces are also the same.

For the $k \geq d = 3$ case, we use the stability of the $\boldsymbol{\mathcal{P}}_d - \mathcal{P}_0$ pair provided in [27, Example 6.3] together with a local inf-sup stability result [Lemma 2.4.4] following the exact same steps from the proof of Lemma(2.4.6) to show Theorem(3.3.1).

Corollary 3.3.2. *The following stability is satisfied*

$$\theta_* \|q\|_{L^2(\Omega)} \leq \sup_{\substack{\boldsymbol{v} \in \boldsymbol{V}_h \\ \text{supp}(\boldsymbol{v}) \subset \Omega_h^i}} \frac{b(\boldsymbol{v}, q)}{\|\boldsymbol{v}\|_{\boldsymbol{V}_{0,h}}} + J_h^{1/2}(q, q) \qquad \forall\ q \in Q_h, \tag{3.3.2}$$

where $\theta_* > 0$ is independent of h and the position of Γ in the mesh.

Proof. Fix some $q \in Q_h$, such that $q|_{\Omega_h^i} \in L_0^2(\Omega_h^i)$. By [40, Lemma 5.1] for each pair of triangles K_1 and K_2 in $\mathcal{T}_h^{ct}$ where K_1 and K_2 share a common face, we have

$$\|q\|_{L^2(K_1)}^2 \leq C\Big(\|q\|_{L^2(K_2)}^2 + \sum_{l=0}^{k-1} h_F^{2l+1} \int_F [\partial_n^l q]^2 ds\Big).$$

Iterating this estimate and using the definition of $J_h(\cdot, \cdot)$, we have that

$$\|q\|_{L^2(\Omega)}^2 \leq \|q\|_{L^2(\Omega_h^e)}^2 \leq C\big(\|q\|_{L^2(\Omega_h^i)} + J_h(q, q)\big). \tag{3.3.3}$$

Using the inf-sup stability we get from Theorem 3.3.1 we have

$$\|q\|^2_{L^2(\Omega)} \leq C(\|q\|^2_{L^2(\Omega_h^i)} + J_h(q,q)) \leq C\theta^{-1}\Big(\frac{\int_{\Omega_h^i}(\operatorname{div}\boldsymbol{v})q}{\|\boldsymbol{v}\|_{H^1(\Omega_h^i)}} + J_h(q,q)\Big) \tag{3.3.4}$$

for some $\boldsymbol{v} \in \boldsymbol{V}_h$ with $\operatorname{supp}(\boldsymbol{v}) \subset \Omega_h^i$.

Then, since we have $\boldsymbol{v} = 0$ on Ω_h^Γ, $j_h(\boldsymbol{v},\boldsymbol{v}) = 0$. Then by an inverse inequality we have

$$\begin{aligned}\mathbf{j}_h(\boldsymbol{v},\boldsymbol{v}) &= \sum_{\substack{F\in\mathcal{F}^{ct,\Gamma}\\ F\subset\partial\Omega_h^i}}\sum_{\ell=1}^{k} h_F^{2\ell-1}\int_F [\partial_n^\ell \boldsymbol{v}]^2 \\ &\leq C\sum_{K\in\widetilde{\mathcal{T}}_h^{ct,\Gamma}\cap\mathcal{T}_h^{ct,i}} \|\nabla\boldsymbol{v}\|^2_{L^2(K)} \leq C\|\boldsymbol{v}\|^2_{H^1(\Omega_h^i)}.\end{aligned}$$

Thus we have $\|\boldsymbol{v}\|_{\boldsymbol{V}_{0,h}} \leq C\|\boldsymbol{v}\|_{H^1(\Omega_h^i)}$. Combining this with (3.3.4), we have (3.3.2). □

3.3.2 A Priori Estimates for the CutFEM

In this section, we derive a priori estimates of the CutFEM, thus showing the discrete problem (3.2.1) is well-posed.

We first show that the norm $\|\cdot\|_{\boldsymbol{V}_h}$ is continuous and coercive.

Lemma 3.3.3. *There exists constants $C_a, C_0 > 0$ such that*

$$\begin{aligned} a_h(\boldsymbol{u},\boldsymbol{v}) &\leq C_a\|\boldsymbol{u}\|_{\boldsymbol{V}_h}\|\boldsymbol{v}\|_{\boldsymbol{V}_h} \quad && \forall \boldsymbol{u},\boldsymbol{v} \in \boldsymbol{V}_h + \boldsymbol{H}^{k+1}(\Omega_h^e), \\ C_0\|\boldsymbol{v}\|^2_{\boldsymbol{V}_h} &\leq a_h(\boldsymbol{v},\boldsymbol{v}) && \forall \boldsymbol{v} \in \boldsymbol{V}_h. \end{aligned}$$

The proof of the continuity and coervicity of the norm $\|\cdot\|_{\boldsymbol{V}_{0,h}}$ can be found in [27]. Using the fact that $\|\boldsymbol{z}\|_{\boldsymbol{V}_h} \leq (1+\gamma)^{1/2}\|\boldsymbol{z}\|_{\boldsymbol{V}_{0,h}}$ and $\|\boldsymbol{z}\|_{\boldsymbol{V}_{0,h}} \leq \|\boldsymbol{z}\|_{\boldsymbol{V}_h}$, for all $\boldsymbol{z} \in \boldsymbol{V}_h$, we easily extend the results to $\|\cdot\|_{\boldsymbol{V}_h}$.

Theorem 3.3.4. *Suppose that* $(\boldsymbol{u}_h, p_h) \in \boldsymbol{V}_h \times Q_h$ *satisfies* (3.2.1). *Then*

$$\|p_h\|_{L^2(\Omega)} \leq C(1+\gamma)^{\frac{1}{2}} \|\boldsymbol{f}\|_{\boldsymbol{V}_h'}, \quad \|\boldsymbol{u}_h\|_{\boldsymbol{V}_h} \leq C\|\boldsymbol{f}\|_{\boldsymbol{V}_h'}, \tag{3.3.5}$$

for some $C > 0$ *independent of* γ, h, *and the position of* Γ *in the mesh. Consequently,* (3.2.1) *has a unique solution.*

Proof. We set $\boldsymbol{v}_h = \boldsymbol{u}_h$ in the first equation in (3.2.1), and $q_h = p_h$ in the second equation of (3.2.1) and subtract the resulting expressions:

$$a_h(\boldsymbol{u}_h, \boldsymbol{u}_h) + \frac{1}{1+\gamma} J_h(p_h, p_h) = (\boldsymbol{f}, \boldsymbol{u}_h).$$

By the coercivity of $a_h(.,.)$ stated in Lemma 3.3.3 and the Cauchy-Schwarz inequality, we have

$$C_0 \|\boldsymbol{u}_h\|_{\boldsymbol{V}_h}^2 + \frac{1}{1+\gamma} J_h(p_h, p_h) \leq (\boldsymbol{f}, \boldsymbol{u}_h) \leq \|\boldsymbol{f}\|_{\boldsymbol{V}_h'} \|\boldsymbol{u}_h\|_{\boldsymbol{V}_h}.$$

Using the Cauchy-Schwarz inequality again on the right-hand side, we have

$$\|\boldsymbol{f}\|_{\boldsymbol{V}_h'} \|\boldsymbol{u}_h\|_{\boldsymbol{V}_h} \leq \frac{1}{2}(\|\boldsymbol{f}\|_{\boldsymbol{V}_h'}^2 + \|\boldsymbol{u}_h\|_{\boldsymbol{V}_h}^2),$$

and so

$$\frac{C_0}{2} \|\boldsymbol{u}_h\|_{\boldsymbol{V}_h}^2 + \frac{1}{1+\gamma} J_h(p_h, p_h) \leq \frac{1}{2C_0} \|\boldsymbol{f}\|_{\boldsymbol{V}_h'}^2. \tag{3.3.6}$$

By the inf-sup stability estimate (3.3.2) and the fact that $\|\boldsymbol{z}\|_{\boldsymbol{V}_h} \leq (1+\gamma)^{1/2} \|\boldsymbol{z}\|_{\boldsymbol{V}_{0,h}}$ for all $\boldsymbol{z} \in \boldsymbol{V}_h$, there exists $\boldsymbol{z} \in \boldsymbol{V}_h$ with $(1+\gamma)^{-\frac{1}{2}} \|\boldsymbol{z}\|_{\boldsymbol{V}_h} \leq \|\boldsymbol{z}\|_{\boldsymbol{V}_{0,h}} = \|p_h\|_{L^2(\Omega)}$ and

$$\begin{aligned} \theta_* \|p_h\|_{L^2(\Omega)}^2 &\leq b(\boldsymbol{z}, p_h) + J_h^{1/2}(p_h, p_h) \|p_h\|_{L^2(\Omega)} \\ &= (\boldsymbol{f}, \boldsymbol{z}) - a_h(\boldsymbol{z}, \boldsymbol{u}_h) + J_h^{1/2}(p_h, p_h) \|p_h\|_{L^2(\Omega)}. \end{aligned}$$

By Lemma 3.3.3 and the Cauchy-Schwarz inequality, we have

$$\begin{aligned}\theta_*\|p_h\|^2_{L^2(\Omega)} &\le \big(\|\boldsymbol{f}\|_{\boldsymbol{V}_h'}\|\boldsymbol{z}\|_{\boldsymbol{V}_h} + C_a\|\boldsymbol{z}\|_{\boldsymbol{V}_h}\|\boldsymbol{u}_h\|_{\boldsymbol{V}_h}\big) + J_h^{1/2}(p_h,p_h)\|p_h\|_{L^2(\Omega)}\\ &\le \big((1+\gamma)^{\frac{1}{2}}(\|\boldsymbol{f}\|_{\boldsymbol{V}_h'} + C_a\|\boldsymbol{u}_h\|_{\boldsymbol{V}_h}) + J_h^{1/2}(p_h,p_h)\big)\|p_h\|_{L^2(\Omega)}.\end{aligned}$$

Dividing by $\|p_h\|_{L^2(\Omega)}$ and using (3.3.6), we conclude

$$\begin{aligned}\theta_*^2\|p_h\|^2_{L^2(\Omega)} &\le 3\big((1+\gamma)(\|\boldsymbol{f}\|^2_{\boldsymbol{V}_h'} + C_a^2\|\boldsymbol{u}_h\|^2_{\boldsymbol{V}_h}) + J_h(p_h,p_h)\big)\\ &\le 3(1+\gamma)\Big(1 + C_a^2C_0^{-2} + \frac{1}{2C_0}\Big)\|\boldsymbol{f}\|^2_{\boldsymbol{V}_h'}.\end{aligned}$$

This estimate and (3.3.6) yields the desired result (3.3.5). □

3.4 Convergence Analysis of the CutFEM

In this section we assume that the solution to the Stokes problem (3.1.1a) is sufficiently smooth, i.e., $\boldsymbol{u} \in \boldsymbol{H}^{k+2}(\Omega)$, $p \in H^{k+1}(\Omega)$, where we recall k is the polynomial degree in the definition of finite element spaces. Without loss of generality, we assume that $\operatorname{dist}(\partial S, \partial\Omega) = O(1)$.

Because $\partial\Omega$ is Lipschitz there exists an extension of p, which we also denote by p, such that $p \in H^{k+1}(S)$ and (cf. [53])

$$\|p\|_{H^\ell(S)} \le C\|p\|_{H^\ell(\Omega)} \quad \text{for } \ell = 0,1,\dots,k+1. \tag{3.4.1a}$$

An analogous extension of $\boldsymbol{u}$ is done in the following manner. First, write the velocity in terms of a potential function $\boldsymbol{u} = \nabla\times\boldsymbol{\psi}$. Then for $\boldsymbol{u} \in \boldsymbol{H}^{k+2}(\Omega)$, it satisfies that $\boldsymbol{\psi} \in \boldsymbol{H}^{k+3}(\Omega)$ and $\|\boldsymbol{\psi}\|_{H^{\ell+1}(\Omega)} \le C\|\boldsymbol{u}\|_{H^\ell(\Omega)}$ for $\ell = 0,1,\dots k+2$ [24, 18]. We extend $\boldsymbol{\psi}$ to S in a way such that $\|\boldsymbol{\psi}\|_{H^\ell(S)} \le C\|\boldsymbol{\psi}\|_{H^\ell(\Omega)}$ for $\ell = 0,1,\dots,k+3$, and let ω

be a smooth cut-off function with compact support in S and $\omega \equiv 1$ in Ω. We then define the velocity extension as $\boldsymbol{u} = \nabla \times (\omega \boldsymbol{\psi})$, so that $\boldsymbol{u}$ is divergence-free, vanishes on ∂S, and

$$\|\boldsymbol{u}\|_{H^\ell(S)} \leq C \|\boldsymbol{u}\|_{H^\ell(\Omega)} \quad \text{for } \ell = 0, 1, \ldots, k+2. \tag{3.4.1b}$$

Remark 3.4.1 (Consistency). Since we assume the exact solution to be smooth enough, all the ghost-penalty terms and Nitsche term from the discrete problem will vanish when we insert $\boldsymbol{u}$ and p into (3.2.1). Thus, the method (3.2.1) is consistent. In particular, there holds

$$\begin{cases} a_h(\boldsymbol{u}, \boldsymbol{v}_h) + b(p, \boldsymbol{v}_h) = (\boldsymbol{f}, \boldsymbol{v}_h), \\ b(q_h, \boldsymbol{u}) - \frac{1}{1+\gamma} J_h(p, q_h) = 0 \end{cases} \tag{3.4.2}$$

for all $\boldsymbol{v}_h \in \boldsymbol{V}_h$, $q_h \in Q_h$.

The following lemma is a direct application of [20, Lemma 4.10].

Lemma 3.4.2. *For $T \in \mathcal{T}_h^e$, define $\omega_T = \cup_{\substack{T' \in \mathcal{T}_h^e \\ \bar{T} \cap \bar{T}' \neq \emptyset}} \bar{T}'$ to be the patch of neighboring elements of T. We further define the $O(h)$ strip around Γ:*

$$\omega_\Gamma = \bigcup_{T \in \mathcal{T}_h^\Gamma} \omega_T.$$

Then there holds

$$\|v\|_{L^2(\omega_\Gamma)} \leq C h^{\frac{1}{2}} \|v\|_{H^1(S)} \qquad \forall v \in H^1(S).$$

We also require a trace inequality suitable for the CutFEM discretization (see, e.g., [29, 27]).

Lemma 3.4.3. *For every $K \in \mathcal{T}_h^{ct,\Gamma}$ it holds*

$$\|v\|_{L^2(K_\Gamma)} \leq C(h_K^{-\frac{1}{2}}\|v\|_{L^2(K)} + h_K^{\frac{1}{2}}\|\nabla v\|_{L^2(K)}) \qquad \forall v \in H^1(K), \tag{3.4.3}$$

with a constant C independent of v, T, how Γ intersects T, and $h < h_1$ for some fixed $h_1 > 0$.

Consider the finite element subspace of pointwise divergence-free functions:

$$\boldsymbol{Z}_h = \{\boldsymbol{w}_h \in \boldsymbol{V}_h \,:\, \operatorname{div} \boldsymbol{w}_h = 0 \text{ in } \Omega_h^e\}.$$

This subspace enjoys full approximation properties in the sense of the following lemma.

Lemma 3.4.4. *For $\boldsymbol{u}$, the divergence-free extension of the solution to* (3.1.1)*, it holds*

$$\inf_{\boldsymbol{w}_h \in \boldsymbol{Z}_h} \|\boldsymbol{u} - \boldsymbol{w}_h\|_{H^1(T)} \leq C h_T^k |\boldsymbol{u}|_{H^{k+1}(\omega_T)} \qquad \forall T \in \mathcal{T}_h^e. \tag{3.4.4}$$

Consequently, if $\boldsymbol{u} \in \boldsymbol{H}^{k+2}(\Omega)$,

$$\inf_{\boldsymbol{w}_h \in \boldsymbol{Z}_h} \|\boldsymbol{u} - \boldsymbol{w}_h\|_{\boldsymbol{V}_h} \leq C\big(h^k \|\boldsymbol{u}\|_{H^{k+1}(\Omega)} + \eta^{\frac{1}{2}} h^{k+\frac{1}{2}} \|\boldsymbol{u}\|_{H^{k+2}(\Omega)}\big).$$

Proof. We first prove the approximation property (3.4.4).Here we consider the three-dimensional case; the analogous 2D arguments are similar (and simpler).

We first construct a Fortin operator using the recent results in [22]. For $T \in \mathcal{T}_h^e$, let T^{ct} denote the local triangulation of four (sub)tetrahedra, obtained by performing a barycenter refinement of T.

We define the polynomial spaces:

$$\mathcal{P}_k(T^{ct}) = \{v \in L^2(D) :\ v|_K \in \mathcal{P}_k(K)\ \forall K \in T^{ct}\}, \quad \mathring{\mathcal{P}}_k(T^{ct}) = \mathcal{P}_k(T^{ct}) \cap L_0^2(D),$$
$$\boldsymbol{\mathcal{P}}_k^c(T^{ct}) = [\mathcal{P}_k(T^{ct}) \cap H^1(D)]^3, \qquad \mathring{\boldsymbol{\mathcal{P}}}_k^c(T^{ct}) = \boldsymbol{\mathcal{P}}_k^c(T^{ct}) \cap \boldsymbol{H}_0^1(D),$$

where $D = \mathrm{int}(\cup_{K\in T^{ct}} \bar{K})$. We also define the smooth space

$$\mathring{\boldsymbol{M}}_{k+1}(T^{ct}) = \{\boldsymbol{\kappa} \in \mathring{\boldsymbol{\mathcal{P}}}^c_{k+1}(T^{ct}) : \mathbf{curl}\,\boldsymbol{\kappa} \in \mathring{\boldsymbol{\mathcal{P}}}^c_{k}(T^{ct})\}.$$

It follows from [22, Lemma 4.16] that there exists an operator $\boldsymbol{\Pi}_{0,T} : \boldsymbol{H}^1(T) \to \mathring{\boldsymbol{\mathcal{P}}}^c_k(T^{ct})$ uniquely determined by the conditions

$$\int_T (\boldsymbol{\Pi}_{0,T}\boldsymbol{v}) \cdot \mathbf{curl}\,\boldsymbol{\kappa} = \int_T \boldsymbol{v} \cdot \mathbf{curl}\,\boldsymbol{\kappa} \qquad \forall \boldsymbol{\kappa} \in \mathring{\boldsymbol{M}}_{k+1}(T^{ct}), \tag{3.4.5a}$$

$$\int_T (\mathrm{div}\,(\boldsymbol{\Pi}_{0,T}\boldsymbol{v}))\kappa = \int_T (\mathrm{div}\,\boldsymbol{v})\kappa \qquad \forall \kappa \in \mathring{\mathcal{P}}_{k-1}(T^{ct}). \tag{3.4.5b}$$

Next we show a stability estimate for the operator using a scaling argument.

To ease presentation, set $\boldsymbol{v}_T = \boldsymbol{\Pi}_{0,T}\boldsymbol{v}$. Let $\hat{T} = \{\frac{x}{h_T} : x \in T\}$ be a dilation of T, and define $\hat{\boldsymbol{v}}_T \in \mathring{\boldsymbol{\mathcal{P}}}_k(\hat{T}^{ct})$ as $\hat{\boldsymbol{v}}_T(\hat{x}) = \boldsymbol{v}_T(x)$ with $x = h_T\hat{x}$, so that $\partial \boldsymbol{v}_T = h_T^{-1}\hat{\partial}\hat{\boldsymbol{v}}_T$. In particular, $\mathrm{div}\,\boldsymbol{v}_T = h_T^{-1}\widehat{\mathrm{div}}\,\hat{\boldsymbol{v}}_T$ and $\mathbf{curl}\ \boldsymbol{\kappa} = h_T^{-1}\widehat{\mathbf{curl}}\ \hat{\boldsymbol{\kappa}}$. Using a change of variables and equivalence of norms, we compute

$$\begin{aligned}
h_T^{-1}\|\nabla \boldsymbol{v}_T\|^2_{L^2(T)} &= \|\hat{\nabla}\hat{\boldsymbol{v}}_T\|^2_{L^2(\hat{T})} \\
&\approx \sup_{\hat{\boldsymbol{\kappa}}\in\mathring{\boldsymbol{M}}_{k+1}(\hat{T}^{ct})} \Big|\frac{\int_{\hat{T}} \hat{\boldsymbol{v}}_T \cdot \widehat{\mathbf{curl}}\ \hat{\boldsymbol{\kappa}}}{\|\widehat{\mathbf{curl}}\ \hat{\boldsymbol{\kappa}}\|_{L^2(\hat{T})}}\Big|^2 + \sup_{\hat{\kappa}\in\mathring{\mathcal{P}}_{k-1}(\hat{T}^{ct})} \Big|\frac{\int_{\hat{T}} \widehat{\mathrm{div}}\,\hat{\boldsymbol{v}}_T\hat{\kappa}}{\|\hat{\kappa}\|_{L^2(\hat{T})}}\Big|^2 \\
&= \sup_{\hat{\boldsymbol{\kappa}}\in\mathring{\boldsymbol{M}}_{k+1}(T^{ct})} \Big|\frac{h_T^{-3}\int_T \boldsymbol{v}_T \cdot (h_T\mathbf{curl}\ \boldsymbol{\kappa})}{h_T^{-1/2}\|\mathbf{curl}\,\boldsymbol{\kappa}\|_{L^2(T)}}\Big|^2 + \sup_{\kappa\in\mathring{\mathcal{P}}_{k-1}(T^{ct})} \Big|\frac{h_T^{-3}\int_T (h_T\mathrm{div}\,\boldsymbol{v}_T)\kappa}{h_T^{-3/2}\|\kappa\|_{L^2(T)}}\Big|^2 \\
&= h_T^{-3} \sup_{\hat{\boldsymbol{\kappa}}\in\mathring{\boldsymbol{M}}_{k+1}(T^{ct})} \Big|\frac{\int_T \boldsymbol{v} \cdot \mathbf{curl}\ \boldsymbol{\kappa}}{\|\mathbf{curl}\,\boldsymbol{\kappa}\|_{L^2(T)}}\Big|^2 + h_T^{-1} \sup_{\kappa\in\mathring{\mathcal{P}}_{k-1}(T^{ct})} \Big|\frac{\int_T (\mathrm{div}\,\boldsymbol{v})\kappa}{\|\kappa\|_{L^2(T)}}\Big|^2 \\
&\le h_T^{-3}\|\boldsymbol{v}\|^2_{L^2(T)} + h_T^{-1}\|\mathrm{div}\,\boldsymbol{v}\|^2_{L^2(T)}.
\end{aligned}$$

Hence, we have

$$\|\nabla\boldsymbol{\Pi}_{0,T}\boldsymbol{v}\|_{L^2(T)} \le C\big(\|\nabla\boldsymbol{v}\|_{L^2(T)} + h_T^{-1}\|\boldsymbol{v}\|_{L^2(T)}\big) \qquad \forall \boldsymbol{v} \in \boldsymbol{H}^1(T). \tag{3.4.6}$$

Then we first set $\boldsymbol{I}_h : \boldsymbol{H}^1(\Omega) \to \boldsymbol{\mathcal{P}}_k^c(\mathcal{T}_h^e) \subset \boldsymbol{V}_h$ be the kth degree Scott-Zhang interpolant which satisfies ($k \geq 3$) [52]

$$\int_F \boldsymbol{I}_h \boldsymbol{v} = \int_F \boldsymbol{v} \qquad \text{for all faces in } \mathcal{T}_h^e \qquad \forall \boldsymbol{v} \in \boldsymbol{H}^1(\Omega_h^e), \tag{3.4.7}$$

and $\boldsymbol{\Pi}_0 : \boldsymbol{H}^1(\Omega^e) \to \boldsymbol{V}_h$ such that $\boldsymbol{\Pi}_0|_T = \boldsymbol{\Pi}_{0,T}$ for all $T \in \mathcal{T}_h^e$.

Then we define the operator $\boldsymbol{\Pi}_h : \boldsymbol{H}^1(\Omega_h^e) \to \boldsymbol{V}_h$ as

$$\boldsymbol{\Pi}_h = \boldsymbol{I}_h + \boldsymbol{\Pi}_0(\mathbf{1} - \boldsymbol{I}_h),$$

where $\mathbf{1}$ is the identity operator. Moreover, for all $\boldsymbol{v} \in \boldsymbol{H}^1(\Omega^e)$, we have

$$\int_{\Omega_h^e} (\operatorname{div}(\boldsymbol{\Pi}_h \boldsymbol{v}))q = \int_{\Omega_h^e} (\operatorname{div} \boldsymbol{v})q \qquad \forall q \in \mathcal{P}_{k-1}(\mathcal{T}_h^{ct,e}).$$

If $\boldsymbol{u}$ is divergence–free, then $\boldsymbol{\Pi}_h \boldsymbol{u} \in \boldsymbol{Z}_h$. Therefore by the definition of $\boldsymbol{\Pi}_h$ and the $\boldsymbol{H}^1$-stability of this operator,

$$\begin{aligned}
\inf_{\boldsymbol{w}_h \in \boldsymbol{Z}_h} \|\nabla(\boldsymbol{u} - \boldsymbol{w}_h)\|_{L^2(T)} &\leq \|\nabla(\boldsymbol{u} - \boldsymbol{\Pi}_h \boldsymbol{u})\|_{L^2(T)} \\
&\leq \|\nabla(\boldsymbol{u} - \boldsymbol{I}_h \boldsymbol{u})\|_{L^2(T)} + \|\nabla(\boldsymbol{\Pi}_0(\mathbf{1} - \boldsymbol{I}_h)\boldsymbol{u})\|_{L^2(T)} \\
&\leq C(\|\nabla(\boldsymbol{u} - \boldsymbol{I}_h \boldsymbol{u})\|_{L^2(T)} + h_T^{-1} \|\boldsymbol{u} - \boldsymbol{I}_h \boldsymbol{u}\|_{L^2(T)}).
\end{aligned}$$

We then use the approximation properties of the Scott-Zhang interpolant to obtain the result (3.4.4).

Note that by the extension of $\boldsymbol{u}$, we have $\operatorname{div} \boldsymbol{u} = 0$ in Ω_h^e. Thus we have $\operatorname{div}(\boldsymbol{u} - \boldsymbol{w}_h) = 0$ in Ω_h^e for $\boldsymbol{w}_h \in \boldsymbol{Z}_h$.

Using Lemma 3.4.3, we bound the penalty part in $\|\boldsymbol{u}-\boldsymbol{w}_h\|_{\boldsymbol{V}_h}$ as follows:

$$\begin{aligned} j_h(\boldsymbol{u}-\boldsymbol{w}_h,\boldsymbol{u}-\boldsymbol{w}_h) &= \sum_{K\in\mathcal{T}_h^{ct,\Gamma}} h_K^{-1}\|\boldsymbol{u}-\boldsymbol{w}_h\|^2_{L^2(K_\Gamma)} \\ &\leq C\sum_{K\in\mathcal{T}_h^{ct,\Gamma}} \big(h_K^{-2}\|\boldsymbol{u}-\boldsymbol{w}_h\|^2_{L^2(K)} + \|\nabla(\boldsymbol{u}-\boldsymbol{w}_h)\|^2_{L^2(K)}\big) \quad (3.4.8) \\ &\leq Ch^{2k}\|\boldsymbol{u}\|^2_{H^{k+1}(\omega_\Gamma)} \leq Ch^{2k+1}\|\boldsymbol{u}\|^2_{H^{k+2}(\Omega)}, \end{aligned}$$

where for the last inequality we used an inverse estimate, (3.4.1) and Lemma 3.4.2. This yields the bound $\|\boldsymbol{u}-\boldsymbol{w}_h\|_{\boldsymbol{V}_h} \leq C\big(h^k\|\boldsymbol{u}\|_{H^{k+1}(\Omega)} + \eta^{\frac{1}{2}}h^{k+\frac{1}{2}}\|\boldsymbol{u}\|_{H^{k+2}(\Omega)}\big)$. □

Theorem 3.4.5. *The following error estimate holds*

$$\begin{aligned} \|\boldsymbol{u}-\boldsymbol{u}_h\|_{\boldsymbol{V}_h}+(1+\gamma)^{-\frac{1}{2}}\|p-p_h\|_{L^2(\Omega)} \leq C\Bigg(& h^k\|\boldsymbol{u}\|_{H^{k+1}(\Omega)}+(1+\gamma^{\frac{1}{2}}+\eta^{\frac{1}{2}})h^{k+\frac{1}{2}}\|\boldsymbol{u}\|_{H^{k+2}(\Omega)} \\ & + (\eta^{-\frac{1}{2}}+(1+\gamma)^{-\frac{1}{2}})h^{k+\frac{1}{2}}\|p\|_{H^{k+1}(\Omega)} + (1+\gamma)^{-\frac{1}{2}}h^k\|p\|_{H^k(\Omega)}\Bigg). \quad (3.4.9) \end{aligned}$$

Proof. To show the error bounds, we start with a standard argument. Let $\boldsymbol{w}_h \in \boldsymbol{Z}_h$ be a function in the discrete kernel satisfying estimate (3.4.4). Setting $\boldsymbol{e}_I = \boldsymbol{u}_h - \boldsymbol{w}_h \in \boldsymbol{V}_h$ we have, thanks to the coercivity result in Lemma 3.3.3:

$$C_0\|\boldsymbol{e}_I\|^2_{\boldsymbol{V}_h} \leq a_h(\boldsymbol{e}_I,\boldsymbol{e}_I). \quad (3.4.10)$$

Denote by $\widehat{p}_h \in Q_h$ the L^2-projection of p onto Q_h, and set $q_I = p_h - \widehat{p}_h$. It follows from (3.3.2) that there exists $\boldsymbol{v} \in \boldsymbol{V}_h$ with $\mathrm{supp}(\boldsymbol{v}) \subset \Omega_h^i$ such that

$$C_1\|q_I\|^2_{L^2(\Omega)} \leq b(\boldsymbol{v},q_I) + C_1^{-1}J_h(q_I,q_I), \quad \text{with } (1+\gamma)^{-\frac{1}{2}}\|\boldsymbol{v}\|_{\boldsymbol{V}_h} \leq \|\boldsymbol{v}\|_{\boldsymbol{V}_{0,h}} = \|q_I\|_{L^2(\Omega)}, \quad (3.4.11)$$

where $C_1 = \frac{\theta_*}{2}$, and θ_* is the inf-sup constant given in Corollary 3.3.2.

From (3.4.10), (3.4.11), (3.2.1), and the consistency identity (3.4.2), we conclude that for any $\alpha \geq 0$ it holds

$$
\begin{aligned}
&C_0\|\boldsymbol{e}_I\|_{\boldsymbol{V}_h}^2 + C_1\alpha\|q_I\|_{L^2(\Omega)}^2 + \big((1+\gamma)^{-1} - \alpha C_1^{-1}\big) J_h(q_I, q_I) \qquad (3.4.12)\\
&\quad \leq a_h(\boldsymbol{e}_I, \boldsymbol{e}_I) + b(\alpha\boldsymbol{v}, q_I) + (1+\gamma)^{-1} J_h(q_I, q_I)\\
&\quad = a_h(\boldsymbol{e}_I, \boldsymbol{e}_I + \alpha\boldsymbol{v}) + b(\boldsymbol{e}_I + \alpha\boldsymbol{v}, q_I) - b(\boldsymbol{e}_I, q_I) + (1+\gamma)^{-1} J_h(q_I, q_I) - a_h(\boldsymbol{e}_I, \alpha\boldsymbol{v})\\
&\quad = a_h(\boldsymbol{u} - \boldsymbol{w}_h, \boldsymbol{e}_I + \alpha\boldsymbol{v}) + b(\boldsymbol{e}_I + \alpha\boldsymbol{v}, p - \widehat{p}_h) - b(\boldsymbol{u} - \boldsymbol{w}_h, q_I)\\
&\qquad\quad + (1+\gamma)^{-1} J_h(p - \widehat{p}_h, q_I) - a_h(\boldsymbol{e}_I, \alpha\boldsymbol{v})\\
&\quad =: I_1 + I_2 + I_3 + I_4 + I_5.
\end{aligned}
$$

We now estimate the right-hand side of (3.4.12) term-by-term.

Using the continuity result in Lemma 3.3.3 and the approximation results in Lemma 3.4.4, we bound

$$
\begin{aligned}
I_1 &\leq C_a\|\boldsymbol{e}_I + \alpha\boldsymbol{v}\|_{\boldsymbol{V}_h}\|\boldsymbol{u} - \boldsymbol{w}_h\|_{\boldsymbol{V}_h} \qquad (3.4.13)\\
&\leq C\|\boldsymbol{e}_I + \alpha\boldsymbol{v}\|_{\boldsymbol{V}_h}\left(h^k\|\boldsymbol{u}\|_{H^{k+1}(\Omega)} + \eta^{\frac{1}{2}} h^{k+\frac{1}{2}}\|\boldsymbol{u}\|_{H^{k+2}(\Omega)}\right)\\
&\leq C\big(\|\boldsymbol{e}_I\|_{\boldsymbol{V}_h} + \alpha(1+\gamma)^{\frac{1}{2}}\|q_I\|_{L^2(\Omega)}\big)\left(h^k\|\boldsymbol{u}\|_{H^{k+1}(\Omega)} + \eta^{\frac{1}{2}} h^{k+\frac{1}{2}}\|\boldsymbol{u}\|_{H^{k+2}(\Omega)}\right),
\end{aligned}
$$

where we used (3.4.11) in the last inequality.

We now estimate the second term in the right-hand side of (3.4.12) in two steps. First, using approximation properties of the L^2-projection, we get

$$
(\widehat{p}_h - p, \operatorname{div}\boldsymbol{e}_I) \leq (1+\gamma)^{-\frac{1}{2}}\|\widehat{p}_h - p\|_{L^2(\Omega)}\|\boldsymbol{e}_I\|_{\boldsymbol{V}_h} \leq (1+\gamma)^{-\frac{1}{2}} h^k\|p\|_{H^k(\Omega)}\|\boldsymbol{e}_I\|_{\boldsymbol{V}_h}. \qquad (3.4.14)
$$

Likewise,

$$
(\widehat{p}_h - p, \alpha\operatorname{div}\boldsymbol{v}) \leq C\alpha h^k\|p\|_{H^k(\Omega)}\|q_I\|_{L^2(\Omega)}. \qquad (3.4.15)
$$

We apply the trace inequality (3.4.3) and standard approximation properties of the L^2-projection to estimate the boundary integral in $b(\boldsymbol{e}_I+\alpha\boldsymbol{v}, p-\widehat{p}_h)$, noting that $\boldsymbol{v}=0$ on Γ:

$$\begin{aligned}\int_\Gamma(\widehat{p}_h-p)(\boldsymbol{e}_I+\alpha\boldsymbol{v})\cdot\boldsymbol{n} &\le \sum_{K\in\mathcal{T}_h^{ct,\Gamma}}\|\widehat{p}_h-p\|_{L^2(K_\Gamma)}\|\boldsymbol{e}_I\|_{L^2(K_\Gamma)}\\ &\le \Big(\sum_{K\in\mathcal{T}_h^{ct,\Gamma}}\eta^{-1}h_K\|\widehat{p}_h-p\|^2_{L^2(K_\Gamma)}\Big)^{1/2}\Big(\sum_{K\in\mathcal{T}_h^{ct,\Gamma}}\eta h_K^{-1}\|\boldsymbol{e}_I\|_{L^2(K_\Gamma)}\Big)^{1/2}\\ &\le C\eta^{-\frac12}h^k\|p\|_{H^k(\omega_\Gamma)}\|\boldsymbol{e}_I\|_{\boldsymbol{V}_h}\le C\eta^{-\frac12}h^{k+\frac12}\|p\|_{H^{k+1}(\Omega)}\|\boldsymbol{e}_I\|_{\boldsymbol{V}_h},\end{aligned}\tag{3.4.16}$$

where we used the Cauchy-Schwarz inequality in the second inequality and Lemma 3.4.2 in the last inequality. Summing (3.4.14)–(3.4.16) we obtain

$$I_2\le C\Big(\alpha h^k\|p\|_{H^k(\Omega)}\|q_I\|_{L^2(\Omega)}+\Big((1+\gamma)^{-\frac12}h^k\|p\|_{H^k(\Omega)}+\eta^{-\frac12}h^{k+\frac12}\|p\|_{H^{k+1}(\Omega)}\Big)\|\boldsymbol{e}_I\|_{\boldsymbol{V}_h}\Big).\tag{3.4.17}$$

To estimate I_3, we first note that, due to (3.4.3), finite element inverse inequalities, and (3.3.3), there holds

$$\sum_{K\in\mathcal{T}_h^{ct,\Gamma}}h_K\|q_I\|^2_{L^2(K_\Gamma)}\le C\sum_{K\in\mathcal{T}_h^{ct,\Gamma}}\|q_I\|^2_{L^2(K)}\le C\big(\|q\|^2_{L^2(\Omega)}+J_h(q_I,q_I)\big).$$

Therefore, thanks to $\operatorname{div}(\boldsymbol{u}-\boldsymbol{w}_h)=0$ and the estimate (3.4.8), we have

$$\begin{aligned}I_3&\le\Big(\sum_{K\in\mathcal{T}_h^{ct,\Gamma}}h_K\|q_I\|^2_{L^2(K_\Gamma)}\Big)^{1/2}\Big(\sum_{K\in\mathcal{T}_h^{ct,\Gamma}}h_K^{-1}\|\boldsymbol{u}-\boldsymbol{w}_h\|^2_{L^2(K_\Gamma)}\Big)^{1/2}\\ &\le C(\|q_I\|^2_{L^2(\Omega)}+J_h(q_I,q_I))^{\frac12}h^{k+\frac12}\|\boldsymbol{u}\|_{H^{k+2}(\Omega)}.\end{aligned}$$

We proceed with estimating terms in the right-hand side of (3.4.12). For the fourth term we get, using the trace inequality (3.4.3), approximation properties of the L^2-projection, and Lemma 3.4.2,

$$I_4 \leq (1+\gamma)^{-1} J_h^{\frac{1}{2}}(p-\widehat{p}_h, p-\widehat{p}_h) J_h^{\frac{1}{2}}(q_I, q_I) \leq C h^{k+\frac{1}{2}} (1+\gamma)^{-1} \|p\|_{H^{k+1}(\Omega)} J_h^{\frac{1}{2}}(q_I, q_I). \tag{3.4.18}$$

For the last term in (3.4.12) we have (using (3.4.11))

$$I_5 \leq \frac{C_0}{4}\|\boldsymbol{e}_I\|_{\boldsymbol{V}_h}^2 + \frac{C_a^2\alpha^2}{C_0}\|\boldsymbol{v}\|_{\boldsymbol{V}_h}^2 \leq \frac{C_0}{4}\|\boldsymbol{e}_I\|_{\boldsymbol{V}_h}^2 + \frac{C_a^2\alpha^2(1+\gamma)}{C_0}\|q_I\|_{L^2(\Omega)}^2. \tag{3.4.19}$$

We apply the estimates (3.4.13)–(3.4.19) to (3.4.12) getting

$$\begin{aligned}
&C_0\|\boldsymbol{e}_I\|_{\boldsymbol{V}_h}^2 + C_1\alpha\|q_I\|_{L^2(\Omega)}^2 + ((1+\gamma)^{-1} - \alpha C_1^{-1}) J_h(q_I, q_I) \\
&\leq C\Bigg(\big(\|\boldsymbol{e}_I\|_{\boldsymbol{V}_h} + \alpha(1+\gamma)^{\frac{1}{2}}\|q_I\|_{L^2(\Omega)}\big)\big(h^k\|\boldsymbol{u}\|_{H^{k+1}(\Omega)} + \eta^{\frac{1}{2}}h^{k+\frac{1}{2}}\|\boldsymbol{u}\|_{H^{k+2}(\Omega)}\big) \\
&\quad + \alpha h^k\|q_I\|_{L^2(\Omega)}\|p\|_{H^k(\Omega)} + \Big((1+\gamma)^{-\frac{1}{2}}h^k\|p\|_{H^k(\Omega)} + \eta^{-\frac{1}{2}}h^{k+\frac{1}{2}}\|p\|_{H^{k+1}(\Omega)}\Big)\|\boldsymbol{e}_I\|_{\boldsymbol{V}_h} \\
&\quad + (\|q_I\|_{L^2(\Omega)} + J_h^{\frac{1}{2}}(q_I, q_I))h^{k+\frac{1}{2}}(\|\boldsymbol{u}\|_{H^{k+2}(\Omega)} + (1+\gamma)^{-1}\|p\|_{H^{k+1}(\Omega)})\Bigg) \\
&\quad + \frac{C_0}{4}\|\boldsymbol{e}_I\|_{\boldsymbol{V}_h}^2 + \frac{C_a^2\alpha^2(1+\gamma)}{C_0}\|q_I\|_{L^2(\Omega)}^2.
\end{aligned}$$

We apply the Cauchy-Schwarz inequality several times and rearrange terms to obtain

$$\begin{aligned}
&C_0\|\boldsymbol{e}_I\|_{\boldsymbol{V}_h}^2 + \big(C_1\alpha - C\alpha^2(1+\gamma)\big)\|q_I\|_{L^2(\Omega)}^2 + ((1+\gamma)^{-1} - \alpha C_1^{-1}) J_h(q_I, q_I) \\
&\quad \leq C\Bigg(\Big(h^{2k}\|\boldsymbol{u}\|_{H^{k+1}(\Omega)}^2 + \eta h^{2k+1}\|\boldsymbol{u}\|_{H^{k+2}(\Omega)}^2\Big) + (\alpha+1)(1+\gamma)^{-1}h^{2k}\|p\|_{H^k(\Omega)}^2 \\
&\qquad + \eta^{-1}h^{2k+1}\|p\|_{H^{k+1}(\Omega)}^2 + \alpha^{-1}h^{2k+1}\big(\|\boldsymbol{u}\|_{H^{k+2}(\Omega)}^2 + (1+\gamma)^{-2}\|p\|_{H^{k+1}(\Omega)}^2\big)\Bigg).
\end{aligned}$$

We now take $\alpha = \widetilde{C}(1+\gamma)^{-1}$, with $\widetilde{C} > 0$ sufficiently small to obtain

$$
\begin{aligned}
&C_0\|\boldsymbol{e}_I\|^2_{\boldsymbol{V}_h} + C(1+\gamma)^{-1}\big(\|q_I\|^2_{L^2(\Omega)} + J_h(q_I, q_I)\big) \\
&\qquad \leq C\Bigg(h^{2k}\|\boldsymbol{u}\|^2_{H^{k+1}(\Omega)} + (1+\gamma)^{-1}h^{2k}\|p\|^2_{H^k(\Omega)} + \big(1+\eta+\gamma\big)h^{2k+1}\|\boldsymbol{u}\|^2_{H^{k+2}(\Omega)} \\
&\qquad\qquad + (\eta^{-1} + (1+\gamma)^{-1})h^{2k+1}\|p\|^2_{H^{k+1}(\Omega)}\Bigg).
\end{aligned}
$$

Finally, we apply the triangle inequality, the divergence-free property of $\boldsymbol{u}$ and $\boldsymbol{w}_h$, and approximation properties (3.4.4) to obtain the error estimate (3.4.9).

□

Remark 3.4.6. The pressure dependence in velocity error (3.4.9) arises from the violation of mass conservation in the boundary strip and the penalty treatment of the boundary condition. The violation of the divergence-free constraint in a boundary strip can be partially mitigated by taking grad-div parameter $\gamma = O(h^{-1})$ and Nitsche parameter $\eta = O(h^{-1})$, which seem to be the optimal choice with respect to the error analysis in the energy norm. This can be contrasted to $\gamma = O(1)$ for the Taylor-Hood element.

4.0 Numerical Experiments

This Chapter consists of three sections. In the first two sections, we perform two numerical experiments for FEM with boundary correction developed in Chapter 2, and two numerical experiments using Netgen/NGSolve [48] with ngsxfem add-on [37] for CutFEM in Chapter 3, respectively. We also compare the numerical results with the theories developed in the respective chapters; In the third section, we present two numerical experiments for the stationary Navier-Stokes problem using CutFEM.

4.1 Boundary Correction

4.1.1 Circle

In this numerical experiment, we perform a series of tests of the finite element method (2.3.1). The domain for these tests is a circle given via a level set function:

$$\Omega = \{(x, y) \in \mathbb{R}^2 : \phi(x, y) < 0\}, \tag{4.1.1}$$

where

$$\phi(x, y) = \sqrt{(x - 0.5)^2 + (y - 0.5)^2} - 0.2.$$

We use the Scott-Vogelius pair $\boldsymbol{\mathcal{P}}_2 - \mathcal{P}_1^{disc}$ on Clough-Toucher splits for the finite element spaces.

We set the background polygon to be the unit square $S = (0, 1)^2$, and the background mesh $\mathcal{S}_h$ to be a sequence of type I triangulations of S, i.e., a mesh obtained by

drawing diagonals of a cartesian mesh. Then we perform the barycenter refinement to obtain $\mathcal{S}_h^{ct}$.

We obtain the extension direction $\boldsymbol{d}$ by solving an auxiliary 2×2 nonlinear system at each quadrature point of each boundary edge of $\mathcal{T}_h^{ct}$. In particular, for each quadrature point $(x, y) \in \partial\Omega_h$, we find $(x_*, y_*) \in \partial\Omega$ such that

$$\phi(x_*, y_*) = 0, \quad (\nabla\phi(x_*, y_*))^\perp \cdot ((x, y) - (x_*, y_*)) = 0,$$

and set $\boldsymbol{d} = ((x, y) - (x_*, y_*))/|(x, y) - (x_*, y_*)|$ and $\delta(x, y) = |(x, y) - (x_*, y_*)|$. The first equation ensures that (x_*, y_*) is on the boundary $\partial\Omega$, whereas the second equation states that $\boldsymbol{d}$ is parallel to the outward unit normal of $\partial\Omega$ at (x_*, y_*).

For the Nitsche penalty parameter in $a_h(\cdot, \cdot)$, we set the value $\eta = 40$ throughout the experiment.

The experiment consists of two groups of tests, where the difference of the two groups of tests is the viscosity parameter ν in the bilinear form $a_h(\cdot, \cdot)$. In the first group, we set $\nu = 10^{-1}$; in the second group, we set $\nu = 10^{-5}$. For each group, we perform the tests 5 times on a sequence of meshes with the mesh parameter h being 0.200, 0.100, 0.050, 0.025 and 0.013.

The exact velocity solution and exact pressure solution are set to be

$$\boldsymbol{u} = \begin{pmatrix} 2(x^2 - x + 0.25 + y^2 - y)(2y - 1) \\ -2(x^2 - x + 0.25 + y^2 - y)(2x - 1) \end{pmatrix}, \quad p = 10(x^2 - y^2)^2. \tag{4.1.2}$$

Correspondingly, we have the right-hand function

$$f = \begin{pmatrix} \nu(16 - 32y) + 40x(x^2 - y^2) \\ \nu(32x - 16) - 40y(x^2 - y^2) \end{pmatrix}.$$

We state the L^2 error results for the velocity $\|\boldsymbol{u}-\boldsymbol{u}_h\|_{L^2(\Omega_h)}$, the L^2 error results for the pressure $\|p-p_h\|_{L^2(\Omega_h)}$, and the H^1-type error results for the velocity $\|\nabla(\boldsymbol{u}-\boldsymbol{u}_h)\|_{L^2(\Omega_h)}$ and their respective rate of convergence in Table 1 and Table 2.

Results for $\nu = 10^{-1}$			Results for $\nu = 10^{-1}$		
h	$\|\boldsymbol{u}-\boldsymbol{u}_h\|_{L^2(\Omega_h)}$	Rate	h	$\|\nabla(\boldsymbol{u}-\boldsymbol{u}_h)\|_{L^2(\Omega_h)}$	Rate
0.200	9.244e-03		0.200	1.998e-01	
0.100	2.050e-03	2.173	0.100	2.633e-02	2.924
0.050	3.229e-04	2.667	0.050	7.150e-03	1.881
0.025	3.578e-05	3.174	0.025	1.862e-03	1.941
0.013	3.798e-06	3.236	0.013	4.750e-04	1.971
Results for $\nu = 10^{-5}$			Results for $\nu = 10^{-5}$		
h	$\|\boldsymbol{u}-\boldsymbol{u}_h\|_{L^2(\Omega_h)}$	Rate	h	$\|\nabla(\boldsymbol{u}-\boldsymbol{u}_h)\|_{L^2(\Omega_h)}$	Rate
0.200	1.324e+01		0.200	1.517e+02	
0.100	2.328e-01	5.830	0.100	2.842e+00	5.738
0.050	3.282e-02	2.826	0.050	4.134e-01	2.782
0.025	3.172e-03	3.371	0.025	5.385e-02	2.941
0.013	2.177e-04	3.865	0.013	8.199e-03	2.715

Table 1: L^2 error and H^1-type error for velocity and their respective rate of convergence with $\nu = 10^{-1}$ and $\nu = 10^{-5}$ on domain (4.1.1) with exact solution (4.1.2).

Results for $\nu = 10^{-1}$		
h	$\|p - p_h\|_{L^2(\Omega_h)}$	Rate
0.200	5.115e-02	
0.100	1.754e-02	1.544
0.050	4.190e-03	2.065
0.025	1.060e-03	1.983
0.013	2.672e-04	1.988
Results for $\nu = 10^{-5}$		
h	$\|p - p_h\|_{L^2(\Omega_h)}$	Rate
0.200	2.887e-02	
0.100	9.424e-03	1.615
0.050	2.863e-03	1.719
0.025	7.992e-04	1.841
0.013	2.103e-04	1.926

Table 2: L^2 error for pressure and rate of convergence with $\nu = 10^{-1}$ and $\nu = 10^{-5}$ on domain (4.1.1) with exact solution (4.1.2).

From Table 1 and Table 2, we see that, for $\nu = 10^{-5}$, the velocity error is larger than that for $\nu = 10^{-1}$. However, the pressure error is less than that for $\nu = 10^{-1}$. This is consistent with the theoretic results from the error analysis. In both cases when $\nu = 10^{-1}$ and $\nu = 10^{-5}$, the pressure error in L^2 norm converges with order 2, which is the optimal order convergence rate. When $\nu = 10^{-1}$, we find that the convergence rate for the velocity error in L^2 norm is of order 3, and the velocity error in H^1-type norm is of order 2, which both are the optimal order convergence rates

with respect to the respective space and norm; However when $\nu = 10^{-5}$, we find that the convergence rate for the velocity error in L^2 norm is of order 4 and the velocity error in H^1-type norm is of order 3. This behavior is consistent with the results from Theorem 2.5.5. By Theorem 2.5.5, we have that, if the solution is smooth, then $\|\nabla(\boldsymbol{u} - \boldsymbol{u}_h)\|_{L^2(\Omega_h)} = \mathcal{O}(h^2 + \nu^{-1}h^3)$. Since $\nu = 10^{-5}$, ν^{-1} is a large number. Therefore h^3 becomes the dominant term, and increases the rate of convergence of the error estimate by 1.

We plot the errors from Table 1 and Table 2 in Figure 8 to illustrate the convergence rate of the solutions in graph.

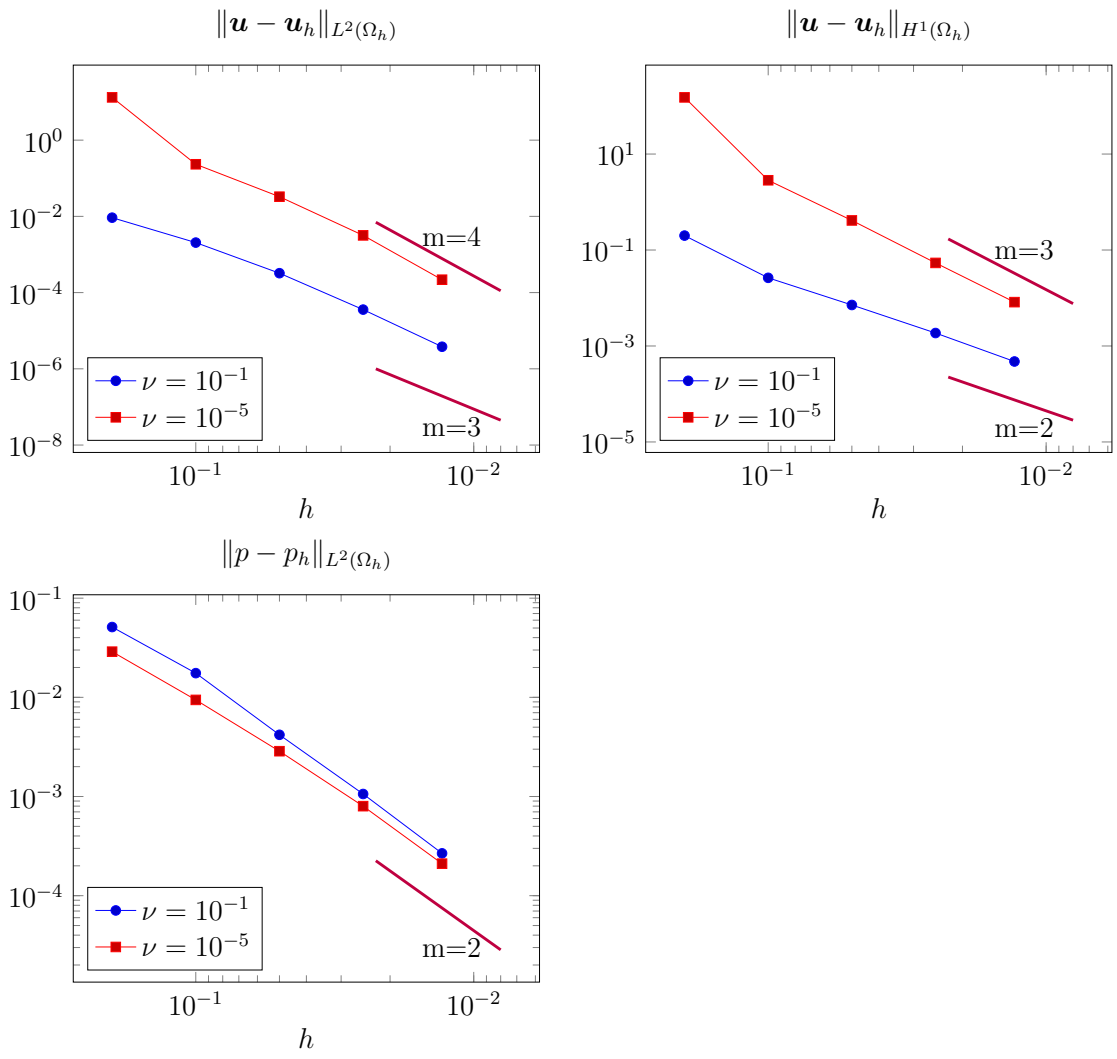

Figure 8: Errors for the velocity and pressure on domain (4.1.1) with varying mesh size.

The data in Table 3 is the divergence of the velocity $\|\operatorname{div} \boldsymbol{u}_h\|_{L^2(\Omega_h)}$ for the two groups of tests with $\nu = 10^{-1}$ and $\nu = 10^{-5}$.

$\nu = 10^{-1}$		$\nu = 10^{-5}$	
h	$\|\text{div}\, \boldsymbol{u}_h\|_{L^2(\Omega_h)}$	h	$\|\text{div}\, \boldsymbol{u}_h\|_{L^2(\Omega_h)}$
0.200	6.951e-12	0.200	6.881e-08
0.100	7.949e-14	0.100	4.884e-10
0.050	3.375e-13	0.050	2.551e-10
0.025	1.096e-12	0.025	3.795e-10
0.013	5.176e-12	0.013	2.286e-10

Table 3: Divergence of velocity in L^2 norm on the domain (4.1.1).

For $\nu = 10^{-1}$, the divergence of velocity slightly increases as the mesh is refined due to round-off error and the increase in condition number for the linear system, but it remains close to 0; when $\nu = 10^{-5}$, the divergence of velocity decreases as the mesh is refined, and it remains close to 0. This observation is consistent with the results from Lemma 2.3.1.

4.1.2 Flower-shaped domain

In this numerical experiment, we perform a series of tests of the finite element method (2.3.1). The domain for these tests is a flower-shaped domain given via a level set function [36]:

$$\Omega = \{(x, y) \in \mathbb{R}^2 : \phi(x, y) < 0\}, \tag{4.1.3}$$

where

$$\phi(x, y) = \sqrt{(x - 0.5)^2 + (y - 0.5)^2} - \sqrt{0.1} - \frac{1}{12}\sin(6\tan^{-1}(\frac{y - 0.5}{x - 0.5})).$$

We use the Scott-Vogelius pair $\boldsymbol{\mathcal{P}}_2 - \mathcal{P}_1^{disc}$ on Clough-Toucher splits for the finite element spaces.

We set the background polygon to be the unit square $S = (0,1)^2$, and the background mesh $\mathcal{S}_h$ to be a sequence of type I triangulations of S, i.e., a mesh obtained by drawing diagonals of a cartesian mesh. Then we perform the barycenter refinement to obtain $\mathcal{S}_h^{ct}$.

We obtain the extension direction $\boldsymbol{d}$ by solving an auxiliary 2×2 nonlinear system at each quadrature point of each boundary edge of $\mathcal{T}_h^{ct}$. In particular, for each quadrature point $(x, y) \in \partial\Omega_h$, we find $(x_*, y_*) \in \partial\Omega$ such that

$$\phi(x_*, y_*) = 0, \quad (\nabla\phi(x_*, y_*))^{\perp} \cdot ((x, y) - (x_*, y_*)) = 0,$$

and set $\boldsymbol{d} = ((x, y) - (x_*, y_*))/|(x, y) - (x_*, y_*)|$ and $\delta(x, y) = |(x, y) - (x_*, y_*)|$. The first equation ensures that (x_*, y_*) is on the boundary $\partial\Omega$, whereas the second equation states that $\boldsymbol{d}$ is parallel to the outward unit normal of $\partial\Omega$ at (x_*, y_*).

For the Nitsche penalty parameter in $a_h(\cdot, \cdot)$, we set the value $\eta = 40$ throughout the experiment.

The experiment consists of two groups of tests, where the difference of the two groups of tests is the viscosity parameter ν in the bilinear form $a_h(\cdot, \cdot)$. In the first group, we set $\nu = 10^{-1}$; in the second group, we set $\nu = 10^{-5}$. For each group, we perform the tests 5 times on a sequence of meshes with the mesh parameter h being 0.200, 0.100, 0.050, 0.025 and 0.013.

The exact velocity solution and exact pressure solution are set to be

$$\boldsymbol{u} = \begin{pmatrix} 2(x^2 - x + 0.25 + y^2 - y)(2y - 1) \\ -2(x^2 - x + 0.25 + y^2 - y)(2x - 1) \end{pmatrix}, \quad p = 10(x^2 - y^2)^2. \tag{4.1.4}$$

Correspondingly, we have the right-hand function

$$f = \begin{pmatrix} \nu(16 - 32y) + 40x(x^2 - y^2) \\ \nu(32x - 16) - 40y(x^2 - y^2) \end{pmatrix}.$$

We state the L^2 error results for the velocity $\|\boldsymbol{u} - \boldsymbol{u}_h\|_{L^2(\Omega_h)}$, the L^2 error results for the pressure $\|p - p_h\|_{L^2(\Omega_h)}$, and the H^1-type error results for the velocity $\|\nabla(\boldsymbol{u} - \boldsymbol{u}_h)\|_{L^2(\Omega_h)}$ and their respective rate of convergence in Table 4 and Table 5.

Results for $\nu = 10^{-1}$			Results for $\nu = 10^{-1}$		
h	$\|\boldsymbol{u}-\boldsymbol{u}_h\|_{L^2(\Omega_h)}$	Rate	h	$\|\nabla(\boldsymbol{u}-\boldsymbol{u}_h)\|_{L^2(\Omega_h)}$	Rate
0.200	2.045e-02		0.200	4.814e-01	
0.100	3.467e-03	2.561	0.100	8.760e-02	2.458
0.050	2.074e-05	4.183	0.050	2.019e-03	3.081
0.025	2.673e-06	3.239	0.025	5.512e-04	2.052
0.013	4.215e-07	2.636	0.013	1.393e-04	1.963
Results for $\nu = 10^{-5}$			Results for $\nu = 10^{-5}$		
h	$\|\boldsymbol{u}-\boldsymbol{u}_h\|_{L^2(\Omega_h)}$	Rate	h	$\|\nabla(\boldsymbol{u}-\boldsymbol{u}_h)\|_{L^2(\Omega_h)}$	Rate
0.200	8.312e+00		0.200	1.404e+02	
0.100	2.335e-01	5.154	0.100	6.294e+00	4.479
0.050	2.954e-03	3.571	0.050	1.163e-01	3.261
0.025	3.086e-04	3.571	0.025	1.174e-02	3.625
0.013	2.078e-05	3.849	0.013	1.047e-03	3.449

Table 4: L^2 error and H^1-type error for velocity and their respective rate of convergence with $\nu = 10^{-1}$ and $\nu = 10^{-5}$ on domain (4.1.3) with exact solution (4.1.4).

Results for $\nu = 10^{-1}$		
h	$\|p - p_h\|_{L^2(\Omega_h)}$	Rate
0.200	2.113e+00	
0.100	1.648e-01	3.681
0.050	1.155e-03	4.053
0.025	2.902e-04	2.184
0.013	7.341e-05	1.961
Results for $\nu = 10^{-5}$		
h	$\|p - p_h\|_{L^2(\Omega_h)}$	Rate
0.200	4.411e-02	
0.100	6.201e-03	2.830
0.050	7.179e-04	1.762
0.025	2.189e-04	1.878
0.013	5.592e-05	1.947

Table 5: L^2 error for pressure and rate of convergence with $\nu = 10^{-1}$ and $\nu = 10^{-5}$ on domain (4.1.3) with exact solution (4.1.4).

From Table 4 and Table 5, we see that, for $\nu = 10^{-5}$, the velocity error is larger than that for $\nu = 10^{-1}$. However, the pressure error is less than that for $\nu = 10^{-1}$. This is consistent with the theoretic results from the error analysis.. In both cases when $\nu = 10^{-1}$ and $\nu = 10^{-5}$, the pressure error in L^2 norm converges with order 2, which is the optimal order convergence rate. When $\nu = 10^{-1}$, we find that the convergence rate for the velocity error in L^2 norm is of order 3, and the velocity error in H^1-type norm is of order 2, which both are the optimal order convergence rates

with respect to the respective space and norm; However when $\nu = 10^{-5}$, we find that the convergence rate for the velocity error in L^2 norm is of order 4 and the velocity error in H^1-type norm is of order 3. This behavior is consistent with the results from Theorem 2.5.5. By Theorem 2.5.5, we have that, if the solution is smooth, then $\|\nabla(\boldsymbol{u} - \boldsymbol{u}_h)\|_{L^2(\Omega_h)} = \mathcal{O}(h^2 + \nu^{-1}h^3)$. Since $\nu = 10^{-5}$, ν^{-1} is a large number. Therefore h^3 becomes the dominant term, and increases the rate of convergence of the error estimate by 1.

We plot the errors from Table 4 and Table 5 in Figure 9 to illustrate the convergence rate of the solutions in graph.

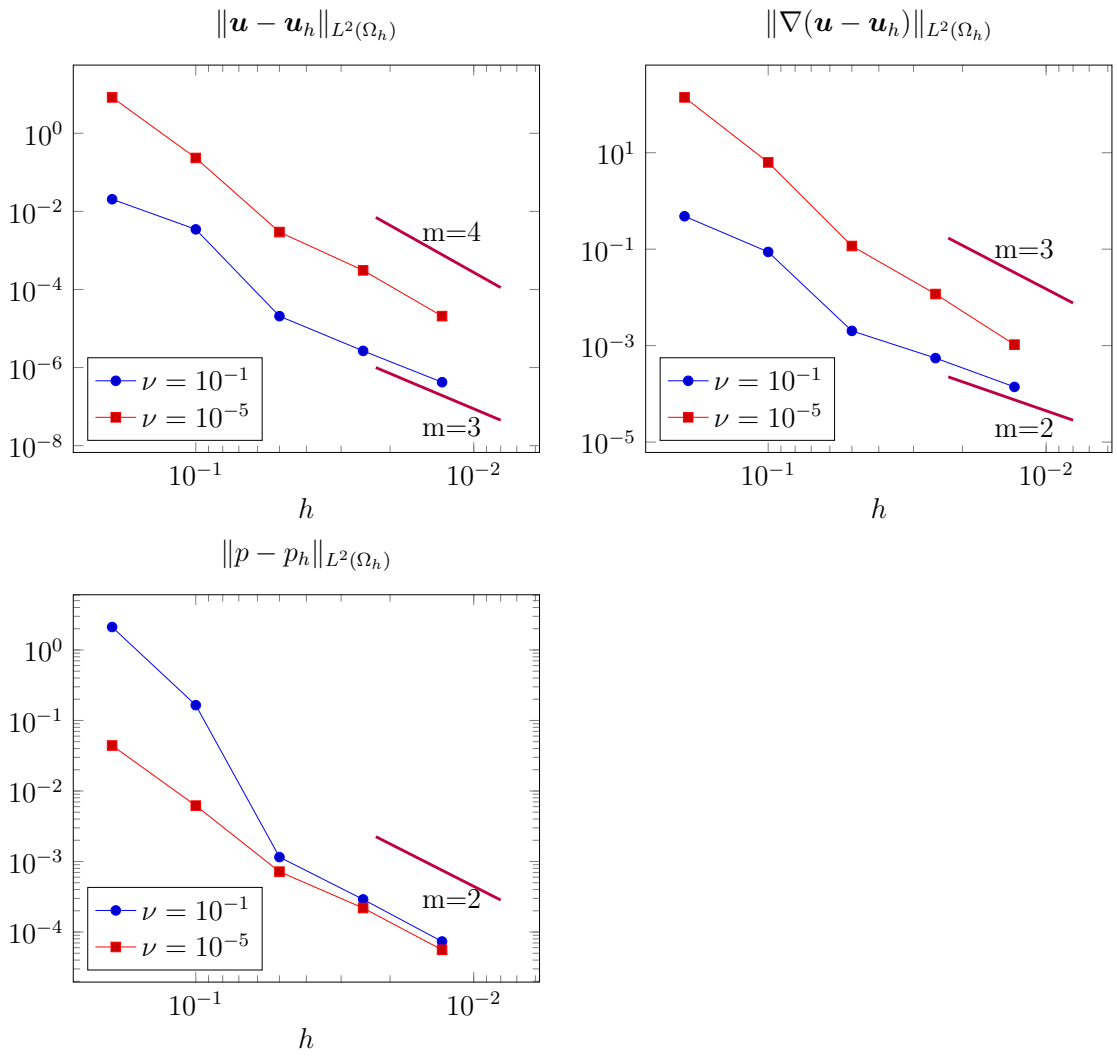

Figure 9: Errors for the velocity and pressure on domain (4.1.3) with varying mesh size.

The data in Table 6 is the divergence of the velocity $\|\operatorname{div} \boldsymbol{u}_h\|_{L^2(\Omega_h)}$ for the two groups of tests with $\nu = 10^{-1}$ and $\nu = 10^{-5}$.

$\nu = 10^{-1}$		$\nu = 10^{-5}$	
h	$\|\text{div}\, \boldsymbol{u}_h\|_{L^2(\Omega_h)}$	h	$\|\text{div}\, \boldsymbol{u}_h\|_{L^2(\Omega_h)}$
0.200	1.112e-12	0.200	1.11013e-08
0.100	5.049e-13	0.100	5.17554e-09
0.050	3.384e-13	0.050	4.26814e-10
0.025	1.776e-13	0.025	4.83809e-11
0.013	4.032e-12	0.013	1.09424e-12

Table 6: Divergence of velocity in L^2 norm on the domain (4.1.3)

For $\nu = 10^{-1}$, the divergence of velocity slightly increases as the mesh is refined due to round-off error and the increase in condition number for the linear system, but it remains close to 0; when $\nu = 10^{-5}$, the divergence of velocity decreases as the mesh is refined, and it remains close to 0. This observation is consistent with the results from Lemma 2.3.1.

4.2 CutFEM

In this section, we use Netgen/NGSolve [48] with the ngsxfem extension [37] for the CutFEM numerical experiments. Throughout this section, we use the finite element methods (3.2.1) introduced in the third chapter for our numerical experiments, with one slight modification for the ghost penalty terms stated in [44] as we now explain.

For any $F \in \mathcal{F}^{ct,\Gamma}$, we define $\omega_F := K_1 \cup K_2$, where $F \subset \partial K_1 \cap \partial K_2$. Then, for

a polynomial v that is defined on ω_F, we denote v_i to be v restricted to K_i, where $i = 1, 2$. Then we canonically extend both v_1 and v_2 to K_2 and K_1, respectively. Finally, we define $[v]_{\omega_F}(x) = v_1(x) - v_2(x)$ for $x \in \omega_F$. Then we define the two modified stabilization term:

$$\mathbf{j}_{h,m}(\boldsymbol{u}, \boldsymbol{v}) = \frac{1}{h^2} \sum_{F \in \mathcal{F}^{ct,\Gamma}} \int_{\omega_F} [\boldsymbol{u}]_{\omega_F} [\boldsymbol{v}]_{\omega_F}, \tag{4.2.1}$$

$$J_{h,m}(p, q) = \sum_{F \in \mathcal{F}^{ct,\Gamma}} \int_{\omega_F} [p]_{\omega_F} [q]_{\omega_F}. \tag{4.2.2}$$

From [44, Lemma 3.1] and [44, Remark 6] we see that both $\mathbf{j}_{h,m}(\cdot, \cdot)$ and $J_{h,m}(\cdot, \cdot)$ have ghost penalty mechanisms, and are bounded above by $\mathbf{j}_h(\cdot, \cdot)$ from the bilinear form $a_h(\cdot, \cdot)$ in (3.2.1) and $J_h(\cdot, \cdot)$ from the second equation of (3.2.1).

For the convenience of implementation, we use $\mathbf{j}_{h,m}(\cdot, \cdot)$ and $J_{h,m}(\cdot, \cdot)$ to replace $\mathbf{j}_h(\cdot, \cdot)$ and $J_h(\cdot, \cdot)$ in (3.2.1) during the following numerical experiments.

We conduct total of two numerical experiments. For each experiment, we perform a series of tests of the finite element method (3.2.1). The domain for these tests is a 6-petal flower-shaped domain given via a level set function [36]:

$$\Omega = \{(x, y) \in \mathbb{R}^2 : \phi(x, y) < 0\}, \tag{4.2.3}$$

where

$$\phi(x, y) = \sqrt{(x - 0.5)^2 + (y - 0.5)^2} - \sqrt{0.1} - \frac{1}{12} \sin(6 \tan^{-1}(\frac{y - 0.5}{x - 0.5})).$$

In the first experiment, we use the Scott-Vogelius pair $\boldsymbol{\mathcal{P}}_2 - \mathcal{P}_1^{disc}$ on Clough-Toucher splits for the finite element spaces; in the second experiment, we use the Scott-Vogelius pair $\boldsymbol{\mathcal{P}}_3 - \mathcal{P}_2^{disc}$ on Clough-Toucher splits for the finite element spaces.

We set the background polygon to be the unit square $S = (0,1)^2$, and the background mesh $\mathcal{S}_h$ to be a sequence of Delaunay triangulations. Then we perform the barycenter refinement to obtain $\mathcal{S}_h^{ct}$.

Each experiment consists of three groups of tests, where the difference of the three groups of tests is the Nitsche penalty parameter η and the grad-div parameter γ in the bilinear form $a_h(\cdot,\cdot)$. In the first group, we set $\eta = 100$ and $\gamma = 0$; in the second group, we set $\eta = 100$ and $\gamma = 10h^{-1}$; in the third group, we set $\eta = 10h^{-1}$ and $\gamma = 10h^{-1}$. For each group, we perform the tests 5 times on a sequence of meshes with the mesh parameter h being 0.200, 0.100, 0.050, 0.025 and 0.013.

The exact velocity solution and exact pressure solution are set to be

$$\boldsymbol{u} = \begin{pmatrix} (x^2+y^2-1)(8x^2y+x^2+5y^2-1) \\ -4x(x^2+y^2-1)(3x^2+y^2+y-1) \end{pmatrix}, \quad p = 10((x^2-y^2)^2 - \frac{1}{6}). \tag{4.2.4}$$

Correspondingly, we have the right-hand function

$$f = \begin{pmatrix} (-144x^2y - 16y^3 - 24x^2 - 72y^2 + 16y + 16) + 40x(x^2-y^2) \\ 16x(17x^2+9y^2+3y-7) - 40y(x^2-y^2) \end{pmatrix}.$$

4.2.1 Scott-Vogelius pair when $k = 2$

In Table 7 and Table 8, we have the results for L^2 error of velocity $\|\boldsymbol{u}-\boldsymbol{u}_h\|_{L^2(\Omega)}$, the H^1-type error of velocity $\|\nabla(\boldsymbol{u}-\boldsymbol{u}_h)\|_{L^2(\Omega)}$ and L^2 error of pressure $\|p-p_h\|_{L^2(\Omega)}$ and their respective rates of convergence for each of the three groups. In each of the three groups, we find that the convergence rate for the velocity error in L^2 norm is of order 3, and the velocity error in H^1-type norm is of order 2, and the pressure error in L^2 norm is of order 2, which are all the optimal order convergence rates with respect to the respective space and norm.

We plot the error results from Table 7 and Table 8 in Figure 10 to illustrate the convergence rates.

We present divergence of the velocity for the three groups of tests in Table 9. We notice that the divergence of velocity solution on the domain decreases drastically in the cases where $\gamma = 10h^{-1}$ from that in the case where $\gamma = 0$. This behavior aligns with the theoretic results that the violation of the divergence-free constraint in a boundary strip can be partially mitigated by taking grad-div parameter $\gamma = \mathcal{O}(h^{-1})$.

Finally, we have the plot of both velocity solution and pressure solution in L^2-norm, where the Nitsche parameter is set to be $\eta = 10h^{-1}$ and the grad-div parameter is set to be $\gamma = 10h^{-1}$, on the mesh with mesh parameter $h = 0.025$ in Figure 11.

$\eta = 100$, $\gamma = 0$				
h	$\|\boldsymbol{u} - \boldsymbol{u}_h\|_{L^2(\Omega)}$	Rate	$\|\nabla(\boldsymbol{u} - \boldsymbol{u}_h)\|_{L^2(\Omega)}$	Rate
0.200	2.372e-03		1.180e-01	
0.100	4.533e-04	2.388	3.882e-02	1.604
0.050	5.657e-05	3.002	1.097e-02	1.823
0.025	7.627e-06	2.891	3.045e-03	1.849
0.013	1.018e-06	2.905	8.100e-04	1.910
$\eta = 100$, $\gamma = 10h^{-1}$				
h	$\|\boldsymbol{u} - \boldsymbol{u}_h\|_{L^2(\Omega)}$	Rate	$\|\nabla(\boldsymbol{u} - \boldsymbol{u}_h)\|_{L^2(\Omega)}$	Rate
0.200	4.507e-03		1.689e-01	
0.100	5.926e-04	2.927	4.662e-02	1.857
0.050	7.036e-05	3.074	1.270e-02	1.876
0.025	8.710e-06	3.014	3.257e-03	1.963
0.013	1.076e-06	3.017	8.392e-04	1.956
$\eta = 10h^{-1}$, $\gamma = 10h^{-1}$				
h	$\|\boldsymbol{u} - \boldsymbol{u}_h\|_{L^2(\Omega)}$	Rate	$\|\nabla(\boldsymbol{u} - \boldsymbol{u}_h)\|_{L^2(\Omega)}$	Rate
0.200	4.027e-03		1.575e-01	
0.100	5.926e-04	2.765	4.662e-02	1.756
0.050	7.511e-05	2.980	1.308e-02	1.834
0.025	9.998e-06	2.909	3.347e-03	1.966
0.013	1.161e-06	3.106	8.572e-04	1.965

Table 7: L^2 and H^1-type error for velocity and respective convergence rates with different Nitsche penalty parameters η and grad-div parameters γ on domain (4.2.3) with exact solution (4.2.4).

$\eta = 100$, $\gamma = 0$		
h	$\|p - p_h\|_{L^2(\Omega)}$	Rate
0.200	1.132e-01	
0.100	2.343e-02	2.272
0.050	7.250e-03	1.692
0.025	2.208e-03	1.715
0.013	6.176e-04	1.838
$\eta = 100$, $\gamma = 10h^{-1}$		
h	$\|p - p_h\|_{L^2(\Omega)}$	Rate
0.200	2.780e-01	
0.100	4.152e-02	2.743
0.050	1.185e-02	1.809
0.025	2.678e-03	2.146
0.013	6.947e-04	1.947
$\eta = 10h^{-1}$, $\gamma = 10h^{-1}$		
h	$\|p - p_h\|_{L^2(\Omega)}$	Rate
0.200	2.129e-01	
0.100	4.152e-02	2.358
0.050	1.404e-02	1.564
0.025	3.561e-03	1.979
0.013	1.089e-03	1.709

Table 8: L^2 error for pressure and convergence rate with different Nitsche penalty parameters η and grad-div parameters γ on domain (4.2.3) with exact solution (4.2.4).

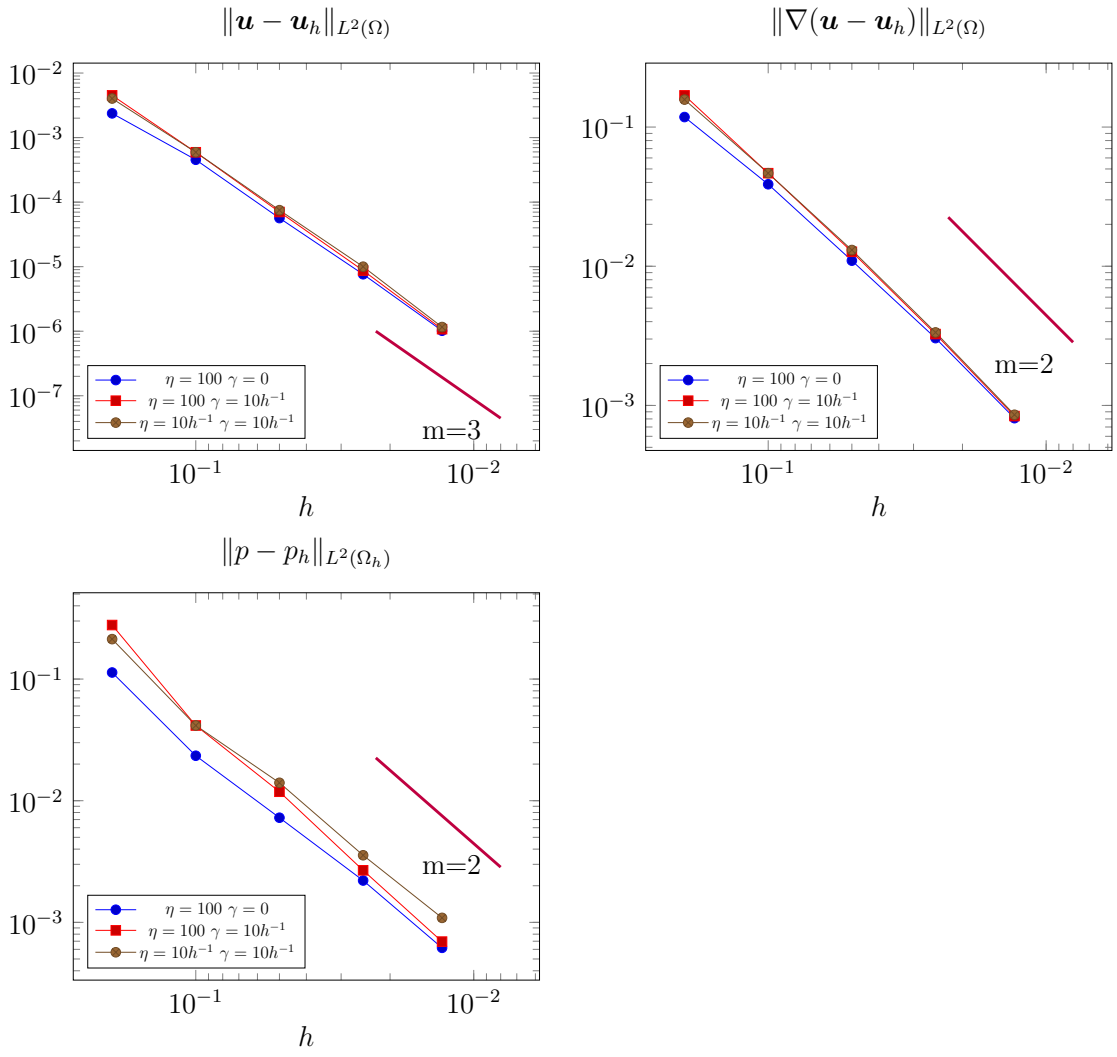

Figure 10: Errors for the velocity and pressure on domain(4.2.3) with varying mesh sizes.

$\|\mathrm{div}\, \boldsymbol{u}_h\|_{L^2(\Omega)}$			
h	$\eta = 100,\ \gamma = 0$	$\eta = 100,\ \gamma = 10h^{-1}$	$\eta = 10h^{-1},\ \gamma = 10h^{-1}$
0.200	4.505e-02	5.959e-03	4.346e-03
0.100	9.165e-03	7.992e-04	7.992e-04
0.050	2.502e-03	8.346e-05	1.190e-04
0.025	3.984e-04	8.650e-06	2.124e-05
0.013	6.464e-05	1.088e-06	3.710e-06

Table 9: Divergence of velocity in L^2 norm on the domain (4.2.3).

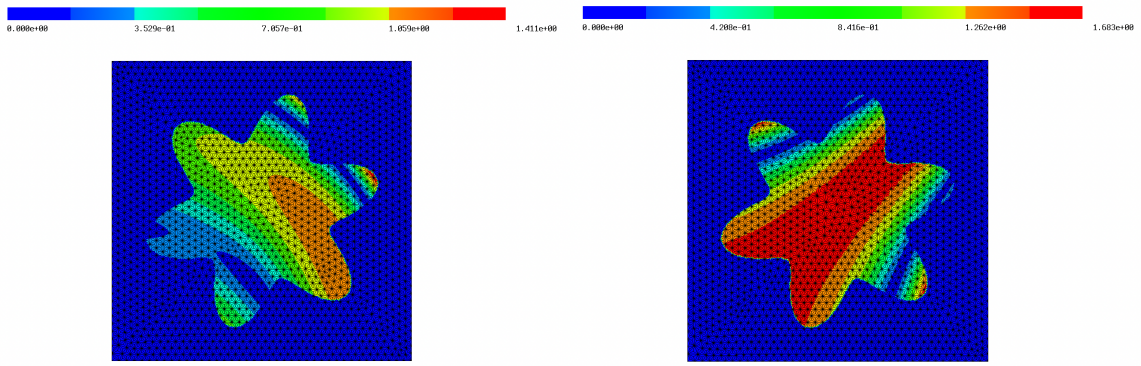

Figure 11: Aboslute values of velocity (left) and pressure (right) solutions on a flower-shaped domain, when $h = 0.025$ and $\eta = \gamma = 10h^{-1}$.

4.2.2 Scott-Vogelius pair when $k = 3$

In Table 10 and Table 11, we have the results for L^2 error of velocity $\|\boldsymbol{u}-\boldsymbol{u}_h\|_{L^2(\Omega)}$, the H^1-type error of velocity $\|\nabla(\boldsymbol{u}-\boldsymbol{u}_h)\|_{L^2(\Omega)}$ and L^2 error of pressure $\|p-p_h\|_{L^2(\Omega)}$ and their respective rates of convergence for each of the three groups. In each of the three groups, we find that the convergence rate for the velocity error in L^2 norm is of order 4, and the velocity error in H^1-type norm is of order 3, and the pressure error in L^2 norm is of order 3, which are all the optimal order convergence rates with respect to the respective space and norm.

We plot the error results from Table 10 and Table 11 in Figure 12 to illustrate the convergence rates.

We present divergence of the velocity for the three groups of tests in Table 12. We notice that the divergence of velocity solution on the domain decreases drastically in the cases where $\gamma = 10h^{-1}$ from that in the case where $\gamma = 0$. This behavior aligns with the theoretic results that the violation of the divergence-free constraint in a boundary strip can be partially mitigated by taking grad-div parameter $\gamma = \mathcal{O}(h^{-1})$.

Finally, we have the plot of both velocity solution and pressure solution in L^2-norm, where the Nitsche parameter is set to be $\eta = 10h^{-1}$ and the grad-div parameter is set to be $\gamma = 10h^{-1}$, on the mesh with mesh parameter $h = 0.025$ in Figure 13.

$\eta = 100$, $\gamma = 0$				
h	$\|\boldsymbol{u} - \boldsymbol{u}_h\|_{L^2(\Omega)}$	Rate	$\|\nabla(\boldsymbol{u} - \boldsymbol{u}_h)\|_{L^2(\Omega)}$	Rate
0.200	7.504e-03		2.864e-01	
0.100	1.081e-05	9.439	5.775e-04	8.954
0.050	5.527e-07	4.290	6.179e-05	3.224
0.025	3.385e-08	4.029	7.093e-06	3.123
0.013	2.181e-09	3.956	9.030e-07	2.974
$\eta = 100$, $\gamma = 10h^{-1}$				
h	$\|\boldsymbol{u} - \boldsymbol{u}_h\|_{L^2(\Omega)}$	Rate	$\|\nabla(\boldsymbol{u} - \boldsymbol{u}_h)\|_{L^2(\Omega)}$	Rate
0.200	1.209e-02		3.747e-01	
0.100	1.138e-05	10.05	6.151e-04	9.251
0.050	5.763e-07	4.304	6.530e-05	3.236
0.025	3.435e-08	4.068	7.285e-06	3.164
0.013	2.207e-09	3.960	9.155e-07	2.992
$\eta = 10h^{-1}$, $\gamma = 10h^{-1}$				
h	$\|\boldsymbol{u} - \boldsymbol{u}_h\|_{L^2(\Omega)}$	Rate	$\|\nabla(\boldsymbol{u} - \boldsymbol{u}_h)\|_{L^2(\Omega)}$	Rate
0.200	1.182e-02		3.306e-01	
0.100	1.138e-05	10.02	6.151e-04	9.070
0.050	5.801e-07	4.294	6.650e-05	3.209
0.025	3.474e-08	4.062	7.423e-06	3.163
0.013	2.224e-09	3.965	9.304e-07	2.996

Table 10: L^2 and H^1-type error for velocity and respective convergence rates with different Nitsche penalty parameters η and grad-div parameters γ on domain (4.2.3) with exact solution (4.2.4).

$\eta = 100$, $\gamma = 0$		
h	$\|p - p_h\|_{L^2(\Omega)}$	Rate
0.200	2.614e-01	
0.100	1.013e-03	8.011
0.050	1.313e-04	2.948
0.025	1.719e-05	2.933
0.013	2.336e-06	2.879
$\eta = 100$, $\gamma = 10h^{-1}$		
h	$\|p - p_h\|_{L^2(\Omega)}$	Rate
0.200	6.384e-01	
0.100	1.157e-03	9.108
0.050	1.441e-04	3.005
0.025	1.786e-05	3.012
0.013	2.399e-06	2.896
$\eta = 10h^{-1}$, $\gamma = 10h^{-1}$		
h	$\|p - p_h\|_{L^2(\Omega)}$	Rate
0.200	5.873e-01	
0.100	1.157e-03	8.988
0.050	1.464e-04	2.982
0.025	1.814e-05	3.013
0.013	2.423e-06	2.904

Table 11: L^2 error for pressure and convergence rate with different Nitsche penalty parameters η and grad-div parameters γ on domain (4.2.3) with exact solution (4.2.4).

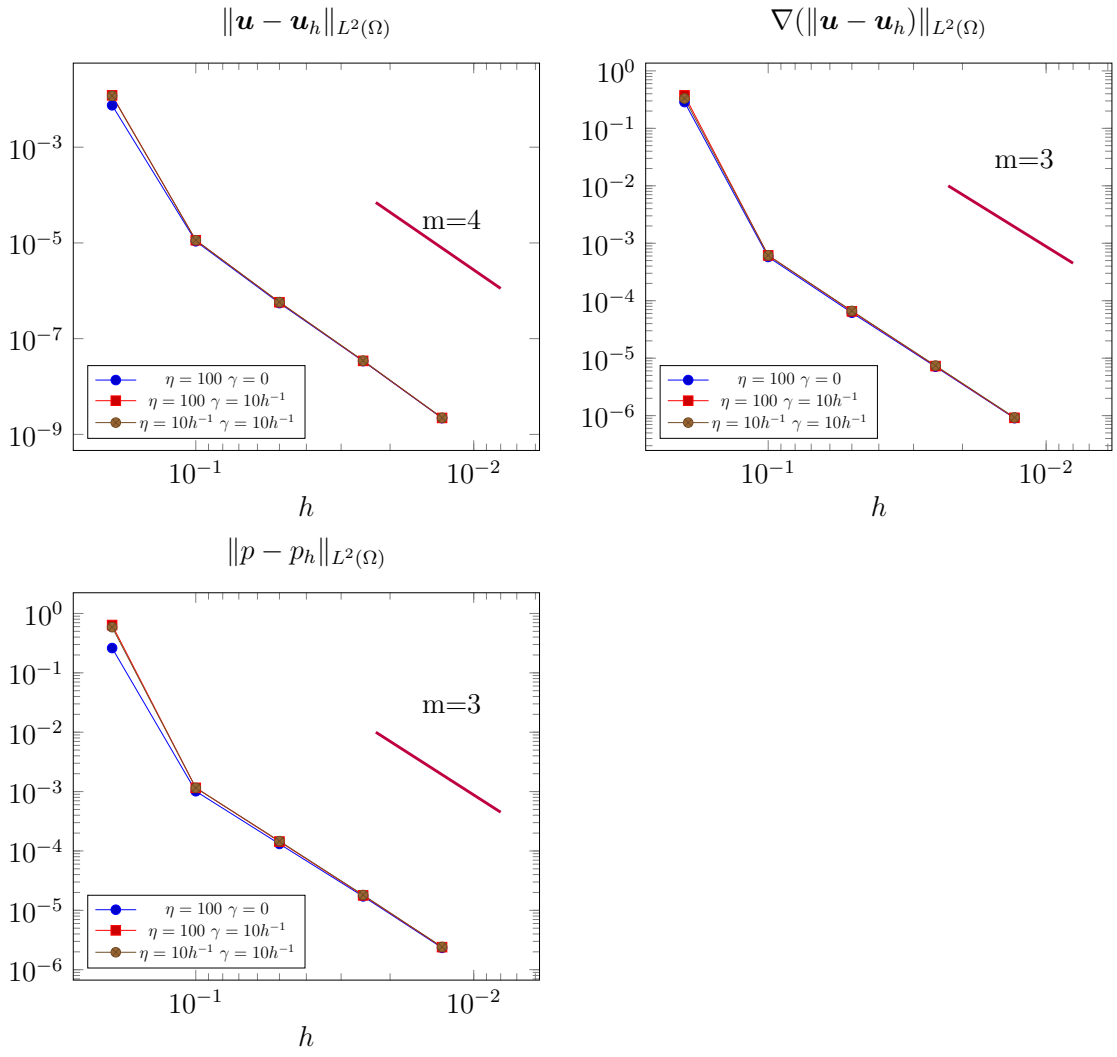

Figure 12: Errors for the velocity and pressure on domain(4.2.3) with varying mesh sizes.

$\|\mathrm{div}\, \boldsymbol{u}_h\|_{L^2(\Omega)}$			
h	$\eta = 100,\ \gamma = 0$	$\eta = 100,\ \gamma = 10h^{-1}$	$\eta = 10h^{-1},\ \gamma = 10h^{-1}$
0.200	2.092e-01	2.021e-02	1.487e-02
0.100	1.966e-04	1.002e-05	1.002e-05
0.050	1.832e-05	5.644e-07	6.999e-07
0.025	1.583e-06	3.494e-08	5.567e-08
0.013	1.372e-07	1.984e-09	4.556e-09

Table 12: Divergence of velocity in L^2 norm on the domain (4.2.3).

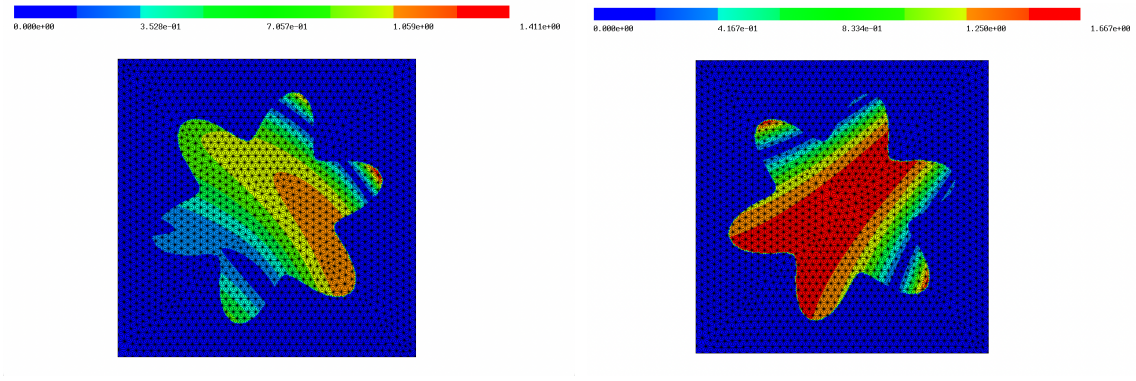

Figure 13: Aboslute values of velocity (left) and pressure (right) solutions on a flower-shaped domain, when $h = 0.025$ and $\eta = \gamma = 10h^{-1}$.

4.3 CutFEM for the stationary Navier-Stokes Problem

In this section, we use Netgen/NGSolve [48] with ngsxfem add-on [37] to conduct two numerical tests for the stationary Navier-Stokes equations:

$$-\nu\Delta \boldsymbol{u} + (\boldsymbol{u}\cdot\nabla)\boldsymbol{u} + \nabla p = \boldsymbol{f} \qquad \text{in } \Omega, \tag{4.3.1a}$$

$$\operatorname{div} \boldsymbol{u} = 0 \qquad \text{in } \Omega \tag{4.3.1b}$$

$$\boldsymbol{u} = 0 \qquad \text{on } \partial\Omega \tag{4.3.1c}$$

4.3.1 CutFEM for the stationary Navier-Stokes Problem on a flower-shaped domain

For this test, the domain is a 6-petal flower-shaped domain given via a level set function [36]:

$$\Omega = \{(x,y) \in \mathbb{R}^2 : \phi(x,y) < 0\}, \tag{4.3.2}$$

where

$$\phi(x,y) = \sqrt{(x-0.5)^2 + (y-0.5)^2} - \sqrt{0.1} - \frac{1}{12}\sin(6\tan^{-1}(\frac{y-0.5}{x-0.5})).$$

We use the finite element methods (3.2.1) introduced in chapter 3 for our numerical experiments with two modifications.

1. For the convenience in implementing this method, we use $\mathbf{j}_{h,m}(\cdot,\cdot)$ and $J_{h,m}(\cdot,\cdot)$ in (4.2.1) and (4.2.2) to replace $\mathbf{j}_h(\cdot,\cdot)$ and $J_h(\cdot,\cdot)$ in (3.2.1).
2. We add the non-linear term $(\boldsymbol{u}\cdot\nabla\boldsymbol{u}, \boldsymbol{v})$ and a skew-symmetrize term $(\frac{1}{2}(\operatorname{div}\boldsymbol{u})\boldsymbol{u}, \boldsymbol{v})$ to the bilinear form $a_h(\cdot,\cdot)$ in (3.2.1).

We set the background polygon to be the unit square $S = (0,1)^2$, and the background mesh $\mathcal{S}_h$ to be a sequence of Delaunay triangulations of S. Then we perform the barycenter refinement to obtain $\mathcal{S}_h^{ct}$.

We set the Nitsche parameter $\eta = 10h^{-1}$.

The experiment consists of three groups of tests, where the difference of the three groups of tests is the grad-div parameter γ in the bilinear form $a_h(\cdot,\cdot)$. In the first group, we set $\gamma = 0$; in the second group, we set $\gamma = 100$; in the third group, we set $\gamma = 10h^{-1}$.

For each group, we perform the tests 5 times on a sequence of meshes with the mesh parameter h being 0.200, 0.100, 0.050, 0.025 and 0.013.

The exact velocity solution and exact pressure solution are set to be

$$\boldsymbol{u} = \begin{pmatrix} 2(x^2 - x + 0.25 + y^2 - y)(2y-1) \\ -2(x^2 - x + 0.25 + y^2 - y)(2x-1) \end{pmatrix}, \quad p = 10(x^2 - y^2)^2. \tag{4.3.3}$$

Correspondingly, we have the right-hand function

$$f = \begin{pmatrix} (16 - 32y) + 40x(x^2 - y^2) - 8(-1+2x)(\frac{1}{4} - x + x^2 - y + y^2)^2 \\ (32x - 16) - 40y(x^2 - y^2) - 8(-1+2y)(\frac{1}{4} - x + x^2 - y + y^2)^2 \end{pmatrix}.$$

We use the lowest order Scott-Vogelius pair $\boldsymbol{\mathcal{P}}_2 - \mathcal{P}_1^{disc}$.

In Table 13 and Table 14, we state the results for the L^2 error of velocity $\|\boldsymbol{u} - \boldsymbol{u}_h\|_{L^2(\Omega)}$, the H^1-type error of velocity $\|\nabla(\boldsymbol{u} - \boldsymbol{u}_h)\|_{L^2(\Omega)}$, the L^2 error of pressure $\|p - p_h\|_{L^2(\Omega)}$, and $\|\mathrm{div}\, \boldsymbol{u}_h\|_{L^2(\Omega)}$ and their respective rates of convergence. When $\gamma = 0$, we find that the convergence rate for the velocity error in L^2 norm is of order 3, and the velocity error in H^1-type norm is of order 2, the pressure error in L^2 norm is of order 2, which are are of optimal order with respect to the space and norm. In the cases $\gamma = 100$ and $\gamma = 10h^{-1}$, the velocity error in L^2 norm and the velocity

error in H^1-type norm exhibit optimal order convergence rate. However, the rate of convergence of pressure error $\|p - p_h\|_{L^2(\Omega)}$ drops to 1.674 when $\gamma = 100$; the rate of convergence of pressure error $\|p - p_h\|_{L^2(\Omega)}$ drops to 0.411 when $\gamma = 10h^{-1}$. On the other hand, we observe the size of the divergence of velocity decreases significantly as the grad-div parameter γ increases.

We plot the error results from Table 13 and Table 14 in Figure 14 to illustrate the convergence rates.

Finally, in Figure 15, we plot the absolute values of velocity solution and pressure solution, where the Nitsche parameter is set to be $\eta = 10h^{-1}$ and the grad-div parameter is set to be $\gamma = 10h^{-1}$, on the mesh with mesh parameter $h = 0.05$ in Figure 15.

$\gamma = 0$						
h	$\|\boldsymbol{u} - \boldsymbol{u}_h\|_{L^2(\Omega)}$	Rate	$\|\nabla(\boldsymbol{u} - \boldsymbol{u}_h)\|_{L^2(\Omega)}$	Rate	$\|\mathrm{div}\,(\boldsymbol{u}_h)\|_{L^2(\Omega)}$	Rate
0.200	6.812e-04		2.460e-02		1.060e-02	
0.100	9.643e-05	2.821	6.671e-03	1.883	2.866e-03	1.887
0.050	8.172e-06	3.561	1.491e-03	2.162	4.978e-04	2.525
0.025	8.664e-07	3.238	3.780e-04	1.980	1.072e-04	2.215
0.013	1.089e-07	2.992	9.714e-05	1.960	3.120e-05	1.781
$\gamma = 100$						
h	$\|\boldsymbol{u} - \boldsymbol{u}_h\|_{L^2(\Omega)}$	Rate	$\|\nabla(\boldsymbol{u} - \boldsymbol{u}_h)\|_{L^2(\Omega)}$	Rate	$\|\mathrm{div}\,(\boldsymbol{u}_h)\|_{L^2(\Omega)}$	Rate
0.200	5.733e-04		2.348e-02		6.522e-04	
0.100	8.049e-05	2.832	6.351e-03	1.886	1.835e-04	1.830
0.050	7.531e-06	3.418	1.454e-03	2.127	6.483e-05	1.501
0.025	9.106e-07	3.048	3.695e-04	1.976	2.183e-05	1.570
0.013	1.041e-07	3.129	9.352e-05	1.982	7.504e-06	1.541
$\gamma = 10h^{-1}$						
h	$\|\boldsymbol{u} - \boldsymbol{u}_h\|_{L^2(\Omega)}$	Rate	$\|\nabla(\boldsymbol{u} - \boldsymbol{u}_h)\|_{L^2(\Omega)}$	Rate	$\|\mathrm{div}\,(\boldsymbol{u}_h)\|_{L^2(\Omega)}$	Rate
0.200	5.720e-04		2.330e-02		9.033e-04	
0.100	8.049e-05	2.328	6.351e-03	1.875	1.835e-04	2.299
0.050	8.071e-06	3.318	1.467e-03	2.114	5.950e-05	1.625
0.025	1.061e-06	2.927	3.747e-04	1.969	2.074e-05	1.520
0.013	1.388e-07	2.934	9.659e-05	1.956	7.182e-06	1.530

Table 13: L^2 and H^1-type error for velocity and divergence of velocity in L^2-norm and respective convergence rates with different grad-div parameters $\gamma = 0$, $\gamma = 100$, $\gamma = 10h^{-1}$ on domain (4.3.2) with exact solution (4.3.3).

$\|p - p_h\|_{L^2(\Omega)}$						
h	$\gamma = 0$	Rate	$\gamma = 100$	Rate	$\gamma = 10h^{-1}$	Rate
0.200	5.053e-02		7.720e-02		7.504e-02	
0.100	6.889e-03	2.875	6.882e-03	3.488	6.882e-03	3.447
0.050	1.297e-03	2.409	1.904e-03	1.854	2.835e-03	1.279
0.025	2.942e-04	2.140	4.444e-04	2.099	1.124e-03	1.335
0.013	7.527e-05	1.967	1.393e-04	1.674	8.451e-04	0.411

Table 14: L^2 error for pressure and convergence rate with different grad-div parameters $\gamma = 0$, $\gamma = 100$, $\gamma = 10h^{-1}$ on domain (4.3.2) with exact solution (4.3.3).

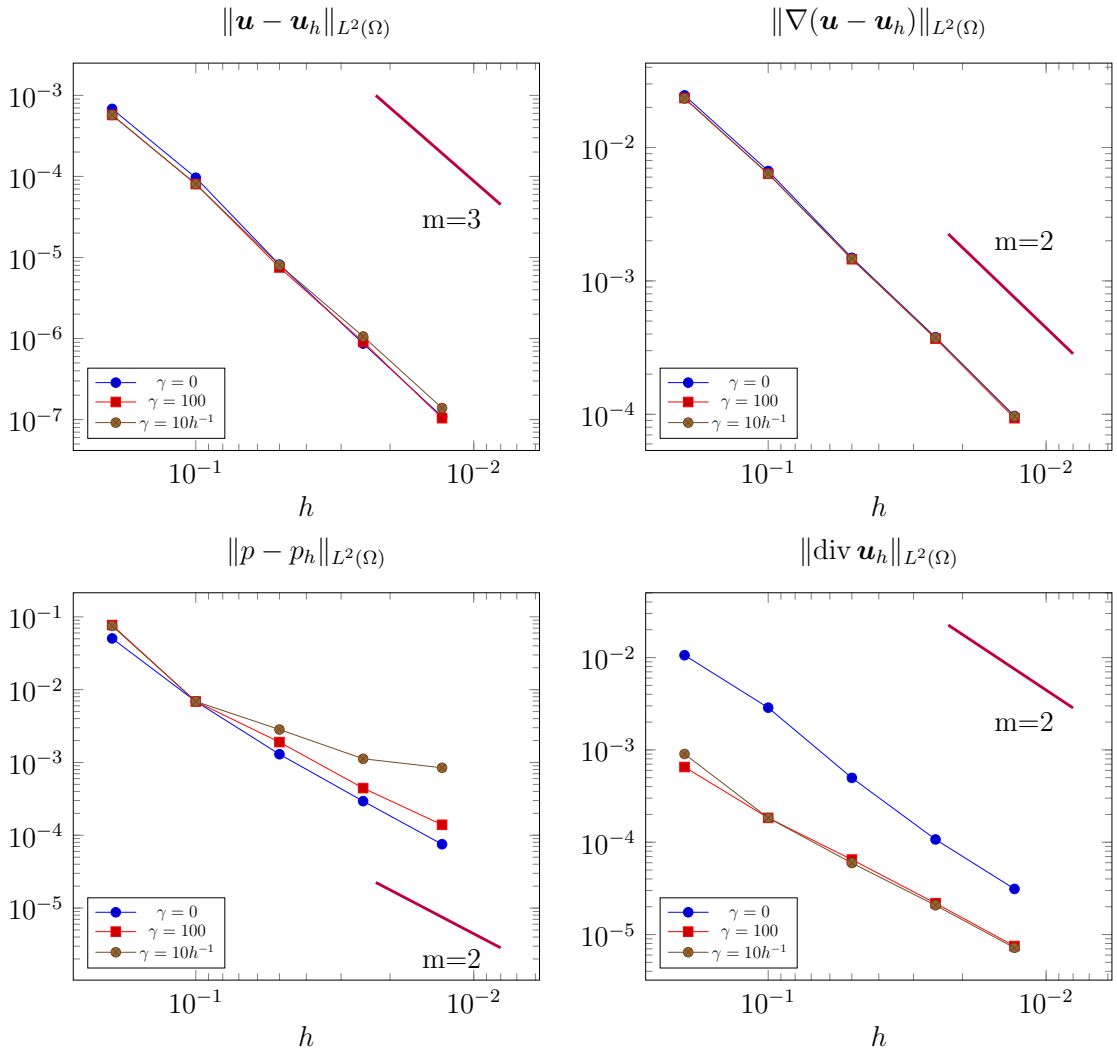

Figure 14: Errors for the velocity and pressure and the divergence of velocity in L^2-norm on domain(4.3.2) with varying mesh sizes.

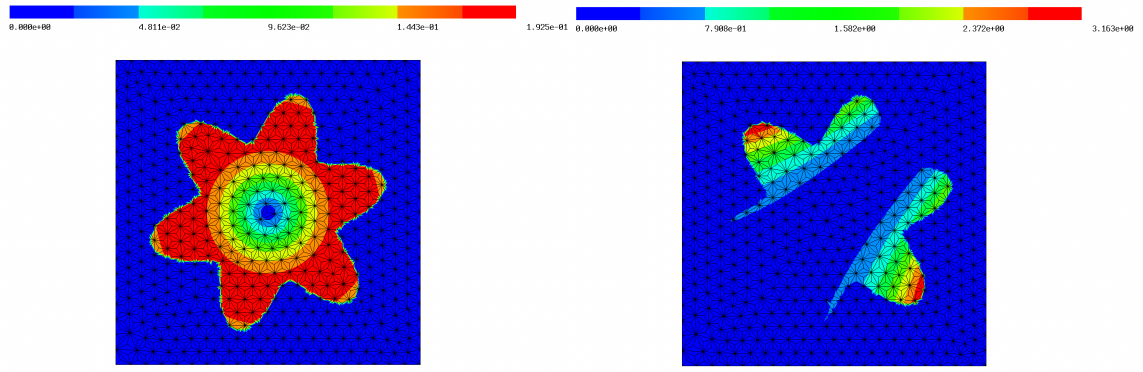

Figure 15: Aboslute values of velocity (left) and pressure (right) solutions on a flower-shaped domain, when $h = 0.05$ and $\eta = \gamma = 10h^{-1}$.

4.3.2 Schäfer-Turek benchmark

In this subsection, we conduct the Schäfer-Turek benchmark test [47] for the stationary Navier–Stokes problem (4.3.1) using the CutFEM scheme (3.2.1) with the same modification as the previous test:

1. For the convenience in implementing this method, we use $\mathbf{j}_{h,m}(\cdot,\cdot)$ and $J_{h,m}(\cdot,\cdot)$ in (4.2.1) and (4.2.2) to replace $\mathbf{j}_h(\cdot,\cdot)$ and $J_h(\cdot,\cdot)$ in (3.2.1).
2. We add the non-linear term $(\boldsymbol{u}\cdot\nabla\boldsymbol{u},\boldsymbol{v})$ and a skew-symmetrize term $(\frac{1}{2}(\operatorname{div}\boldsymbol{u})\boldsymbol{u},\boldsymbol{v})$ to the bilinear form $a_h(\cdot,\cdot)$ in (3.2.1).

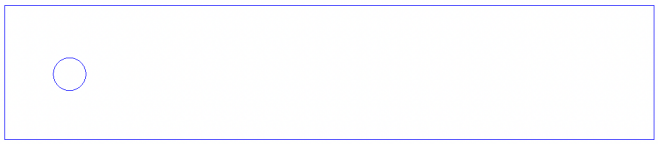

Figure 16: Domain of the Schäfer-Turek benchmark test.

The domain of the test Ω is the interior of a rectangle with length 2 and width 0.41 with a circle removed as shown in Figure16. The circle is given by the following level set:

$$\sqrt{(x-0.2)^2+(y-0.2)^2}-0.0025=0. \tag{4.3.4}$$

The geometry of the domain represents a 2D channel with a circular obstacle which is positioned slightly off the center of the channel. The flow comes in from the left side of the channel and goes out from the right side of the channel. We set the viscosity of the flow $\nu = 0.001$.

We name parts of the boundary of Ω as follows:

1. Γ_{inlet} is the left side of the rectangle;
2. Γ_{wall} is the top and bottom sides of the rectangle;
3. Γ_{outlet} is the right side of the rectangle;
4. Γ_{cyl} is the circle given by (4.3.4).

We set the background polygon to be the 2×0.41 rectangle S, and the background mesh $\mathcal{S}_h$ to be the Delaunay triangulations of S with $h = 0.05$. In this test, the cut elements are the elements that are cut by the circle (4.3.4). The test problem has

the following Dirichlet conditions:

$$\boldsymbol{u} = \begin{pmatrix} \frac{6y(0.41-y)}{0.41^2} \\ 0 \end{pmatrix} \qquad \text{on } \Gamma_{\text{inlet}}, \tag{4.3.5a}$$

$$\boldsymbol{u} = 0 \qquad \text{on } \Gamma_{\text{cyl}}, \tag{4.3.5b}$$

$$\boldsymbol{u} = 0 \qquad \text{on } \Gamma_{\text{wall}}. \tag{4.3.5c}$$

We enforce the boundary conditions (4.3.5a) and (4.3.5c) strongly by including those conditions into the finite element space, while we enforce the boundary condition (4.3.5b) weakly though the CutFEM scheme (3.2.1). We set the Nitsche parameter $\eta = 10h^{-1}$ and the grad-div parameter $\gamma = 10h^{-1}$. We use the Scott-Vogelius pair $\boldsymbol{\mathcal{P}}_3 - \mathcal{P}_2^{disc}$. We plot the norm of the velocity approximation of this test in Figure 17.

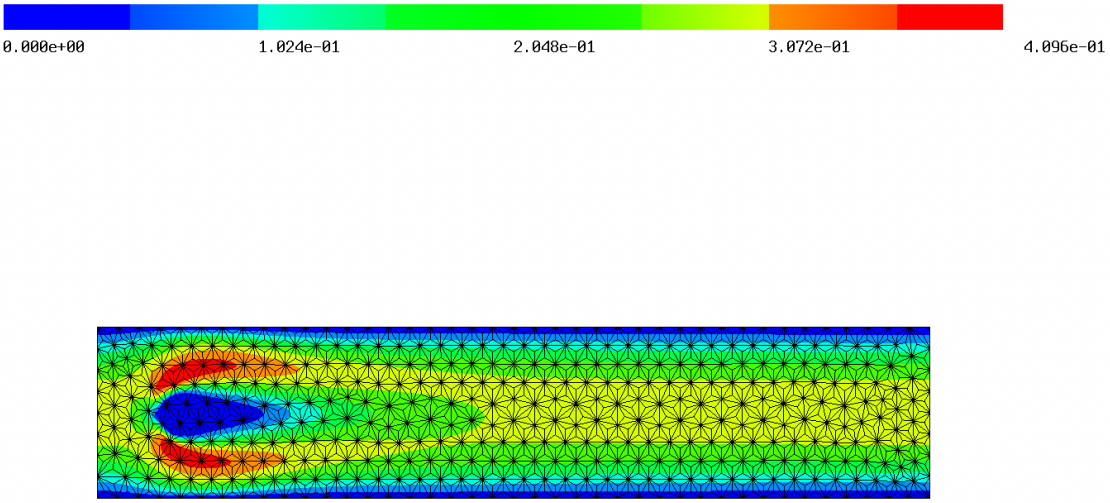

Figure 17: Absolute value of velocity solution of Schäfer-Turek benchmark test, with $h = 0.05$ and $\nu = 0.001$.

5.0 Conclusions

In this thesis, we constructed two unfitted finite element methods for the Stokes problem based on the Scott-Vogelius pair on Clough-Tocher splits and provided numerical experiments using these two schemes.

In Chapter 2, we constructed a uniformly stable and divergence-free method on an unfitted domain for Stokes problem on 2D domains. Although the method is not pressure robust, by using a Lagrange multiplier to enforce normal boundary condition, we reduced the influence of pressure on the velocity error. The theoretical analysis showed that the method converges with optimal order.

In Chapter 3, we constructed a uniformly stable CutFEM on an unfitted domain for Stokes problem on both 2D and 3D domains. Although this scheme does not produce an exact divergence–free velocity approximation, the discrete velocity is divergence–free outside an $O(h)$ neighborhood of the boundary. We used local grad-div stablization to mitigate the error caused by the violation of the divergence-free condition around the boundary. We showed the scheme converges with optimal order even with a rather heavy penalty for the violation of mass conservation.

In chapter 4, we conducted numerical experiments for both the boundary correction method proposed in chapter 2 and the CutFEM proposed in chapter 3. The numerical results were consistent with the theoretical analysis for both methods provided in the respective chapters. In addition, we extended the CutFEM numerical experiments to a stationary Navier-Stokes problem on a simply connected domain and a non-simply connected domain.

Although the discussion in chapter 2 does not go beyond the scope of the 2D setting, some of the results can be easily extended to 3D. For example, the discrete

inf-sup condition (LBB) in Lemma 2.4.6 can be extend seamlessly into 3D. However, the extension of some other results may not be as obvious. For instance, the proof of the inf-sup condition for the velocity-Lagrange multiplier pair relies heavily on the geometry of the computational domain, and its extension to the 3D setting requires a more careful study in the future.

It is also worth mentioning that although for the proposed method in Chapter 3, the finite element space is the Scott-Vogelius pair on Clough-Tocher splits, the results can be extended to the Scott-Vogelius pair on Powell-Sabin splits in a 2D setting.

Bibliography

[1] D. N. Arnold, F. Brezzi, and M. Fortin. *A stable finite element for the Stokes equations*. Calcolo, 21:337-344, 1984.

[2] D. N. Arnold and J. Qin. *Quadratic velocity/linear pressure Stokes elements*. in Advances in Computer Methods for Partial Differential Equations, VII, R. Vichnevetsky, D. Knight, and G. Richter, eds., IMACS, New Brunswick, NJ, pp. 28-34., 1992.

[3] N. M. Atallah, C. Canuto, and G. Scovazzi. *Analysis of the Shifted Boundary Method for the Poisson Problem in General Domains*. arXiv:2006.00872, 2020.

[4] N. M. Atallah, C. Canuto, and G. Scovazzi. *Analysis of the shifted boundary method for the Stokes problem*. Comput. Methods Appl. Mech. Engrg. 358, 2020.

[5] N. M. Atallah, C. Canuto, and G. Scovazzi. *The second-generation shifted boundary method and its numerical analysis*. Comput. Methods Appl. Mech. Engrg., 372:113–3471,, 2020.

[6] J. W. Barrett and C. M. Elliott. *A Finite-Element Method for Solving Elliptic Equations with Neumann Data on a Curved Boundary Using Unfitted Meshes*. IMA Journal of Numerical Analysis, 4(3):309–325, 1984.

[7] M. A. Belenli, L. G. Rebholz, and F. Tone. *A note on the importance of mass conservation in long-time stability of Navier-Stokes simulations using finite elements*. Appl. Math. Lett., 45:98–102, 2015.

[8] D. Boffi, F. Brezzi, and M. Fortin. *Finite elements for the Stokes problem, in Mixed finite Elements Compatibility Conditions, and Applications*. Lecture given at the C.I.M.E Summer school, Springer-Verlag, Berlin, 2008.

[9] S. C. Brenner and L. R. Scott. *The Mathematical Theory of Finite Element Methods*. 3rd ed., Texts in Applied Mathematics, vol. 15, Springer, New York, 2008.

[10] E. Burman, S. Claus, P. Hansbo, M. G. Larson, and A. Massing. *CutFEM: discretizing geometry and partial differential equations*. Internat. J. Numer. Methods Engrg., 104(7): 472–501, 2015.

[11] E. Burman and P. Hansbo. *Fictitious domain methods using cut elements: III. A stabilized Nitsche method for Stokes problem*. ESAIM Math. Model. Numer. Anal., 2014.

[12] E. Burman, P. Hansbo, and M. G. Larson. *Dirichlet boundary value correction using Lagrange multipliers*. BIT, 60(1):235–260, 2020.

[13] E. Burman, P. Hansbo, and M. G. Larson. *Dirichlet boundary value correction using Lagrange multipliers*. BIT, 60(1):235–260, 2020.

[14] M. Case, V. Ervin, A. Linke, and L. Rebholz. *A Connection Between Scott–Vogelius and Grad-Div Stabilized Taylor–Hood FE Approximations of the Navier–Stokes Equations*. SIAM Journal on Numerical Analysis, 49(4):1461-1481, 2011.

[15] L. Cattaneo, L. Formaggia, G. F. Iori, A. Scotti, and P. Zunino. *Stabilized extended finite elements for the approximation of saddle point problems with unfitted interfaces*. Calcolo, 52(2):123–152, 2015.

[16] L. Cattaneo, L. Formaggia, G. F. Iori, A. Scotti, and P. Zunino. *Stabilized extended finite elements for the approximation of saddle point problems with unfitted interfaces*. Calcolo, 52(2):123–152,, 2015.

[17] S. Charnyi, T. Heister, M.A. Olshanskii, and L.G. Rebholz. *On conservation laws of Navier-Stokes Galerkin discretizations*. J. Comput. Phys., 337:289–308, 2017.

[18] M. Costabel and A. McIntosh. *On Bogovskiĭ and regularized Poincaré integral operators for de Rham complexes on Lipschitz domains*. Math. Z., 265(2):297–320, 2010.

[19] J. Douglas Jr., T. Dupont, P. Percell, and L. R. Scott. *A family of C^1 finite elements with optimal approximation properties for various Galerkin methods for 2nd and 4th order problems*. ESAIM: Mathematical Modelling and Numerical Analysis - Modélisation Mathématique et Analyse Numérique, Tome 13(3), pp. 227-255, 1979.

[20] C. M. Elliott and T. Ranner. *Finite element analysis for a coupled bulk–surface partial differential equation*. IMA J. Numer. Anal., 33(2):377–402, 2013.

[21] R. S. Falk and M. Neilan. *Stokes Complexes and the construction of Stable Finite Elements with Pointwise Mass Conservation*. SIAM J. Numer. Anal., vol. 51, pp. 1308-1326, 2013.

[22] G. Fu, J. Guzmán, and M. Neilan. *Exact smooth piecewise polynomial sequences on Alfeld splits*. Mathematics of Computation, 89(323):1059–1091, 2020.

[23] D. Gilbarg and N. S. Trudinger. *Elliptic partial differential equations of second order*. Reprint of the 1998 edition. Classics in Mathematics.Springer–Verlag, Berlin, 2001.

[24] V. Girault and P. A. Raviart. *Finite element methods for Navier-Stokes equations: theory and algorithms*. Springer Series in Computational Mathematics 5, Springer-Verlag, Berlin, 1986.

[25] J. Guzmán and M. Neilan. *Conforming and divergence-free Stokes elements on general triangular meshes*. Mathematics of Computation, 83(285):15-36, 2014.

[26] J. Guzmán and M. Neilan. *inf-sup stable finite elements on barycentric refinements producing divergence-free approximations in arbitrary dimensions.* SIAM J. Numer. Anal., 56(5):2826–2844, 2018.

[27] J. Guzmán and M. Olshanskii. *Inf-sup stability of geometrically unfitted Stokes finite elements.* Mathematics of Computation., 87(313):2091–2112,, 2018.

[28] J. Guzmán and L. Scott. *The Scott-Vogelius finite elements revisited.* Math. Comp. 88 (2019), 515-529, 2018.

[29] A. Hansbo and P. Hansbo. *An unfitted finite element method, based on Nitsches method, for elliptic interface problems.* Comput. Methods Appl. Mech. Engrg., 191(47-48):5537–5552,, 2002.

[30] P. Hansbo, M. G. Larson, and S. Zahedi. *A cut finite element method for a Stokes interface problem.* Appl. Numer. Math., 85:90–114, 2014.

[31] T. Heister, L. G. Rebholz, and M. Xiao. *Flux-preserving enforcement of inhomogeneous Dirichlet boundary conditions for strongly divergence–free mixed finite element methods for flow problems.* J. Math. Anal. Appl., 438(1):507–513, 2016.

[32] J. S. Howell and N. J. Walkington. *Inf-sup conditions for twofold saddle point problems.* Numer. Math., 118(4):663–693, 2011.

[33] M. Kirchhart, S. Gross, and A. Reusken. *Analysis of an XFEM Discretization for Stokes Interface Problems.* SIAM J. Sci. Comput., 38(2):A1019-A1043, 2016.

[34] M. Kirchhart, S. Groß, and A. Reusken. *Analysis of an XFEM discretization for Stokes interface problems.* SIAM J. Sci. Comput, 38(2):A1019–A1043, 2016.

[35] G. Legrain, N. Moës, and A. Huerta. *Stability of incompressible formulations enriched with X-FEM.* Comput. Methods Appl. Mech. Engrg., 197(21-24):1835–1849, 2008.

[36] C. Lehrenfeld. *High order unfitted finite element methods on level set domains using isoparametric mappings.* Comput. Methods Appl. Mech. Engrg., 300:716–733, 2016.

[37] C. Lehrenfeld, F. Heimann, J. Preuß, and H. von Wahl. *ngsxfem: Add-on to NGSolve for geometrically unfitted finite element discretizations.* The Journal of Open Source Software, 6(64):3237, 2021.

[38] A. Linke. *Collision in a cross-shaped domain–a steady 2d Navier-Stokes example demonstrating the importance of mass conservation in CFD.* Comput. Methods Appl. Mech. Engrg., 198(41–44):3278–3286, 2009.

[39] A. Main and G. Scovazzi. *The shifted boundary method for embedded domain computations. Part I: Poisson and Stokes problems.* J. Comput. Phys., 372:972–995, 2018.

[40] A. Massing, M.G. Larson, A. Logg, and M. E. Rognes. *A stabilized Nitsche fictitious domain method for the Stokes problem.* J. Sci. Comput., 61(3):604–628, 2018.

[41] J. Nitsche. *Über ein Variationsprinzip zur Lösung von Dirichlet-Problemen bei Verwendung von Teilruämen die keinen Randbedingungen unterworfen sind.* Abh. Math. Sem. Univ. Hamburg, 36:9–15, 1971.

[42] M.A. Olshanskii. *A low order Galerkin finite element method for the Navier–Stokes equations of steady incompressible flow: a stabilization issue and iterative methods.* Comput. Methods Appl. Mech. Engrg., 191(47-48):5515–5536, 2002.

[43] R. Oyarzúa, M. Solano, and P. Zúñiga. *A high order mixed-FEM for diffusion problems on curved domains*. J. Sci. Comput., 79(1):49–78, 2019.

[44] J. Preuß. *Higher order unfitted isoparametric space-time FEM on moving domains*. Master's thesis, NAM, University of Göttingen, 2018.

[45] J. Qin. *On the Convergence of Some Low Order Mixed Finite Elements for Incompressible Fluids*. Ph.D. thesis, The Pennsylvania State University, State College, PA, 1994.

[46] B. Rivière. *Discontinuous Galerkin methods for solving elliptic and parabolic equations*. heory and implementation. Frontiers in Applied Mathematics, 35. Society for Industrial and Applied Mathematics (SIAM), Philadelphia, PA, 2008.

[47] M. Schafer and S. Turek. *Recent Benchmark Computations of Laminar Flow around a Cylinder*. , 1996.

[48] J. Schöberl. *C++11 implementation of finite elements in NGSolve*. Technical report, ASC-2014-30, Institute for Analysis and Scientific Computing, 2014.

[49] P.W. Schroeder, C. Lehrenfeld, A. Linke, and G. Lube. *Towards computable flows and robust estimates for inf-sup stable FEM applied to the time-dependent incompressible Navier-Stokes equations*. SeMA J., 75(4):629–653, 2018.

[50] P.W. Schroeder and G. Lube. *Divergence-free $H(div)$-FEM for time-dependent incompressible flows with applications to high Reynolds number vortex dynamics*. J. Sci. Comput., 75(2):830–858, 2018.

[51] L. Scott and M. Vogelius. *Norm estimates for a maximal right inverse of the divergence operator in spaces of piecewise polynomials*. ESAIM: M2AN, 19(1): 111-143, 1985.

[52] L. R. Scott and S. Zhang. *Finite element interpolation of nonsmooth functions satisfying boundary conditions.* Mathematics of Computation, 54(190):483–493, 1990.

[53] E. M. Stein. *Singular Integrals and Differentiability Properties of Functions.* Princeton Mathematical Series, No. 30 Princeton University Press, Princeton, N.J, 1970.

[54] M. Vogelius. *A right-inverse for the divergence operator in spaces of piecewise polynomials. Application to the p-version of the finite element method.* Numer. Math., 41:19-37, 1983.

[55] S. Zhang. *A new family of stable mixed finite elements for the 3d Stokes equations.* Mathematics of Computation, 74(250):543–554, 2005.